Revised version 4 – May 15th 2014

Title: Saturn's dynamic magnetotail: A comprehensive magnetic field and plasma survey of plasmoids and travelling compression regions, and their role in global magnetospheric dynamics

Paper revised for re-submission to Journal of Geophysical Research, Space Physics

Authors:

C.M. Jackman[1,2,3], J. A Slavin[4], M.G. Kivelson[4,5], D. J. Southwood[6], N. Achilleos[1,2], M.F. Thomsen[7], G. A. DiBraccio[4], J.P. Eastwood[6], M.P. Freeman[8], M.K. Dougherty[6], M.F. Vogt[9,10]

Affiliations

1 Department of Physics and Astronomy, University College London, Gower Place, London, WC1E 6BT.

2 Centre for Planetary Sciences, UCL/Birkbeck, London, UK

3 Now at: University of Southampton, Southampton, SO17 1BJ, UK

[4]Department of Atmospheric, Oceanic and Space Sciences, University of Michigan, Ann Arbor, Michigan, USA

5 Department of Earth, Planetary and Space Sciences, University of California, Los Angeles, California, USA.

6 Imperial College London, London, UK

7 Planetary Science Institute, Tucson, AZ, USA

8 British Antarctic Survey, Cambridge, UK.

[9] University of Leicester, Leicester, UK

10 Now at: Boston University, Boston, USA.

Abstract:

We present a comprehensive study of the magnetic field and plasma signatures of reconnection events observed with the Cassini spacecraft during the tail orbits of 2006. We

examine their "local" properties in terms of magnetic field reconfiguration and changing plasma flows. We also describe the "global" impact of reconnection in terms of the contribution to mass loss, flux closure, and large scale tail structure. The signatures of 69 plasmoids, 17 travelling compression regions (TCRs), and 13 planetward-moving structures have been found. The direction of motion is inferred from the sign of the change in the B_θ component of the magnetic field in the first instance, and confirmed through plasma flow data where available. The plasmoids are interpreted as detached structures, observed by the spacecraft tailward of the reconnection site and the TCRs are interpreted as the effects of the draping and compression of lobe magnetic field lines around passing plasmoids. We focus on the analysis and interpretation of the tailward-moving (south-to-north field change) plasmoids and TCRs in this work, considering the planetward-moving signatures only from the point of view of understanding the reconnection x-line position and recurrence rates. We discuss the location spread of the observations, showing that where spacecraft coverage is symmetric about midnight, reconnection signatures are observed more frequently on the dawn flank than on the dusk flank. We show an example of a chain of two plasmoids and two TCRs over three hours, and suggest that such a scenario is associated with a single reconnection event ejecting multiple successive plasmoids. Plasma data reveal that one of these plasmoids contains H+ at lower energy and W+ at higher energy, consistent with an inner magnetospheric source, and the total flow speed inside the plasmoid is estimated with an upper limit of 170 km/s. We probe the interior structure of plasmoids and find that the vast majority of examples at Saturn show a localized decrease in field magnitude as the spacecraft passes through the structure. We take the trajectory of Cassini into account, as, during 2006, the spacecraft's largely equatorial position beneath the hinged current sheet meant that it rarely traversed the centre of plasmoids. We present an innovative method of optimizing the window size for minimum variance analysis (MVA) and apply this MVA across several plasmoids to explore their interior morphology in more detail, finding that Saturn's tail contains both loop-like and flux rope-like plasmoids. We estimate the mass lost downtail through reconnection and suggest that the apparent imbalance between mass input and observed plasmoid ejection may mean that alternative mass loss methods contribute to balancing Saturn's mass budget. We also estimate the rate of magnetic flux closure in the tail and find that, where open field line closure is active, it plays a very significant role in flux cycling at Saturn.

1. Introduction

Magnetic reconnection is a process by which stored energy can be explosively released and plasma trapped in separate magnetic domains can move from one region to the other and intermix. Magnetic reconnection can be sampled directly and indirectly by observing changes in the topology of the magnetic field near the reconnection site, and by observing the products of reconnection such as magnetotail plasmoids. The reconnection between the interplanetary and planetary magnetic fields at the dayside magnetopause results in the entry of some solar wind plasma, the escape of magnetospheric charged particles, and the transport of electromagnetic energy to the tail. Reconnection between the open magnetic field lines in the lobes of a magnetotail causes a reduction in the accumulation of open magnetic field flux [e.g. Dungey, 1961]. Reconnection can also occur between oppositely-directed closed magnetic field lines when they become strongly stretched. In that case, previously trapped plasma sheet material can be lost downtail into the solar wind [e.g. Vasyliunas, 1983]. Tail reconnection either of open or closed field lines drives sunward and anti-sunward flows which carry mass and energy toward the dayside magnetosphere and down the tail. The plasma escaping down the tail as a result of reconnection is on magnetic field lines forming either quasi-closed magnetic loops, or "islands", or helical magnetic fields called flux ropes [Schindler, 1974; Hughes and Sibeck, 1987; Slavin et al., 1989; Birn et al., 1989]. Collectively, the plasma and magnetic flux making up these magnetic loops and flux ropes are termed "plasmoids" [Hones, 1976; 1977]. If a spacecraft directly encounters such structures, the primary signature as measured by a magnetometer will take the form of a deflection in the north-south component of the field, usually followed by unipolar northward or southward magnetic field depending upon the location of the spacecraft relative to the flux rope or loop and the X-lines that created it (and also on whether the background planetary field is northward, as at Earth, or southward, as at Jupiter/Saturn) [Slavin et al., 2003a; Eastwood et al., 2005; Li et al., 2013]. The sense of the field deflection tells us which side of the reconnection x-line the spacecraft is on at the time of observation. Tailward-moving events at Saturn are expected to display a southward-to-northward turning of the field (opposite to the Earth due to the oppositely-directed planetary dipole). As we describe later, many plasmoids at Saturn have an azimuthal/corotational component to their motion in addition to purely radial tailward motion. Plasmoids have larger north-south dimensions than the surrounding plasma sheet where they form and this results in the lobe regions being compressed as the plasmoids move sunward or anti-sunward [Slavin et al., 1984]. These

93 "travelling compression regions" (TCRs) are readily observable in magnetic field
94 measurements on the basis of the correlated compression in the total magnetic field and the
95 north-south tilting of the draped magnetic field [Slavin et al., 1993].

96

97 There are two important sub-categories of plasmoid signature: flux ropes and loops. Loop-
98 like plasmoids may be thought of as lossless "magnetic bottles" that transport plasma sheet
99 plasma down the tail. In contrast, flux ropes are cylindrical magnetic structures of twisted
100 flux tubes with a strong axial magnetic field, peaking in the centre, which must connect either
101 to the lobes of the tail or, if the plasmoid extends across the entire plasma sheet, to the IMF in
102 the dawn and dusk magnetosheath. These sub-categories of plasmoid structure are important
103 because they provide clues as to the large-scale structure of the tail prior to reconnection [e.g.
104 Eastwood et al., in press, 2014]. For example, at Earth, strong links have been found between
105 the direction of the IMF B_Y component, large-scale shear in the terrestrial magnetotail, and
106 the formation of flux ropes there [e.g. Moldwin and Hughes, 1992]. In addition, plasmoids
107 with a helical flux rope structure lose much of the plasma sheet plasma as they move, with
108 large pitch-angle ions and electrons being lost first. The plasmoid magnetic field can only
109 relax toward its ultimate force-free configuration as the internal plasma is depleted and the
110 low-beta, strong axial magnetic field region grows [e.g. Hesse and Kivelson, 1998]. Early
111 studies at Earth [e.g. Sibeck et al., 1984; Moldwin and Hughes, 1992] noted that most
112 terrestrial plasmoids have a strong "core" field, characteristic of helical magnetic structures.
113 Later studies went on to successfully model them as "force-free" (i.e. $\mathbf{J}\times\mathbf{B}=0$) flux ropes,
114 which represent the minimum energy state of the field [e.g. Lepping et al., 1995]. This flux
115 rope core field has since been shown to possess up to twice the intensity of the field in the tail
116 lobes [Slavin et al., 1995; 2003b]. Flux ropes have also been found in the solar wind
117 [Moldwin et al, 1995], the ionosphere and induced magnetotail of Venus [Russell and Elphic,
118 1979], and the magnetotail of Mars [Eastwood et al., 2012]. Thus it would seem that flux
119 ropes are ubiquitous throughout the solar system. In Section 4 below we explore whether this
120 is also true of Saturn's magnetosphere.

121 Figure 1 shows a schematic representing the various magnetic field signatures that may arise
122 from spacecraft traversals through or near plasmoids. Briefly, if the plasmoid is flux rope-like
123 we would expect to see a strong increase in the total field strength as the spacecraft passes
124 through (or close to) the centre of the structure. Loop-like plasmoids on the other hand could

be identified by a decrease in the total field strength (which is zero in the exact centre of the circular loop-like plasmoid; i.e. it is an O-line). However we note a strong caveat to this picture, i.e. that the field signature observed is strongly dependent on the trajectory of the spacecraft through the structure [Slavin et al., 2003b; Borg et al. 2012], as shown in the figure. We discuss the implications of this in more detail later (figure 2). In addition to this, modeling of tail plasmoids by Kivelson and Khurana [1995] and observation of magnetopause flux transfer events by Zhang et al. [2010, 2012] indicated that it is possible for flux ropes to display a depressed field strength at their centre due to the presence of significant trapped hot plasma. We have not explored this possibility in this work due to a lack of continuous plasma data and/or multiple spacecraft passes.

The first *in situ* hint at reconnection in Saturn's magnetotail came on the outbound pass of Cassini's Saturn Orbit Insertion (SOI) manoeuvre in 2004. Bunce et al. [2005], analysing magnetic and plasma data, reported evidence of compression-induced tail reconnection accompanied by hot plasma injection. The magnetometer signature at this time was consistent with a dipolarization of the field. Following on from this event, the best chance to search for evidence of reconnection came in 2006 with Cassini's tail orbits season. Jackman et al. [2007] analyzed the magnetometer data for three events, and that work was quickly followed by a presentation of plasma and energetic particle data for two of those events by Hill et al. [2008]. The events, interpreted as plasmoid passage, were characterized by small southward followed by sharp northward turnings of the field, representing tailward-travelling structures, and estimates of the speed were of order ~800 km/s. The suggested location of the X-line, estimated from plasma velocity data and Energetic Neutral Atom (ENA) emission suggested to come from the reconnection site, was in the region of ~26.5 R_S (1 R_S = 60268 km), in line with previous estimates by Mitchell et al. [2005] who reported intense energetic neutral atom (ENA) fluxes emanating from this region. Later, Jackman et al. [2008a] added a further two events to the catalogue, and showed energetic particle information depicting a change of the plasma flow from the corotation direction to a tailward direction with the passage of a plasmoid. Such deflection of the plasma flow from azimuthal to radial was also reported by McAndrews et al. [2009] who showed ion velocity flow measurements from the Cassini plasma spectrometer.

More recently, Jackman et al. [2011] examined the role of plasmoids in flux transport in Saturn's magnetosphere. They found evidence of a significant post-plasmoid plasma sheet (PPPS), a region where open flux is being closed following the release of the plasmoid [Richardson et al., 1987]. They estimated that the average PPPS interval at Saturn closes up to ~3 GWb of flux. From auroral images it is estimated that Saturn's tail contains ~15-50 GWb of flux [e.g., Badman et al., 2005, 2013], and thus 3 GWb represents a significant fraction of this. While the calculation of the flux closed in the PPPS is sensitive to assumptions about the azimuthal extent of plasmoids, the estimates agree very well with the results of the global MHD simulation of Jia et al. [2012], who estimated 3.5 GWb of flux closure from a typical reconnection event at Saturn.

The aim of this paper is to provide a new comprehensive survey of reconnection signatures in Saturn's magnetotail, primarily from the perspective of the Cassini magnetometer data but with the addition of plasma data where appropriate. Since the first observation of a planetward-moving dipolarization [Bunce et al., 2005] and tailward-moving plasmoids [Jackman et al., 2007], many questions have arisen regarding the local properties of the reconnection region (such as magnetic field reconfiguration and plasma flow changes), and the global impact of reconnection in terms of its role as a flux closure and mass removal method. We show the statistics of the location of reconnection events, and describe the size and properties of plasmoids and TCRs. For the first time we probe the interior structure of plasmoids at Saturn to determine the nature of the magnetic fields inside them. We compare and contrast our observations with those in other planetary magnetotails and look to the future of exploration of Saturn's magnetotail. In Section 2 below we introduce the data set used in our study. Section 3 includes several case study examples of reconnection events, as well as superposed epoch analyses showing the average field profiles for reconnection signatures. Section 4 investigates the interior structure of plasmoids, Section 5 provides a general discussion, and Section 6 summarises our key results.

2. Dataset and observations:

As introduced above, reconnection events can be identified by changes in the north-south component of the magnetic field. We have surveyed the data from the Cassini magnetometer

187 [Dougherty et al., 2004] in Saturn's tail during 2006, the period where Cassini executed its
188 deepest orbits of the tail, providing us with some of the best chances to observe the products
189 of reconnection. The co-ordinate system used throughout this paper is the Kronocentric
190 Radial Theta Phi (KRTP) system, where the radial component (B_r) is positive outward from
191 Saturn, the theta component (B_θ) is positive southward, and the azimuthal component (B_φ) is
192 positive in the direction of planetary corotation. Jackman et al. [2009] discussed the merits of
193 this co-ordinate system in detail, particularly emphasizing how it can help to differentiate
194 between plasmoid passage and a wavy current sheet. This is a Saturn-centric co-ordinate
195 system, and Jackman and Arridge [2011] showed that the average B_θ component is small and
196 positive (southward) in the tail during 2006. We are seeking departures from this "steady-
197 state" behavior, and thus we began by defining a background for the B_θ component by taking
198 a running average of 1-minute resolution data over 1 day, similar to the method employed by
199 Vogt et al. [2010] for Jupiter. From this point, we selected a subset of events for further
200 examination, where the magnitude of the B_θ component was close to, or above background
201 levels and the spacecraft was beyond 15 R_S on the nightside. We then selected by eye those
202 events which exhibited clear, unambiguous field deflections. We additionally required that
203 the B_θ component cross through zero at some point during the event. The start and end of the
204 event were assigned as the local south/north extrema in B_θ. The sign of the change in B_θ
205 indicates whether the spacecraft was tailward or planetward of the reconnection x-line. As
206 mentioned in the introduction above, when looking for tailward-moving plasmoids or TCRs
207 we expect a southward-to-northward turning of the field, as evidenced by a positive-to-
208 negative change in B_θ and vice versa for planetward-moving events.

209

210 We used two key methods to differentiate plasmoids from TCRs. Firstly we inspected the
211 magnetic field components. Both plasmoids and TCRs yield a change in the B_θ component.
212 although the amplitude of this change (determined from the local extrema in the north-south
213 component around the central turning) is expected to be smaller for TCRs than plasmoids (as
214 illustrated in Figure 1). TCRs also display a very characteristic signature in terms of the total
215 field strength. As illustrated in Figure 1, the smooth tilting in **B** associated with the wrapping
216 of lobe field lines around passing plasmoids is the key feature which distinguishes TCRs
217 from plasmoids. Flux ropes also feature an increase in the field magnitude, but for a flux rope
218 this increase is very abrupt and is due primarily to the axial field, while the TCR signature is
219 more gradual and lacks a strong axial field. Secondly we took the spacecraft position into

account, to understand whether the spacecraft was in the lobes or plasma sheet when observing passing structures. Here the sign and magnitude of the radial field component can provide clues as to whether the spacecraft is close to the current sheet, or is farther out in the lobes. Additionally, we have supported our analysis with a detailed inspection of data from the Cassini Plasma Spectrometer (CAPS), Electron Spectrometer (ELS), and Ion Mass Spectrometer (IMS) instruments, where electron and ion populations in the lobes and plasma sheet show characteristic differences. If the spacecraft is deep in the lobes we expect to see TCRs rather than plasmoids.

Through our search we found a total of 69 south-north signatures which we interpret as tailward-moving plasmoids, 17 TCRs (15 tailward and 2 planetward) and 13 north-south signatures which we interpret as planetward-moving structures. The "tailward" and "planetward" motion is inferred from the sign of the change in B_θ. When the CAPS instrument look direction was favorable we also inspected the plasma flows, and indeed in the vast majority of plasmoid cases (29/35 for which a flow direction, if not a flow velocity, could be inferred) there was some tailward component to the flow. However, it was also common for a significant component of the flow to be in the corotation/azimuthal direction. Nonetheless, for simplicity, we refer to plasmoids with a south-north field signature as "tailward-moving" for the remainder of this paper. There was a single example (2006 day 261 04:01) where the field displayed a north-south-north turning and the plasma data indicate an inward flow. We have still classed this example as a plasmoid because the south-north turning of the field was dominant (as selected by our automated technique), but such an example warrants further study and may shed light on the existence of multiple reconnection sites in Saturn's tail which may yield such a combination of field and flow signatures. On average, the amplitude of plasmoids ranged from ~0.61 to 4.2 nT and the amplitude of the TCRs from ~0.12 to 2.22 nT. All 69 plasmoids had a value of B_θ that exceeded the background during the event, and 66/69 events had B_θ that exceeded 1.5 × the background. Because we placed minimum requirements on the field change associated with our events, it is possible that there are many smaller-amplitude events in the data that we have not included in our list. Thus our list represents a select set of robust events that may represent a lower limit on the occurrence rate of reconnection in Saturn's tail.

252 Plasmoid signatures can be somewhat more complicated than TCRs. Sophisticated modeling
253 [e.g. Slavin et al., 2003a] and multi-spacecraft data analysis at Earth [e.g. Borg et al., 2012,
254 Henderson et al., 2006] have revealed the complex topology of the tail post-reconnection, and
255 the sensitivity of magnetic field traces to the trajectory through plasmoids. Figure 2 illustrates
256 some example trajectories through model flux ropes and loop-like plasmoids, along with the
257 corresponding expected magnetic field signatures. While a bipolar south-north change in B_θ
258 (of varying amplitude) is common to nearly every encounter with a tailward-moving
259 plasmoid, the sense, magnitude and duration of the changes in the radial and azimuthal field
260 components and field magnitude are highly sensitive to the spacecraft trajectory through the
261 structures. The B_φ component in particular is significantly different for loops and flux ropes.

262

263 The date, time and properties of the plasmoids and TCRs are provided in Table 1. We have
264 listed the duration and peak-to-peak amplitude of all events. The duration is defined as the
265 interval between the local maximum positive (southward) and negative (northward)
266 excursions in the B_θ component. We note (see Figure 5c below) that the duration as defined
267 from the magnetic field signature can be shorter than the duration as inferred from the plasma
268 data), and according to the force-free flux rope model of Kivelson and Khurana [1995], our
269 definition may underestimate the plasmoid size by a factor of ~4-8. We note also that
270 occasionally the endpoints of the signatures can be uncertain due to either the presence of
271 multiple local maxima or minima in B_θ or very broad extrema that smoothly blend into the
272 background tail field. However, this method of defining the duration by the peak
273 northward/southward excursions gives a consistent and reproducible measure of these
274 structures, and has also been used in analysis of plasmoids at Jupiter [Vogt et al., 2014]. The
275 amplitude is the total peak – to – trough amplitude in the B_θ perturbation. Events were also
276 classified in terms of whether they were observed in isolation, or in pairs or groups, following
277 the classification employed by Slavin et al. [1993] (hereafter S93) for the terrestrial tail.
278 "Isolated" events were those observed to be separated from other events by at least 180
279 minutes. "Paired" events were defined as those separated by less than 180 minutes, while
280 "multiple" events were those in which several TCRs or plasmoids were observed without a
281 gap of more than 180 minutes between successive events. We note that this 180-minute
282 timescale is much longer than the analogous 30-minute timescale employed by S93. This
283 reflects the larger system size and inherently longer timescales for plasma circulation and
284 reconnection processes at Saturn compared to Earth. The vast majority of events were

observed in isolation. It is impossible to say with a single spacecraft whether most reconnection events result in the release of a single plasmoid, or whether they release many which may, for one reason or another, be missed by the spacecraft if they travel in relatively narrow channels downtail. We do, however, study the "paired" and "multiple" events with particular interest, such as the series of three plasmoids on day 64 that Jackman et al. [2011] analyzed, and the series of four closely-spaced events on day 60 described in section 3.1 below.

We incorporate both tailward and planetward-moving events in this section, as the full sample helps towards our understanding of reconnection recurrence. However, we focus only on tailward-moving plasmoids and TCRs for the subsequent sections. We leave the analysis and interpretation of events planetward of the x-line to future work as their properties and their ultimate fate as they travel toward the inner magnetosphere warrant a separate and much more detailed discussion.

The locations of all events superimposed on the Cassini trajectory during 2006 are shown in Figures 3a and 3b. As can be seen from Figure 3a, a view of the equatorial plane from the north, Cassini's trajectory over this interval was largely biased toward dawn, with the deepest tail passes occurring post-midnight. We note from Figure 3a that tailward-moving plasmoids are observed at all local times where there is spacecraft coverage. A striking point from figure 3a is that there is no clear division in radial distance between the tailward and planetward observations, other than to say that planetward-moving events are observed within ~50 R_S. By analogy with Earth, where a near-planet x-line might be ~30 R_E downtail [Imber et al., 2011], and a distant x-line might be ~100 R_E downtail [Slavin et al., 1985], we can scale this (based on average magnetopause standoff distances at Earth and Saturn of 10 R_E and 25 R_S respectively) to an expected near-planet x-line distance of ~75 R_S and expected distant x-line distance of ~250 R_S at Saturn. The latter estimate is far beyond the maximum downtail distance of 68 R_S reached by Cassini in 2006. We interpret all of the examples in this work as linked to reconnection processes local to a near-Saturn x-line, which we infer from our observations to be typically significantly closer to the planet than the scaled estimate of 75 R_S. Based on the work of Vogt et al. [2010] at Jupiter, for example, we might have expected with a large statistical sample, to see a clear separatrix between tailward-

317 moving and planetward-moving events. This in turn could indicate the average position of the
318 tail reconnection x-line. However, in our case, there is no such clear demarcation. This may
319 indicate that the reconnection x-line position at Saturn is highly sensitive to magnetospheric
320 conditions. For example, it could be strongly linked to the effect of solar wind compression
321 changing the size of the magnetospheric cavity. The recent modelling work of Jia et al.
322 [2012] indicates that the x-line can be present anywhere between ~25 and 40 R_S. Their model
323 indicated that, for cases when the Dungey cycle is active, reconnection occurs closest to the
324 planet under conditions of strong solar wind compression and further from the planet under
325 expanded magnetospheric conditions.

326

327 Figure 3b illustrates the latitudinal coverage of the spacecraft. The trajectory during 2006 was
328 such that most of the orbits at the start of the interval were in the equatorial plane toward the
329 dawn flank, with the spacecraft only reaching higher latitudes later in the year. The
330 observation of plasmoids and TCRs is highly latitude dependent. TCRs are observed at
331 latitudes ranging from -0.03° to + 0.44°, while plasmoids are observed at latitudes ranging
332 from -0.43° to + 15.2°. We must interpret this latitude spread in the context of the southern
333 hemisphere summer conditions during 2006, where low latitudes tended to correspond to
334 southern lobe, and higher positive latitudes corresponded to the nominal hinged current sheet
335 position (where plasmoids form). We note the strong bias toward plasmoid observation after
336 day 200 of 2006, when the Cassini orbits began to move out of the equatorial plane to higher
337 latitudes. No TCRs were observed beyond day 197 of 2006.

338

339 Knowing that reconnection observations are highly trajectory dependent, it is important to
340 understand not only the nature of the spacecraft trajectory, but also how the events are
341 distributed, such that we can search for specific occurrence trends. Figure 4a shows the
342 amount of the time that the spacecraft spent in different range and local time sectors, figure
343 4b shows the spread of events, and figure 4c shows the number of events normalized to the
344 exploration time. Figure 4a illustrates that most coverage was in the post-midnight sector
345 inside of 40 R_S, with reasonably concentrated coverage just pre-and post-midnight. This
346 figure again illustrates the disparity of observation between dusk and dawn. Figure 4b shows
347 the distribution of the events themselves. Grey bins indicate regions where Cassini flew
348 through without observing any reconnection events. A clustering of events is observed

around midnight in the 30-50 R_S range. There is another noteworthy active region between 40-50 R_S and 03-04 LT. Figure 4c allows us to join the information from Figures 4a and 4b. It shows the occurrence of reconnection events normalized by the time spent by the spacecraft in each spatial bin. This is key because it helps us to understand whether the distribution of our events is due to an observational bias, or to a genuine increased likelihood of reconnection in particular portions of Saturn's tail. Thick yellow lines surround the regions pre- and post-midnight where there has been relatively symmetric coverage by the Cassini spacecraft. Within these regions there is a significantly greater incidence of observation of reconnection post-midnight than pre-midnight; i.e., the likelihood of observing reconnection increases with localtime throughout this region. The implications of this are discussed in section 5 below.

3. Individual and averaged field signatures

3.1 Chain of plasmoids and TCRs: 2006 day 60 (March 1st)

Examples of isolated plasmoids and TCRs in Cassini magnetometer data have been shown in several papers as detailed in the introduction [e.g. Jackman et al., 2007, 2008a]. More recently a "chain" of three plasmoids was observed [Jackman et al., 2011] over three hours, and it was suggested that these were formed either as a result of episodic reconnection events closely spaced in time or simultaneous reconnection at multiple, closely spaced x-lines. In Figure 5a we now show another example of a "chain" of events. The interval is 2006 day 60 07:00-10:00, during which Cassini observed two plasmoids and two TCRs. The panels in Figure 5a displays the field in KRTP co-ordinates as defined above. This system allows us to clearly identify reconnection events, primarily through changes in the north-south (B_θ) component. In addition, the radial and azimuthal components can be used to elucidate the degree of corotation of the plasma (i.e. whether we are observing lagging or leading field lines).

The timings of the plasmoids and TCRs are marked in Figure 5a by vertical dashed lines. The duration of the events and their total ΔB_θ are listed in the top panel. As explained above, the duration is defined as the time between the local southward and northward extrema in the

379 B_θ component either side of the central field deflection. The first of the plasmoids at ~07:32
380 displays the largest field deflection of 2.16 nT. The duration of the signature based on the
381 southward and northward field extrema is ~5 minutes, but we note the extended interval of
382 northward field after the plasmoid passage. The plasma data for this signature are presented
383 in Figure 5c and discussed below. The next plasmoid signature is much smaller, with only a
384 0.94 nT deflection but again the same sense of northward turning of the field. Following on
385 from this, there are two TCRs within 45 minutes of one another, evidenced by the northward
386 turnings of the field and the small localised compressions in the field magnitude. The second
387 TCR has a very small amplitude change in B_θ (0.12 nT), but does display the smooth tilting
388 of the magnetic field characteristic of TCRs. The first plasmoid is seen by the spacecraft at a
389 radial distance of 32.33 R_S, and from inspection of the sign of the field change, we infer that
390 Cassini was tailward of its source, observing the structure propagate down the tail. The same
391 holds for the other three events. We suggest that all of these observations are linked to a
392 common reconnection episode which produced multiple plasmoids.

393

394 With a single spacecraft we are unable to separate temporal from spatial effects, but we can
395 suggest two plausible scenarios which could result in this multi-event observation. In the first
396 scenario, the reconnection episode results in the release of four plasmoids, whose effects are
397 observed sequentially as illustrated in Figure 5b (similar to a terrestrial morphology
398 suggested by Slavin et al. [1993; 2005]). In this case, Cassini (which was sampling the tail at
399 approximately constant latitude during this interval) penetrated relatively deep into the centre
400 of the first, largest plasmoid (decrease in |B| to ~1.4 nT, where |B|=0 would represent the
401 centre of a perfectly loop-like plasmoid). We then suggest that the second plasmoid was
402 smaller, and so the spacecraft only caught the edge of it. This interpretation is borne out by
403 the smaller northward turning and the smaller decrease in |B|. The vertical extent of the third
404 and fourth plasmoids was such that they did not encompass the spacecraft track at all. Rather
405 we suggest that Cassini passed through the compressed lobe field lines draped around the
406 passing plasmoid structures, and observed TCR signatures of decreasing amplitude. Again,
407 this tendency for the amplitude of TCRs, and by implication the north-south extent of
408 plasmoids, to decrease from one TCR to the next in "chain" events is frequently observed at
409 Earth [Slavin et al., 1984; 1993; 2005]. A second plausible scenario also involves the
410 ejections of four plasmoids from a common reconnection episode. However, in this picture
411 the plasmoids may have all been of similar size. A slow flapping of Saturn's tail current sheet

over the spacecraft (which was at constant latitude) could result in Cassini slowly moving north/south relative to the current sheet. Flapping of Saturn's current sheet is a well documented phenomenon [e.g. Arridge et al., 2011; Provan et al., 2012; Volwerk et al., 2013]. The flapping timescale is of order ~10 hours, and thus the 3 hours shown in this plot could represent just the southward motion portion of the flapping. This idea is supported by the radial field component which displays an increasing magnitude throughout the interval, indicating that Cassini could have been moving further away from the current sheet centre. For this case of a slowly moving current sheet, Cassini could hence have crossed near the middle of the first plasmoid, and the edge of the second. As the spacecraft moved further relative to the current sheet, it then observed a TCR, and finally a weak TCR from its position in the southern lobe. The positions of the spacecraft in the plasma sheet/lobes are confirmed by inspection of the plasma data below.

Figure 5c shows measurements from the CAPS instruments for the same interval as Figure 5a. The center panels are the energy-time spectrograms for the ions (above) and electrons (below) observed by the CAPS IMS and ELS, respectively. The data for the first plasmoid confirm that Cassini was inside the first plasmoid structure from ~07:20 to ~07:40, longer than the ~5 minute duration inferred from the southward/northward field extrema above. This inference is based on the duration of the diamagnetic field signature, and the presence of relatively cool dense plasma (including ions with a clear water group signature). The double-peaked ion distribution is characteristic of plasma of inner magnetospheric origin (H+ at low energy, W+ at higher energy). We note that the field remains northward for some time after this interval, during the post-plasmoid plasma sheet interval (as discussed in Jackman et al. [2011]). The three panels above the spectrograms are all-sky images of the ion distribution at 2.4 keV (first two) and 4.1 keV (third). During the first plasmoid event the peak counts are observed near the corotation direction (black triangle) but displaced towards the look direction to Saturn, indicating an outward flow component. The energy of the ions suggests that the total flow speed is ~170 km/s. Based on the angular offset of the peak from the corotation triangle in the all-sky images, we suggest that the radial component of the flow is of the order ~90 km s^{-1}. The plasma data for the second plasmoid support the suggestion that Cassini traversed the edge of this structure (due to the presence of hot magnetospheric electrons near 100 eV) and that the two identified TCRs were in fact observed while the

spacecraft was in the lobe (due to the absence of magnetospheric electrons and the higher spacecraft potential).

3.2 Superposed epoch analysis of tailward-propagating plasmoids and TCRs:

Figures 6a and 6b depict the results of superposed epoch analyses for 69 tailward-moving plasmoids and 15 tailward-moving TCRs (separately), where the zero epoch is the central event time, defined as the point where B_θ changes sign. Jackman et al. [2011] showed a superposed epoch analysis of 34 tailward-moving plasmoids, where they discussed the results in terms of the flux transport through the post-plasmoid plasma sheet. Since then, as discussed in section 2 above, we have re-surveyed the Cassini magnetometer data from 2006 and uncovered more plasmoid examples, more than doubling the list from 34 to 69. Thus Figure 6a is an updated superposed epoch analysis. The basic characteristics of the signature are the same, with slightly amended amplitude and duration. From Figure 6a, we see that the field signature of an average tailward-moving kronian plasmoid is a distinct northward turning of the field. Some individual examples display a southward turning prior to the strong northward turning, but once averaged into the superposed epoch analysis it becomes somewhat smeared out. However, the northward turning persists. The mean plasmoid duration taken from the full set of examples listed in Table 1 is 17.71 minutes (with a standard deviation also of 17.7 minutes, implying a skewed distribution with a long tail), which represents the average duration between the local southward and northward extrema. In the absence of continuous plasma data (such as that in figure 5c which could shed light on longer intervals of plasma energization and local tail disturbance), we interpret the interval between the southward and northward extrema as the passage of the plasmoid itself. For the case of the smeared B_θ signature from the superposed epoch analysis, we have marked the "start" of the event at T=-5 minutes despite the lack of a clear southward extremum in the trace. We obtain this start time by tracking the field fluctuations preceding the event. The B_θ component decreases slightly at T=-6 minutes, before increasing to reach a local southward maximum at T=-5 minutes, beyond which it steadily decreases and then turns northward. We note, however, that this local southward maximum is barely discernible above the statistical field fluctuations. This time can be compared to the mean start time (as determined from the local southward field extremum) based on 69 individual events, which is T=-9.2 minutes. The

476 "end" of the event is marked as T=+3 min (the clear northward extremum). This 8-minute
477 duration is considerably shorter than the 17.71 mean duration obtained from the distribution
478 of events, and is the effect of the smearing due to the superposed epoch analysis. Similarly
479 the mean ΔB_θ event amplitude from the event list is 1.39 nT (with a standard deviation of
480 0.73 nT), while the amplitude of the field change from T=-5 to T=+3 minutes is ~0.75 nT).
481 Following the northward extremum (at T=+3 min), there is an interval ~27 minutes long,
482 where the B_θ component remains northward. We interpret this as representing an interval of
483 closure of previously open flux, analogous to the terrestrial PPPS. We note that there is
484 another possibility that such asymmetry may be due to slowing of the flow as the plasmoid
485 moves downtail, such as in cases where plasmoids associated with the Vasyliunas cycle are
486 blocked from moving downtail by surrounding closed field lines. However, we are not in a
487 position to test this alternative explanation of the extended northward field because the
488 plasma measurements available for the subset of our events simply yield a single bulk flow
489 speed for each event rather than a detailed time series of velocity variations throughout the
490 interval of field change. Exploration of this hypothesis for a small number of case studies,
491 particularly those on the dusk side where Vasyliunas-style reconnection may be more likely,
492 should be the subject of future work. For the purposes of this paper we take the extended
493 interval of northward field following the plasmoid to be representative of the PPPS and flux
494 closure, a scenario which is consistent with auroral observations of flux opening and closing
495 in Saturn's magnetosphere [Badman et al., 2005; 2013] and modeling of reconnection and
496 flux closure [e.g. Jia et al., 2012], and we note that by making this assumption we are taking
497 an upper bound on flux closure for our events. While the average background B_θ at Saturn
498 has been shown to be small and positive by Jackman and Arridge [2011], we define the end
499 of the PPPS as the point where B_θ crosses zero to return from negative to positive for
500 consistency. This point is marked on Figure 6a by a vertical dot-dashed line. We note that this
501 27 minutes is shorter than the ~58-minute PPPS reported by Jackman et al. [2011]. The
502 primary reason for this is that several of the new events added to the list display bipolar
503 signatures which are more symmetric, without the extended PPPS interval of northward field
504 after plasmoid passage. We discuss the implications of these signatures in terms of
505 reconnection on open/closed magnetic field lines further in Section 5.2.

506

507 The fact that the average southward-to-northward turning associated with plasma passage is
508 strongly asymmetric hints at the geometry of the typical pass through a plasmoid, as raised

initially in Section 2 above. Due to the hinged nature of the current sheet during southern hemisphere summer, a spacecraft orbiting in the equatorial plane (as Cassini did for much of 2006) will be situated in the southern lobe, and any encounters with plasmoids will be cuts through the lower portion rather than traversals of the central part of the structures. However, we note, as illustrated in Figure 2, that a spacecraft travelling parallel to the plasmoid edge can still record a symmetric signature, even if it doesn't penetrate through to the centre. The asymmetry arises from the spacecraft encountering the plasmoid at an angle. At the time of the field deflection shown here, there is a small local dip in |B| implying a simple loop-like as opposed to flux rope-like interior structure. However, this is highly sensitive to the spacecraft trajectory through the structures, and a more detailed exploration of the interior morphology of plasmoids will be presented in Section 4 below.

The average absolute value of the radial field component during plasmoid encounters is ~1.2 nT, with an average of ~1.5 nT either side. This shows that the spacecraft did not, on average, encounter plasmoids at the very centre of the current sheet (where $B_R \approx 0$) but rather at some distance away in the outer plasma sheet or lobe, as we understand from the description of the trajectory above. While the magnitude of the radial component (as a function of total field strength) cannot be used as a direct measure for vertical distance from the current sheet centre, it can act as a proxy. For example, if a Harris-sheet type geometry is assumed for the plasma sheet, then fitting of the observed magnetic field to such an assumed structure can yield an estimate of distance from the center of the plasma sheet [e.g. Runov et al., 2006; Arridge et al., 2008b; Jackman and Arridge, 2011]. Because the magnetic field data indicate penetration of the spacecraft into a plasmoid structure, we know that in these examples, a spacecraft sampling a radial field component of magnitude ~1.2-1.5 nT cannot be more than one plasmoid half-width from the centre of the current sheet. As mentioned in section 2 above, events are identified by taking into account not just the B_θ component but the behavior of other components as well. Cassini can pass through the interior of plasmoids from a position in the outer plasma sheet but also from a position in the lobes, if the plasmoids are large enough to extend a significant distance from their formation point at the current sheet centre. The azimuthal component of the field is virtually constant around the time of plasmoid passage, consistent with a loop-like picture as opposed to a flux rope-type structure as mentioned above but this will be explored in more detail in section 4.

We can use the range of observed plasmoid durations, along with the range of observed plasmoid velocities to calculate a range of approximate plasmoid lengths (as done by Kronberg et al. [2008] for Jupiter and S93 for Earth). The first estimate of the velocity of a plasmoid in Saturn's tail from in situ CAPS data was presented by Hill et al. [2008], who reported a value of 800 km/s. Here we significantly expanded the list of events for which we can extract velocity information. From Table 1 we present a set of velocities for 29 plasmoids, ranging from 144 - 1240 km/s, with a mean of 299.8 km/s and a standard deviation of 215.5 km/s. These estimates are obtained from the energy of the peak counts and thus represent upper limits. The case study example in Figure 5c (with a total bulk velocity of 170 km/s) is at the lower end of this velocity range. We can combine this range of velocities for 29 events with the range of plasmoid durations listed in Table 1 (2 minutes to 50 minutes for the subset of 29 events for which plasma data were available). The length of each of these 29 plasmoids has been calculated individually (duration × velocity), and is found to range from 0.44 - 23.9 R_S. The mean plasmoid length is 4.28 R_S with a standard deviation of 5.6 R_S. Figure 7 shows histograms of flow velocity, duration, length and mass for these 29 plasmoids which have both magnetometer and plasma data.

There may be a number of errors in the determination of these plasmoid lengths. Firstly, we note, as mentioned above, that our definition of plasmoid duration as the time between southward and northward extrema may result in an underestimate of plasmoid size by a factor of ~4-8 [Kivelson and Khurana, 1995]. In addition, the duration estimates are based on trajectories which, as discussed earlier, do not necessarily represent the full diameter of the plasmoids. Unless the observing spacecraft passes through the center of the plasmoid along a trajectory that is normal to the long axis of the structure, the effective length of the plasmoid may be significantly under- or over-estimated. There are also errors associated with the velocity measurements. The velocities used to determine the plasmoid "lengths" are the bulk flow velocities, and from the subset of examples where CAPS pointing was favorable we know that in addition to the radial (downtail) component of the velocity there can also be a significant azimuthal motion. Hence the bulk flow velocity is an upper limit. We may compare our estimates of plasmoid length derived here with the output of global models which suggest that plasmoids may be up to 30-40 R_S long [e.g. Jia et al., 2012; Kidder et al.,

573 2012]. Such estimates are higher than our quoted range, but we note that the model estimates
574 consider the full plasmoid and not just a cut through a section, as may be the case for our
575 examples.

576

577 In addition to our estimates of plasmoid length, we can use velocity measurements to
578 estimate the size of the reconnecting region, and in turn estimate the flux closed through
579 reconnection. As mentioned above, the superposed epoch analysis shows a distinct ~27
580 minutes after plasmoid passage where the field remains northward, analogous to the
581 terrestrial PPPS. Jackman et al. [2011] calculated the amount of flux closed during a ~58-
582 minute PPPS as obtained from the superposed epoch analysis of 34 events. They assumed a
583 velocity of 800 km/s [Hill et al., 2008] and took an upper limit of the full tail width (90 R_S)
584 for the azimuthal extent. From this they calculated a flux closure of ~3 GWb per event.

585 We now have an extended sample of events which yield a ~27-minute PPPS, the length of
586 which is also subject the same kind of assumptions made above regarding the orientation of
587 the plasmoid motion relative to the spacecraft. We also have additional in situ data which
588 allows us to make flux estimates based on a range of velocities. Like Jackman et al. [2011],
589 we use the full tail width of ~90 R_S as the azimuthal extent of the plasmoid for our
590 calculation, emphasizing that this 90 R_S value is an upper limit. In reality we expect that the
591 typical width of reconnection-associated flow channels in the tail is much smaller than this,
592 because if plasmoids took up the full width of the tail, Cassini would observe every one as
593 long as its position was tailward of the reconnection site. Based on speeds of 144-1240 km/s,
594 we estimate that 0.26 – 2.2 GWb of flux is closed during the 27-minute PPPS.

595

596 The TCR superposed epoch analysis for 15 tailward-moving events, shown in Figure 6b,
597 shows the localized compression associated with the wrapping of field lines around the
598 passing plasmoid(s). This smooth increase in the total field strength is also mirrored by a
599 smooth increase in the radial field component, peaking at the centre of the TCR. The average
600 amplitude of the southward-to-northward turning from the list of 15 events is ~0.66 nT (with
601 a standard deviation of 0.54, reflecting the wide spread in amplitude of TCR signatures). This
602 amplitude is slightly smaller than for the plasmoid encounters as might be expected
603 (particularly considering that our selection criteria did not require the B_θ component during

TCRs to fluctuate above background levels). The average TCR signature at Saturn displays a mean change in |B| of ~18%. This is compared to typical compression ratios of 1-10% at Earth [Slavin et al., 1993; Slavin et al. 2005]. Thus, this is evidence that plasmoids at Saturn are large enough to significantly distort the magnetotail field lines in their vicinity and could imply that plasmoids at Saturn occupy a larger vertical portion of the magnetotail than plasmoids at Earth, although this cannot be confirmed with a single spacecraft. In some cases at Earth, it is suggested that waves initiated at the centre of the plasma sheet during reconnection can travel through the lobes all the way to the magnetopause, communicating field disturbances such that the magnetopause may even exhibit a corresponding bulge, however this behavior is still not fully understood [Slavin et al., 1993]. The average duration of the 15 observed TCRs, as defined by the time between local maxima/minima in B_θ either side of the central field deflection, and as calculated from the list in Table 1, is 14.4 minutes (with a standard deviation of 9.35 minutes). As with the plasmoid superposed epoch analysis, the TCR superposed epoch trace becomes somewhat smeared out, and thus its amplitude and duration (~0.43 nT from T=-3 to T=+7 minutes) are considerably smaller than those calculated directly from the distribution. However, on inspection of the field magnitude trace, it is clear that |B| undergoes a smooth compression from background levels over a much longer interval, of order ~35 minutes either side of the central epoch time, 70 minutes in total, as bracketed by the vertical dot-dashed lines in the bottom panel.

4. Morphology of reconnection region:

While reconnection undoubtedly has dramatic effects on the local structure of the field lines in the vicinity, it can also affect the global morphology of the magnetotail. As discussed in section 3.2 above, the passage of large plasmoids down tail can cause the surrounding lobe field lines to bend significantly as they wrap around the bulging plasma sheet. In the introduction we mentioned that plasmoids may have loop-like or flux rope-like interior structure, and these structures have implications for the structure of the magnetotail as a whole, perhaps elucidating the degree of shear within the tail prior to reconnection. In this section we examine the Cassini magnetic field data in detail to decipher the nature of the field geometry in Saturn's tail when reconnection is ongoing.

In order to precisely visualize the geometry of the reconnection region, we apply minimum variance analysis (MVA) to several events [Sonnerup and Cahill, 1967]. Transforming the magnetic field data into this co-ordinate system allows us to visualize the orientation of the structures and the location of their central axis. When MVA is performed on a magnetic field dataset, it returns three eigenvectors (corresponding to the minimum, intermediate, and maximum variance directions) and their associated eigenvalues. The direction which corresponds to the axis of the structure depends on the type of structure and on the depth of crossing (known as the impact parameter). For a crossing close to the centre of a cylindrically symmetric force-free flux rope, the intermediate direction is the direction of the axis [e.g. Lundquist, 1950, Lepping et al., 1990]. The perfectly force-free flux rope is a special case, representing the minimum energy state of a structure. At the centre the field is purely axial, and this field weakens with increasing distance from the centre. In practice, many magnetotail plasmoids take the form of non force-free flux ropes, which also have a helical topology but have not yet evolved to a force-free configuration. In this case the structure has a core field (such as those studied at Venus by Russell [1990] and Elphic and Russell [1983]), and the axis may be oriented with the intermediate or maximum directions. A third class of structure is loop-like plasmoids. In reality, it might be difficult to expect perfect loops to form in three dimensional space as this requires perfect alignment of oppositely directed magnetic field lines [e.g. Slavin et al., 2003a]. However, quasi-loop-like structures should be distinctive in terms of having their axes aligned along the minimum variance direction [Farrugia et al., 1987; Elphic and Southwood, 1987]. Clearly, determination of the orientation of the axis of plasmoids is key to the study of their geometry, structure, and their possible formation process.

The interval over which the MVA is performed is crucial to the success of the analysis. A first criterion for a good MVA interval is that it encompasses the largest field change associated with the passage of the plasmoid, TCR or dipolarization. Secondly, a large eigenvalue ratio gives confidence in the transformation. Previous studies have indicated that the ratio of intermediate to minimum eigenvalue should be at least ~8-10 for the analysis to be acceptable [e.g. Paschmann and Daly, 1998; Briggs et al., 2011]. The largest eigenvalue ratios tend to result from the selection of intervals which bracket the turning points of bipolar

magnetic field signatures, thus encompassing the greatest change of magnetic field strength and direction.

4.1 MVA window optimization technique:

Throughout this work we have sought to remove observer biases as much as possible. For example, the selection of an appropriate MVA window is most often done "by eye", and while this may be satisfactory for most cases, we desired to try an automated method to select the interval over which the field changes most significantly, and to then apply the MVA to this interval. This "MVA window optimization" technique is illustrated in Figure 8.

The top panel shows the field in KRTP co-ordinates, colour-coded according to the legend on the right. The feature of interest is a plasmoid at 16:47:30, identified by the strong northward turning of the field (negative B_θ in red). MVA was applied to this field data over a sliding window, with start times marked by the vertical dotted lines. The start times and window sizes are plotted on the axes of the lower three panels, which are colour coded to show the eigenvalue ratios for each MVA start time and window size. Darker colours represent lower eigenvalue ratios, as per the colour bars on the right of each of the lower three panels. The striking feature of this plot is that the eigenvalue ratios corresponding to start times and window sizes away from the main plasmoid observation are low. Meanwhile, the eigenvalue ratios increase significantly in the vicinity of the northward turning. Indeed there is a bank of high eigenvalue ratio intervals surrounding the main northward turning. This gives us confidence that selecting an MVA interval in this region will return sufficiently high eigenvalue ratios such that we can be satisfied that the analysis interval encompasses the most significant field change. While the maximum eigenvalue ratio is not a perfect marker of where the MVA should be applied, it acts as strong guide. We note that the three eigenvalue ratios rarely maximize in precisely the same windows. Nonetheless, the plot indicates that the eigenvalues maximize in broad regions surrounding the field change of interest. This technique then gives us confidence to apply MVA over the window bracketing the south-north extrema in B_θ either side of the primary field deflection. We also recognize that changing the MVA window size may alter the orientation of the axis that we obtain from our analysis. Thus MVA has been tested over several window sizes within this central high eigenvalue ratio region to ensure stability of the orientation.

699

700 4.2 MVA examples

701 For all three subsequent examples we use the optimization technique outlined above to guide
702 our choice of MVA analysis window. The eigenvectors and eigenvalue ratios are listed in
703 Table 2 below.

Eigenvectors	B1 (min)	B2 (int)	B3 (max)	L2/L1	L3/L2
Day 216 Plasmoid 16:47:30	(0.99, 0.08, 0.02)	(0.07, -0.70, -0.71)	(0.05, -0.71, 0.70)	6.53	42.9
Day 63 Plasmoid, 22:07	(-0.89, -0.15, -0.44),	(0.35, 0.39, -0.85)	(-0.30, 0.91, 0.29)	9.26	15.6
Day 63 Plasmoid, 22:59:30	(0.77, -0.27, -0.58)	(-0.61, -0.05, -0.80)	(-0.18, -0.96, 0.19)	44.7	37.0

704 *Table 2: List of eigenvectors and eigenvalue ratios for all MVA intervals described in Section*
705 *4.2*

706

707 4.2.1 MVA example 1: Day 216 (August 4th) Plasmoid 16:47:30

708 Figures 9a and 9b show the results of the application of MVA over a window surrounding the
709 plasmoid on day 216 at 16:47:30. Vertical dashed lines on the top panel of figure 9a bracket
710 the interval on which the MVA was performed. The lower three panels show the magnetic
711 field data transformed into MVA co-ordinates and plotted over the selected interval (less than
712 two minutes long). B1 is the direction of minimum variance, and B2 and B3 refer to the
713 intermediate and maximum variance directions. The spacecraft was 49 R_S downtail and just
714 pre-midnight at 23:41 LT. This event was reported first by Jackman et al. [2007], while
715 Jackman et al. [2008a] showed that the large-scale magnetospheric plasma flow rotated from
716 sub-corotation to tailward with the passage of this plasmoid. Plasma data from CAPS IMS
717 (not shown) indicate the presence of outward-moving W+ ions during the passage of this
718 plasmoid. The field signature is certainly dramatic, with a total field deflection of 3.39 nT.
719 The total field strength rises sharply coincident with plasmoid passage, and this has been
720 interpreted as pile up of newly-closed field lines behind the plasmoid after reconnection,
721 accelerating it downtail. The field in the direction of minimum variance (B1) is near-zero,
722 while the intermediate variance trace (B2) is unipolar. The dominant northward turning of the
723 field associated with plasmoid passage is reflected in the maximum variance direction, which

displays a dramatic bipolar signature. The eigenvectors are (0.996, 0.084, 0.018), (0.072, -0.697, -0.714), (0.047, -0.712, 0.700), indicating that the direction of minimum variance is strongly radial, the intermediate variance direction is split between northward and corotational, and the maximum variance direction is split between northward and corotational. Figure 9b shows hodograms of the field variations in three planes, with most variation in the intermediate-maximum plane. The near-constant, non-zero minimum and intermediate fields combined with the predominantly positive maximum variance argue for Cassini having just passed though the outer portion of this plasmoid along a trajectory that began in the south, but quickly passed into the northern half of the plasmoid (e.g., see trajectory path #4 in figure 2). No flux rope-line core field was observed, but it cannot be determined whether this is due to the plasmoid being loop-like or the off-axis trajectory.

4.2.2. MVA example 2: Day 63 (March 4th) Plasmoid, 22:07

Figure 10 shows the results of MVA on an interval surrounding a tailward-moving plasmoid at 22:07 on day 63 of 2006. At this time the spacecraft was 44.17 R_S downtail and at a local time of 03:10. The plasmoid is identified by the deflection in the B_θ component northward, with an amplitude of 1.7 nT. The more balanced north-south magnetic field variation shows that the spacecraft passed much closer to the center of this plasmoid than the previous event. Once again, B1 is approximately constant near zero and directed largely in the radial direction consistent with a pass not far off the center of the plasmoid. B2 is mostly azimuthal and unipolar, but it does not display any enhancement near the inflection point in the north-south field as would be expected if there were a flux rope-type core field. B3 is closely aligned with the north-south direction and shows a bipolar signature. The eigenvectors are: (-0.887, -0.151, -0.436), (0.350, 0.395, -0.849), (-0.300, 0.906, 0.298), indicating that the direction of minimum variance is primarily radial, the intermediate variance direction is in the corotation direction, and the maximum variance direction is north-south. We suggest that this example could represent a passage through a loop-like plasmoid, along a trajectory similar to path #2 in Figure 2, although closer to the center of the structure than the encounter in MVA Example 1 on day 216. Figure 10b shows hodograms of the field variations in three planes. The B2-B3 hodogram shows a relatively smooth tilting of the field consistent with a loop-like plasmoid. This can be compared to an example of a rare, but well-defined magnetic loop plasmoid at Earth reported by Slavin et al., [1989].

757

758 4.2.3 MVA Example 3: Day 63 (March 4th) Plasmoid, 22:59:30

759 Figure 11a shows high resolution Cassini magnetometer data surrounding a plasmoid
760 observation at 22:59:30 on day 63 of 2006. At this time the spacecraft was 44.17 R_S downtail
761 and at a local time of 03:11, virtually the same location as for the previous example less than
762 an hour before, although in this example the magnitude of the B_R component is somewhat
763 smaller indicating that the spacecraft was situated closer to the current sheet center. The
764 plasmoid is identified by the sharp northward turning of the field of amplitude 3.51 nT, and
765 the balance between northward and southward magnetic field. It is followed by an extended
766 interval of northward field, which we interpret as analogous to a post-plasmoid plasma sheet
767 as at Earth. The field change associated with the plasmoid passage is very rapid, and the
768 MVA is performed over an interval <50 seconds long, using the highest resolution
769 magnetometer data available. The eigenvectors are: (0.772, -0.264, -0.578), (-0.608, -0.045, -
770 0.792), (-0.183, -0.963, 0.195). The field in MVA co-ordinates shows the clear signature of a
771 plasmoid with flux rope topology. The constant, near-zero B1 (min) directed along the radial
772 direction is consistent with a very low inclination spacecraft trajectory passing through the
773 center of the plasmoid similar to the green traces (trajectory path #1) in Fig. 2. The B2 (int)
774 component is unipolar, peaked around the center of the bipolar north-south field variation,
775 and oriented in the azimuthal direction consistent with a cross-tail oriented flux rope (e.g.
776 bottom panel Fig 2; Slavin et al., 2003a; Borg et al., 2012) with the core in the B2
777 (intermediate) direction. The B3 (max) direction is largely in the north-south theta direction
778 and displays the expected clear bipolar trace. The B2-B3 hodogram shows exceptionally
779 smooth rotation indicative of the core magnetic field of a flux rope-type plasmoid.

780

781

782 ## 5. Discussion

783 In this paper we have presented a set of reconnection events observed during Cassini's
784 exploration of Saturn's deep tail during 2006. We now discuss the results by placing them in
785 the framework of several common questions about the nature of reconnection in Saturn's tail.

786

787 5.1 What is the primary mass loss mechanism at Saturn?

In this study we have revealed 69 south-to-north plasmoids tailward of the x-line, 17 TCRs (15 tailward and 2 planetward) and 13 north-to-south events planetward of the x-line, which represent the largest and most significant reconnection signatures from our detailed survey of the 2006 Cassini magnetometer data. The question remains, however, as to whether there are mechanisms other than large-scale reconnection which may allow material to be lost down the magnetotail. For instance, Zieger et al. [2010] suggested on the basis of their modelling work that large-scale plasmoids account for less than 8% of the total mass lost down the tail. Bagenal and Delamere [2011] estimated the average mass of plasmoids at Saturn and compared this to the suggested mass loading rates from the moon Enceladus of 8-250 kg/s [e.g. Fleshman et al., 2010; Jurac and Richardson, 2005; Pontius and Hill, 2009; Chen et al., 2010]. They assumed a plasmoid of volume $(10\ R_S)^3$ with a density of 0.01 cm^{-3} of 18 amu ions. From this, they calculate that plasmoids would need to be ejected at a rate of 200 per day to remove just 100 kg s^{-1}.

We are now in a position to refine the estimates of the plasmoid mass loss rate. We base our calculations on the 29/69 plasmoids which have corresponding plasma data. We calculated the length for each plasmoid as duration × velocity, and obtained a range of 0.44 – 23.9 R_S. We note that these observed speeds sit between the estimates of average Alfvén speeds in Saturn's central plasma sheet (1-10 km/s) and lobes (>4000 km/s) as reported by Arridge et al. [2009]. They also agree reasonably well with analogy from Earth, where plasmoids have been observed to move tailward with speeds typically 1-3 times that of the solar wind [Baker et al., 1987; Richardson et al., 1987; Ieda et al., 1998; Slavin et al., 2003a]. If we average all of the plasmoid lengths obtained in this way we find a mean of 4.28 R_S (whereas if we multiply the mean duration of 13.5 minutes by the mean velocity of 299.8 km/s, we obtain a mean plasmoid length of 4.03 R_S). We take a thickness of 2 R_S, to represent the plasma sheet half-thickness (for a full plasma sheet width of 4 Rs [e.g. *Kellett et al.*, 2009; *Sergis et al.*, 2011; *Arridge et al.*, 2011; Szego et al., 2012]), and we take an upper limit for the azimuthal extent as the full tail width (90 R_S). Because this estimate is intended to represent an upper limit, instead of assuming the same density as Bagenal and Delamere [2011] (0.01 cm^{-3} of 18 amu ions), we take the upper limit from Thomsen et al. [in press, 2014], of 0.1 cm^{-3} of 16 amu ions. We thus calculate a range of plasmoid masses from 4.42×10^4 – 241.0×10^4 kg, with a mean of 43.2×10^4 kg. We would require ~3.6 - 196 tail-width plasmoids per day to remove 100 kg s^{-1} of added mass. In order to estimate the total mass loss for the 99

reconnection events that we observe, we multiply the mean plasmoid mass of 43.2×10^4 kg by 99 events. Our events were observed between days 32 - 264 of 2006. If we calculate how much time the spacecraft spent beyond 20 R_S on the nightside during this interval (to give an approximate likely "viewing region" for downtail mass loss) and express the total mass loss as a fraction of time, we find an average mass loss rate over our observation interval of 2.59 kg/s.

There are several "active" intervals during 2006 where multiple plasmoids and TCRs are clustered together, such as: Days 60-67 inclusive (18 events); Days 193-197 inclusive (13 events); Days 212-219 inclusive (15 events). Indeed, there are 6 events on day 212 alone (~23:00 hours local time, and between 43-45 R_S). Thus it appears that during the most active intervals, the observed rate of mass loss can just about match the lower end of the requirement for removal of 100 kg/s of mass (and easily match the requirement for a lower mass source rate of 8 kg/s). However, there is a huge range on the mass removal requirements, and during less active intervals there is a clear mismatch between the suggested loading rates and observed average removal rates. Thus, it is plausible that during "active" intervals, plasmoid ejection at Saturn is the primary mass loss mechanism. However, we need to explain the significant mismatch in mass addition and loss rates during the more typical, less active intervals. There may be several reasons for this mismatch. Firstly we may only be observing a small fraction of the number of plasmoids that are released in Saturn's tail. We may be missing examples due to spacecraft trajectory out of the plane of the plasma sheet. Similarly we may miss a large number of plasmoids released via the Vasyliunas cycle [Vasyliunas, 1983] down the dusk flank (if, as stated in Section 3.2 above, the real azimuthal extent of plasmoids is much less than 90 R_S). We return to the issue of the difference between Vasyliunas and Dungey cycle reconnection in the next section. A second reason for the mismatch may be in the scale of the events. If a steady stream of small-scale plasmoids were to be released, the cumulative effect could go a long way toward making up the mass deficit. As outlined in Section 2 above, the events that we identify are the clearest, largest amplitude events from the Cassini magnetometer data in 2006. There may be many smaller-scale events with field signatures close to the level of background fluctuation that we have not selected here as we did not deem them to be unambiguous. Thirdly, there may be other mechanisms for mass loss in Saturn's magnetosphere apart from reconnection. Bagenal and Delamere [2011] suggested that perhaps cross-field diffusion, "drizzle" from highly stretched dusk field

854 lines, or other small-scale loss mechanisms may account for much of the mass loss from the
855 tail, particularly down the dusk flank [e.g. Kivelson and Southwood, 2005]. A final possible
856 reason is that the spacecraft did not sample far enough downtail to capture major plasmoid
857 ejections from a possible distant x-line.. The question of how mass is lost from Saturn's
858 magnetosphere is certainly one which warrants further investigation. For comparison, we
859 refer to Vogt et al. [2014] for a discussion of the minor role of plasmoids in mass loss in the
860 jovian magnetotail.

861

862 5.2 What drives reconnection at Saturn?

863 The Dungey and Vasyliunas cycles at Saturn are the primary cycles of magnetospheric
864 convection. The Dungey cycle is driven by interaction with the solar wind, and involves the
865 opening of flux via reconnection at the dayside and the closing of it on the nightside, with
866 return of empty flux tubes to the dayside primarily via dawn. The Vasyliunas cycle is an
867 internally driven process, involving rotation of mass-loaded flux tubes down the dusk flank
868 and pinch off primarily pre-midnight. Reconnection and associated plasmoid loss can
869 complete the cycle of magnetospheric convection at Saturn in both the Dungey and
870 Vasyliunas regimes [Cowley et al., 2004]. Theory predicts that both processes exist at Saturn
871 [Badman and Cowley, 2007], and evidence for Vasyliunas-cycle return flow from plasma
872 data has been presented [Masters et al., 2011]. Jackman et al. [2011] posed the question of
873 whether the nature of the reconnection field signatures could help to distinguish the
874 difference between reconnection of closed (Vasyliunas-cycle) and open (Dungey-cycle) field
875 lines. They interpreted the presence of a significant PPPS at Saturn as evidence of significant
876 closure of open flux. We note that even if reconnection is initially driven by the Vasyliunas
877 cycle, the reconnection can proceed from closed field lines to open within a single episode,
878 thus closing previously open flux via "Dungey-type" reconnection.

879

880 Figure 12 includes a cut from the picture presented by Jackman et al. [2011] and shows two
881 contrasting examples of plasmoids from the newly updated set. The panels show schematic
882 pictures of textbook "bipolar" and "PPPS" signatures, while Figures 12b and 12c show real
883 examples of such events from the magnetometer data. We did not have a large enough
884 number of events such as these to explore any local time dependence of the features. In this

885 work, we found the vast majority of plasmoids at Saturn displayed some extended interval of
886 northward field following plasmoid passage. We have interpreted this as representative of an
887 interval of closure of open flux, or a PPPS. However, we note the alternative explanation for
888 the "PPPS" field signature given in Section 3.2 above, in which plasma can be slowed due to
889 Vasyliunas-style reconnection occurring and plasmoids being trapped within outer closed
890 field lines. The exploration of such a scenario should be the topic of future detailed case
891 study analysis with high resolution plasma data. For the purposes of this paper, we base our
892 PPPS interpretation on analogy with Earth where a PPPS is a common feature [e.g.
893 Richardson et al., 1987] to explain such a distinctive field signature. In doing so, the flux
894 values we derive for Saturn can represent an upper limit to the rate of closure of open flux in
895 this process (within the limit of our assumptions). We also compare with studies of Saturn's
896 aurora which show changes in the auroral oval size linked to changing flux content of the
897 polar cap [e.g. Badman et al., 2005, 2013]. These studies suggest that opening and closing of
898 magnetic flux via dayside and nightside reconnection are significant processes in Saturn's
899 magnetosphere. Plasmoid release and subsequent reconnection of open lobe field lines must
900 play a part in this picture.

901

902 Figure 12b shows an example event from 2006 day 243 . The interval shown is from 07:00-
903 10:00, and the plasmoid in question is observed at 09:05, when the spacecraft was 47.3 R_S
904 downtail at a local time of 00.1 hrs. The B_R trace indicates that the current sheet moved over
905 the spacecraft just before plasmoid passage such that Cassini moved from southern lobe to
906 the plasma sheet north of the current sheet and into the northern lobe during the event.
907 Plasma data (not shown) confirm this picture. The B_θ field signature displays the textbook
908 bipolar signature which may be associated with reconnection on closed field lines as depicted
909 schematically in Figure 12a.

910

911 Figure 12c shows a plot of Cassini magnetometer data from 2006 day 131 13:00-17:00. A
912 plasmoid is observed passing tailward over the spacecraft at 13:55, when the spacecraft was
913 at a radial distance of ~48.3 R_S downtail, at ~02 LT. The duration of the plasmoid itself was
914 36 minutes, during which there was a total field deflection of 1.35 nT. However, this
915 signature was followed by a long interval where the field remained northward. Indeed B_θ

916 only reached zero again at 16:25. This field signature is in sharp contrast to the bipolar
917 signature observed in Figure 12b.

918

919 As mentioned above, plasmoid loss is expected for both the Vasyliunas and Dungey cycles.
920 In some theoretical pictures of Saturn, Dungey cycle reconnection is predisposed toward the
921 dawn flank [e.g. Cowley et al. 2004]. Work at Jupiter has suggested a pattern of reconnection
922 in which stretching empties flux tubes on the evening side and they snap back and then
923 stretch out again post midnight [Kivelson and Southwood, 2005]. We clearly require a large
924 sample of magnetic field and plasma data in order to understand the global patterns of plasma
925 circulation. While the single textbook "Vasyliunas-style" bipolar B_θ signature case study
926 shown here was observed pre-midnight, we do not have a sufficient number of "Vasyliunas"
927 type events to say whether this is the case on average. A longer term goal of the study of
928 Saturn's tail should be to exploit all available dusk coverage by Cassini (albeit at smaller
929 radial distances than the 2006 trajectories) to understand mass loss in this under-studied
930 region.

931

932 5.3 Where does reconnection happen and what is the size of the affected region?

933 In the well-sampled terrestrial magnetosphere, the role of magnetic reconnection in driving
934 magnetospheric convection is well established [Baker et al., 1996]. However, much remains
935 to be understood regarding the nature and effectiveness of external triggers for the onset of
936 reconnection [Hsu and McPherron, 2003] and the factors affecting the number of events and
937 the location of x-line formation [e.g., Imber et al, 2011] In this paper we have reported 69
938 tailward-moving plasmoids, 17 TCRs and 13 planetward-moving events. As mentioned in
939 the introduction, the sign of the change in B_θ over time (north-to-south or south-to-north)
940 indicates which side of the x-line the spacecraft is on. In our case, the vast majority of the
941 events were observed to be moving tailward. Even with an expanded database of planetward-
942 moving events, it has been impossible to derive a statistical separatrix based on field change
943 or flow patterns in the same sense that others have employed at Jupiter [e.g. Woch et al.,
944 2002; Vogt et al., 2010].

945

946 Estimates from ENA observations place the near-planet x-line at radial distances of ~20-30
947 R_S [Mitchell et al., 2005]. However, we note that ENA emission is stimulated when energetic
948 particles interact with the neutral torus at Saturn, and thus the observation of ENA emission
949 from this radial range can simply mean that this is where excitation took place, rather than
950 pinpointing where reconnection originated. Modellers have also sought to explore the issue of
951 the x-line location. Jia et al. [2012] suggested that the x-line position at Saturn can vary from
952 25-40 R_S depending on solar wind dynamic pressure, with the x-line moving towards the
953 planet and becoming narrower when the magnetosphere is compressed. Our results would
954 seem to qualitatively agree with the conclusions of modeling work, suggesting that the
955 position of the x-line is highly variable.

956

957 The timing of reconnection onset was discussed by Russell et al. [2008], who postulated a
958 relationship between reconnection onset and the position of the moon Titan in local time
959 based on six events. We have tested this relationship with the much larger dataset presented
960 in this paper and we do not find that the position of Titan is statistically significant in terms of
961 linking to reconnection event observation.

962

963 We noted above that from the subset of plasmoid events with plasma velocity information,
964 we can estimate the average plasmoid length at ~0.44 – 23.9 R_S. We note, however, that
965 these numbers are highly sensitive to trajectory effects, as spacecraft passes through the
966 plasmoids may take the form of "cords" through the edge as opposed to direct traversals of
967 the central/widest part of the structures. Also this calculation of "length" is based on the
968 assumption that plasmoids travel radially downtail after ejection, and neglects any azimuthal
969 motion. The azimuthal extent of the reconnection region is not well constrained. At Earth,
970 the flow channel widths associated with bursty bulk flows are observed to be ~1-2 R_E
971 [Angelopoulos et al., 1996], just less than 10% of the width of the Earth's tail. However, this
972 applies to the planetward-moving portion, which will be azimuthally limited. At Jupiter,
973 Vogt et al. [2010] found that the mean flow channel width associated with reconnection in the
974 jovian tail is 18 R_J, 6.67-10% of the typical tail width, a value which they suggested to be a
975 lower bound, taking measurement uncertainties into consideration. In the absence of multiple
976 spacecraft or continuous plasma velocity measurements at Saturn, we are unable to constrain
977 the corresponding values. However, one must remember that, once released, plasmoids are

978 free to expand to achieve pressure balance with their local surroundings, and thus we might
979 expect the azimuthal extent to represent a larger portion of the tail width with increasing
980 distance downtail.

981

982 In terms of local time, Figure 4c shows that there are many more observations of
983 reconnection events post-midnight than pre-midnight. The theoretical picture put forward by
984 Cowley et al. [2004] suggested that reconnection on closed field lines occurs predominantly
985 in the dusk sector, with Dungey-cycle open field line reconnection dominating towards dawn.
986 Thomsen et al. [2013] surveyed the dusk orbits of Cassini in 2010 and, other than strong
987 down-tail flows relatively near the magnetopause, found no evidence for outward flow in this
988 region. They interpreted this to mean that Vasyliunas-style reconnection may have occurred
989 on the dusk flank but that these plasmoids are still trapped within outer closed field lines and
990 thus not free to escape downtail until they reach the post-midnight sector. It may also be that
991 Cassini did not sample far enough downtail in this portion of its orbit to observe reconnection
992 outflow (note that their data set had no measurements beyond X_{KSM}~-20 Rs in the
993 premidnight sector). In Section 3 above we present new plasma data showing the composition
994 and velocity of a plasmoid on day 60 of 2006 at a local time of 2.3 hrs. These measurements
995 indicated that this plasmoid contained plasma from an inner magnetospheric source, and was
996 travelling with a total velocity of ~170 km/s, of which ~90 km/s was in the radial direction.

997

998 5.4 What is the morphology of the reconnection region?

999 In Section 4 we explored the morphology of the reconnection regions, applying MVA to
1000 three tailward-moving plasmoids to ascertain the direction of motion, and to search for
1001 evidence of loop-like or flux rope-like structures. We saw a mix of examples; one with a
1002 loop-like geometry, one with a flux rope-like geometry, and one where the trajectory of the
1003 spacecraft through the outer portions of the plasmoid precludes a determination of a flux-
1004 rope-like or loop-like central structure. What yields these particular geometries in the first
1005 place?

1006

A possible reason quoted in the literature for the production of flux rope-type plasmoids is simultaneous or sequential multiple x-line reconnection associated with substorms [e.g. Elphic et al., 1986; Slavin et al., 2003a; Deng et al., 2004]. However, the single-spacecraft Cassini measurements do not allow us to observe multiple reconnection sites in the tail at once, and to date no measurements of the x-line region itself have been made at Saturn. We note that the idea of a near-planet x-line and a distant-tail x-line is a popular picture in the terrestrial magnetosphere. However, this is one which again we are unable to directly infer from Cassini data. We suggest that the reconnection events shown in this paper are all associated with a near-Saturn reconnection site. All are within 68 R_S of the planet, which, by a simple scaling, is analogous to the region inside 30 R_E at Earth. The distant-tail x-line at Earth is thought to be situated beyond ~100 R_E. Thus we cannot know, based on our current data set, whether multiple x-lines exist at different radial distances in Saturn's tail, and hence we cannot conclude anything regarding their potential influence on interior plasmoid structure.

The presence of a cross-tail magnetic field has been shown to be an important factor in the formation of flux rope-like plasmoids [Liu et al., 2013], and suggestion made that this can come about via penetration of the azimuthal component of the interplanetary magnetic field (IMF) into the magnetosphere [e.g. Moldwin and Hughes, 1992]. Magnetic shear in the magnetotail can arise due to solar wind-magnetosphere coupling via magnetic reconnection at the dayside magnetopause. Due to the combination of frozen-in-flux and solar rotation, the IMF becomes increasingly tightly wound with increasing radial distance from the Sun. At 1 AU, this "Parker spiral angle" is ~45°, but by the time the solar wind reaches ~9 AU, the field is strongly azimuthal, with an average angle of ~83° [Jackman et al., 2008b]. However, the strength of the IMF at Saturn's orbit is considerably weakened compared to that at Venus, Earth and Mars. Perhaps the IMF at Saturn is not always sufficiently strong to impose a significant B_y component on the entire magnetosphere, especially given that it is competing against internal rotational dynamics for magnetospheric influence. In the case where Saturn's magnetotail lobes are not sheared to the degree that they are at other planets, flux rope-like plasmoids would be much less likely to be formed.

A second aspect to consider is whether the plasmoids that Cassini observes are the result of reconnection involving open field lines. Early theoretical work at Earth explored the

differences in magnetic topology introduced by reconnection on closed versus open field lines [e.g. Schindler, 1974; Hones, 1977]. Magnetic loops were achievable, at least in two dimensions, from reconnection of anti-parallel field lines from opposite lobes at a single x-line [e.g. Slavin et al., 2003a]. Evidence for reconnection of open lobe field lines at Saturn was presented by Jackman et al. [2011]. However, we note if the lobe magnetic field lines are significantly sheared relative to one another, this may make flux ropes more likely than loops.

Overall, our results on the interior morphology of plasmoids at Saturn are mixed. It is clear that during 2006, the hinging of the current sheet combined with the largely near-equatorial trajectory of the spacecraft has meant that Cassini typically passed through the bottom portion of plasmoids. This would, for example, reduce the duration of the encounters relative to the duration of a pass through the center of the structure and make it likely that the measurements failed to capture the actual core of the structures encountered. Thus, any conclusions we may draw regarding plasmoid-like or flux rope-like structures must be tempered with the knowledge that the field signatures are highly sensitive to the spacecraft trajectory through the structures. Future work will focus on fitting the field signatures using sophisticated flux rope fitting methods such as those employed by Slavin et al. [2003a] and Kivelson and Khurana [1995] to discern the impact parameter and explore statistical trends in plasmoid axis orientation.

6. Summary:

The aim of this study was to provide a comprehensive description of the "local" effects of magnetic reconnection in Saturn's magnetotail (e.g. changing magnetic topology, energization of electrons), and the "global" effects (e.g. mass loss and flux closure). In order to achieve this aim we have surveyed the Cassini magnetometer and plasma spectrometer data from the deep tail orbits of 2006 and found 69 tailward-moving plasmoids, 17 TCRs and 13 planetward-moving events. Events can occur in isolation, as previously reported, but also can be found in chains, likely linked to single reconnection episodes. The vast majority of events observed were tailward of the x-line, and those planetward of the x-line were observed over a wide range of radial distances, making it impossible to derive a statistical separatrix, and indicating that the x-line at Saturn is highly mobile. The average plasmoid observed at

Saturn has a duration of ~17.71 minutes, followed by an extended interval of northward field, interpreted as analogous to the terrestrial post-plasmoid plasma sheet, representing a period of flux closure. The average TCR at Saturn is evidenced by a broad compression of the field and a small deflection in the north-south component of the field. The average TCR compression ratio is 18%. Several important case studies have been shown, including an example of two plasmoids and two TCRs in quick succession, suggested to be linked to a single reconnection episode. Plasma data for one of these plasmoids indicate that it has a composition commensurate with an inner magnetospheric source, and it is travelling with a total velocity of 170 km/s. Plasma data from 29 of the plasmoids have been used to estimate a range in their length from 0.44 – 23.9 R_S, and we estimate that reconnection episodes in Saturn's tail can close between 0.26 and 2.2 GWb of flux. The refinement of the assumptions that are involved in these calculations will be the subject of future work. The morphology of the reconnection region has been explored using MVA, with both loop-like and flux rope-like topologies present, but with results highly sensitive to the trajectory of the spacecraft through the structures. We suggest that the observations presented here likely represent the largest events, and we are not ruling out steadier, smaller-scale mass release, perhaps on the dusk flank where observations thus far have been relatively scarce. The study of mass release at Saturn is key to our understanding of global magnetospheric dynamics, and we hope that future orbits of the Cassini spacecraft will afford us more chances to look in detail at the fascinating kronian magnetotail.

Acknowledgements:

CMJ's work at UCL was supported by a Leverhulme Trust Early Career Fellowship and a Royal Astronomical Society Fellowship and her work at Southampton was supported by a Royal Astronomical Society Fellowship until December 2013. CMJ, JAS and MFV discussed this work within the International Space Science Institute team number 195 on "Investigating the Dynamics of Planetary Magnetotails", led by CMJ. MFT was supported by the NASA Cassini program through JPL contract 1243218 with Southwest Research Institute. The Cassini project is managed by the Jet Propulsion Laboratory for NASA. JPE is supported by an STFC Advanced Fellowship at ICL.

References:

Andrews, D. J., B. Cecconi, S. W. H. Cowley, M. K. Dougherty, L. Lamy, G. Provan, and P. Zarka (2011), Planetary period oscillations in Saturn's magnetosphere: Evidence in magnetic field phase data for rotational modulation of Saturn kilometric radiation emissions, *J. Geophys. Res.*, 116, A09206, doi:10.1029/2011JA016636.

Angelopoulos, V., et al. (1996), Multipoint analysis of a bursty bulk flow event on April 11, 1985, *J. Geophys. Res.*, 101, 4967–4989, doi:10.1029/ 95JA02722.

Arridge, C. S., K. K. Khurana, C. T. Russell, D. J. Southwood, N. Achilleos, M. K. Dougherty, A. J. Coates, and H. K. Leinweber (2008a), Warping of Saturn's magnetospheric and magnetotail current sheets, *J. Geophys. Res.*, 113, A08217, doi:10.1029/2007JA012963.

Arridge, C. S., N. André, N. Achilleos, K. K. Khurana, C. L. Bertucci, L. K. Gilbert, G. R. Lewis, A. J. Coates, and M. K. Dougherty (2008b), Thermal electron periodicities at $20R_S$ in Saturn's magnetosphere, *Geophys. Res. Lett.*, 35, L15107, doi:10.1029/2008GL034132.

Arridge, C.S., H.J. McAndrews, C.M. Jackman, C. Forsyth, A.P. Walsh, E.C. Sittler, L.K. Gilbert, G.R. Lewis, C.T. Russell , A.J. Coates, M.K. Dougherty, G.A. Collinson, A. Wellbrock, D.T. Young, (2009), Plasma electrons in Saturn's magnetotail: structure, distribution and energisation, *Planet. Space. Sci.*, 57 (14-15), 2032-2047, doi:10.1016/j.pss.2009.09.007.

Arridge, C.S., N. André, K.K. Khurana, C.T. Russell, S.W.H. Cowley, G. Provan, D.J. Andrews, C.M. Jackman, A.J. Coates, E.C. Sittler, M.K. Dougherty, and D.T. Young (2011), Periodic motion of Saturn's nightside plasma sheet, *J. Geophys. Res.*, 116, A11205, doi: 10.1029/2011JA016827.

1133 Badman, S. V., E. J. Bunce, J. T. Clarke, S. W. H. Cowley, J.-C. Ge´rard, D. Grodent, and S.
1134 E. Milan (2005), Open flux estimates in Saturn's magnetosphere during the January 2004
1135 Cassini-HST campaign, and implications for reconnection rates, *J. Geophys.Res.*, 110,
1136 A11216, doi:10.1029/2005JA011240.

1137

1138 Badman, S. V., and S. W. H. Cowley (2007), Significance of Dungey cycle flows in Jupiter's
1139 and Saturn's magnetospheres, and their identification on closed equatorial field lines, *Ann.*
1140 *Geophys.*, 25, 941–951, doi:10.5194/angeo-25-941-2007.
1141

1142 Badman, S.V., C.M. Jackman, J.D. Nichols, J.T. Clarke, J.-C. Gérard (2013), Open flux in
1143 Saturn's magnetosphere,, *Icarus*, 231, 137-145,
1144 http://dx.doi.org/10.1016/j.icarus.2013.12.004.

1145

1146 Bagenal, F., and P. A. Delamere (2011), Flow of mass and energy in the magnetospheres of
1147 Jupiter and Saturn, *J. Geophys. Res.*, 116, A05209, doi:10.1029/2010JA016294.
1148

1149 Baker, D.N., R.C. Anderson, R.D. Zwickl, J.A. Slavin, (1987), Average plasma and magnetic
1150 field variations in the distant magnetotail associated with near-Earth substorm effects, *J.*
1151 *Geophys. Res.*, 92, 71.

1152

1153 Baker, D. N., T. I. Pulkkinen, V. Angelopoulos, W. Baumjohann, and R. L. McPherron
1154 (1996), Neutral line model of substorms: Past results and present view, *J. Geophys. Res.*,
1155 101(A6), 12975–13010, doi:10.1029/95JA03753.

1156

1157 Birn, J., Three-dimensional equilibrium for the extended magnetotail and the generation of
1158 field-aligned current sheets, *J. Geophys. Res.*, 94, 252, 1989.

1159

1160 Borg, A.L., M.G.G.T. Taylor, and J.P. Eastwood (2012), Observations of magnetic flux ropes
1161 during magnetic reconnection in the Earth's magnetotail, *Ann. Geophys.*, 30, 761-773.

1162

1163 Briggs, J.A., D.A. Brain, M.L. Cartwright, J.P. Eastwood, J.S. Halekas, (2011), A statistical
1164 study of flux ropes in the Martian magnetospheres, *Planet. Space Sci.*, 59, 1498-1505.
1165

1166 Bunce, E. J., S. W. H. Cowley, D. M. Wright, A. J. Coates, M. K. Dougherty, N. Krupp, W.
1167 S. Kurth, and A. M. Rymer (2005), In situ observations of a solar wind compression-induced
1168 hot plasma injection in Saturn's tail, *Geophys. Res. Lett.*, 32, L20S04,
1169 doi:10.1029/2005GL022888.
1170

1171 Burch, J. L., J. Goldstein, P. Mokashi, W. S. Lewis, C. Paty, D. T. Young, A. J. Coates, M.
1172 K. Dougherty, and N. Andre´ (2008), On the cause of Saturn's plasma periodicity, *Geophys.*
1173 *Res. Lett.*, 35, L14105, doi:10.1029/2008GL034951.
1174

1175 Carbary, J. F., D. G. Mitchell, P. Brandt, C. Paranicas, and S. M. Krimigis (2008), ENA
1176 periodicities at Saturn, *Geophys. Res. Lett.*, 35, L07102, doi:10.1029/2008GL033230.
1177

1178 Carbary, J. F., S. M. Krimigis, D. G. Mitchell, C. Paranicas, and P. Brandt (2009), Energetic
1179 neutral atom (ENA) and charged particle periodicities in Saturn's magnetosphere, *Adv. Space*
1180 *Res.*, 44, 483–493, doi:10.1016/j.asr.2009.04.019.
1181

1182 Chen, Y., T. W. Hill, A. M. Rymer, and R. J. Wilson (2010), Rate of radial transport of
1183 plasma in Saturn's inner magnetosphere, *J. Geophys. Res.,* 115, A10211,
1184 doi:10.1029/2010JA015412.
1185

1186 Cowley, S. W. H. and Bunce, E. J. (2003), Corotation-driven magnetosphere-ionosphere
1187 coupling currents in Saturn's magnetosphere and their relation to the auroras, *Ann. Geophys.*,
1188 21, 1691–1707, 2003.
1189

1190 Cowley, S.W. H., Bunce, E. J., and Prangé, R. (2004), Saturn's polar ionospheric flows and
1191 their relation to the main auroral oval, *Ann. Geophys.*, 22, 1379–1394.

1192

1193 Deng, X. H., Matsumoto, H., Kojima, H., Mukai, T., Anderson, R., Baumjohann, W., and
1194 Nakamura, R. (2004), Geotail encounter with reconnection diffusion region in the Earth's
1195 magnetotail: Evidence of multiple X lines collisionless reconnection?, *J. Geophys. Res.*, 109,
1196 A05 206, doi:10.1029/2003JA010031.
1197

1198 Dougherty, M. K., et al. (2004), The Cassini magnetic field investigation, *Space Sci. Rev.*,
1199 114, 331–383, doi:10.1007/s11214-004-1432-2.

1200

1201 Dungey, J. W., Interplanetary magnetic field and the auroral zones, *Phys. Rev. Lett.*, 6, 47,
1202 1961.

1203

1204 Eastwood, J. P., D. G. Sibeck, J. A. Slavin, M. L. Goldstein, B. Lavraud, M. Sitnov, S. Imber,
1205 A. Balogh, E. A. Lucek, and I. Dandouras (2005), Observations of multiple X-line structure
1206 in the Earth's magnetotail current sheet: A Cluster case study, Geophys. Res. Lett., 32,
1207 L11105, doi:10.1029/2005GL022509.

1208

1209 Eastwood, J.P. et al., (2012), A chain of magnetic flux ropes in the magnetotail of Mars,
1210 *Geophys. Res. Lett.*, 39, ISSN:0094-8276

1211

1212 Eastwood, J.P. and S.A. Kiehas, Origin and evolution of plasmoids and flux ropes in the
1213 magnetotails of Earth and Mars, in 'Magnetotails in the Solar System' (ed. Kieling, Jackman
1214 and Delamere), in press, 2014

1215

1216 Elphic, R. C., Cattell, C. A., Takahashi, K., Bame, S. J., and Russell, C. T., (1986), ISEE-1
1217 and 2 observations of magnetic flux ropes in the magnetotail: FTEs in the plasma sheet?,
1218 *Geophys. Res. Lett.*, 13, 648–651.
1219
1220 Elphic, R. C., and C. T. Russell (1983), Magnetic flux ropes in the Venus ionosphere:
1221 Observations and models, J. Geophys. Res., 88, 58.
1222
1223 Elphic, R. C., and D. J. Southwood (1987), Simultaneous measurements of the magnetopause
1224 and flux transfer events at widely separated sites by AMPTE UKS and ISEE 1 and 2, J.
1225 Geophys. Res., 92, 13,666–13,672.
1226
1227 Farrugia, C. J., R. C. Elphic, D. J. Southwood, and S. W. H. Cowley (1987), Field and flow
1228 perturbations outside the reconnected field region in flux transfer events: Theory, Planet
1229 Space Sci., 35(2), 227– 240.
1230
1231 Fleshman, B. L., P. A. Delamere, and F. Bagenal (2010c), The source of Saturn's extended
1232 neutral cloud, Abstract SM11C-1768 presented at 2010 Fall Meeting, AGU, San Francisco,
1233 Calif., 13–17 Dec.
1234
1235 Henderson, P.D. et al.,(2006), Cluster observations of flux rope structures in the near-tail,
1236 *Ann. Geophys.*, 24, 651-666.
1237
1238 Hesse, M., M.G. Kivelson, (1998), The formation and structure of flux ropes in the
1239 magnetotail, *New Perspectives on the Earth's Magnetotail, Geophysical Monograph*, 105.
1240 Hill, T.W., M.F. Thomsen, M.G. Henderson, R.L. Tokar, A.J. Coates, H.J. McAndrews, G.R.
1241 Lewis, D.G. Mitchell, C.M. Jackman, C.T. Russell, M.K. Dougherty, F.J. Crary, D.T. Young,
1242 (2008), Plasmoids in Saturn's magnetotail, *J. Geophys. Res.,* 113, A01214,
1243 doi:10.1029/2007JA012626.
1244
1245 Hones, E. W. Jr., (1976), The magnetotail: its generation and dissipation, in Physics of Solar
1246 Planetary Environments, Vol. II, edited by D. J. Williams, pp. 558-571, AGU.

Hones, E. W., Jr. (1977), Substorm processes in the magnetotail: Comments on ‘‘On hot tenuous plasma, fireballs, and boundary layers in the Earth’s magnetotail’’ by L.A. Frank et al., *J. Geophys. Res.*, 82, 5633.

Hsu, T.-S., and R. L. McPherron (2003), Occurrence frequencies of IMF triggered and nontriggered substorms, *J. Geophys. Res.*, 108, 1307, doi:10.1029/2002JA009442, A7.

Hughes, W. J., and D. G. Sibeck, On the 3-dimensional structure of plasmoids, Geophys. Res. Lett., 14, 636, 1987.

Ieda, A., S. Machida, T. Mukai, Y. Saito, T. Yamamoto, A. Nishida, T. Terasawa, and S. Kokubun, (1998), Statistical analysis of plasmoid evolution with GEOTAIL observations, *J. Geophys. Res.*, 103, 4435.

Imber, S. M., J. A. Slavin, H. U. Auster, and V. Angelopoulos (2011), A THEMIS survey of flux ropes and travelling compression regions: Location of the near-Earth reconnection site during solar minimum, *J. Geophys. Res.*, 116, A02201, doi:10.1029/2010JA016026.

Jackman, C. M., and C. S. Arridge (2011), Statistical properties of the magnetic field in the Kronian magnetotail lobes and current sheet, *J. Geophys. Res.*, 116, A05224, doi:10.1029/2010JA015973.

Jackman, C.M., C.T. Russell, D.J. Southwood, C.S. Arridge, N. Achilleos, and M.K. Dougherty, (2007), Strong field dipolarizations in Saturn’s magnetotail: In situ evidence of reconnection, *Geophys. Res. Lett.*, 34, (11), Art. No. L11203.

Jackman, C.M., C.S. Arridge, N. Krupp, E.J. Bunce, D.G. Mitchell, W.S. Kurth, H.J. McAndrews, M.K. Dougherty, C.T. Russell, N. Achilleos, A.J. Coates, G.H. Jones, (2008a), A multi-instrument view of tail reconnection at Saturn, *J. Geophys. Res.*, 113, A11213, doi:10.1029/2008JA013592.

Jackman, C.M., R.J. Forsyth, M.K. Dougherty, (2008b), The overall configuration of the interplanetary magnetic field upstream of Saturn as revealed by Cassini observations, *J. Geophys. Res.,* 113, A08114, doi:10.1029/2008JA013083.

Jackman, C.M., C.S. Arridge, H.J. McAndrews, M.G. Henderson, R.J. Wilson, Northward field excursions in Saturn's magnetotail and their relationship to magnetospheric periodicities, (2009), *Geophys. Res. Lett.*, 36, L16101, doi:10.1029/2009GL039149.

Jackman, C. M., J. A. Slavin, and S. W. H. Cowley (2011), Cassini observations of plasmoid structure and dynamics: Implications for the role of magnetic reconnection in magnetospheric circulation at Saturn, *J. Geophys. Res.*, 116, A10212, doi:10.1029/2011JA016682.

Jackman, C.M., N. Achilleos, S.W.H. Cowley, E.J. Bunce, A. Radioti, D. Grodent, S.V. Badman, M.K. Dougherty, W. Pryor (2013), Auroral counterpart of magnetic field dipolarizations in Saturn's tail, *Planet. Space Sci.*, 82-83, 34-42, doi: 10.1016/j.pss.2013.03.010

Jia, X., K. C. Hansen, T. I. Gombosi, M. G. Kivelson, G. Tóth, D. L. DeZeeuw, and A. J. Ridley (2012), Magnetospheric configuration and dynamics of Saturn's magnetosphere: A global MHD simulation, *J. Geophys. Res.*, 117, A05225, doi:10.1029/2012JA017575.

Jurac, S., and J. D. Richardson (2005), A self-consistent model of plasma and neutrals at Saturn: Neutral cloud morphology, *J. Geophys. Res.*, 110, A09220, doi:10.1029/2004JA010635.

1305 Kanani, S. J., et al. (2010), A new form of Saturn's magnetopause using a dynamic pressure
1306 balance model, based on in situ, multi-instrument Cassini measurements, *J. Geophys. Res.*,
1307 115, A06207, doi:10.1029/2009JA014262.
1308
1309 Kellett, S., E. J. Bunce, A. J. Coates, and S. W. H. Cowley (2009), Thickness of Saturn's ring
1310 current determined from north-south Cassini passes through the current layer, *J. Geophys.*
1311 *Res.*, 114, A04209, doi:10.1029/2008JA013942.
1312
1313 Kidder, A., C. S. Paty, R. M. Winglee, and E. M. Harnett (2012), External triggering of
1314 plasmoid development at Saturn, J. Geophys. Res., 117, A07206,
1315 doi:10.1029/2012JA017625.
1316
1317 Kivelson, M.G., and K.K. Khurana, (1995), Models of flux ropes embedded in a Harris
1318 neutral sheet: Force-free solutions in low and high beta plasmas, *J. Geophys. Res.*, 100, A12,
1319 23,657-23,645.
1320
1321 Kivelson, M. G., and D. J. Southwood (2005), Dynamical consequences of two modes of
1322 centrifugal instability in Jupiter's outer magnetosphere, J. Geophys. Res., 110, A12209,
1323 doi:10.1029/2005JA011176.
1324
1325 Kronberg, E. A., J. Woch, N. Krupp, and A. Lagg (2008), Mass release process in the Jovian
1326 magnetosphere: Statistics on particle burst parameters, *J. Geophys. Res.*, 113, A10202,
1327 doi:10.1029/2008JA013332.
1328
1329 Lepping, R. P., J. A. Jones, and L. F. Burgala (1990), Magnetic field structure of
1330 interplanetary magnetic clouds at 1 AU, J. Geophys. Res., 95, 11,957.

1331 Lepping, R. P., D. H. Fairfield, J. Jones, L. A. Frank, W. R. Paterson, S. Kokubun, and T.
1332 Yamamoto (1995), Cross-tail magnetic flux ropes as observed by the Geotail spacecraft,
1333 *Geophys. Res. Lett.*, 22, 1193.

1334

1335 Li, S.-S., V. Angelopoulos, A. Runov, S. A. Kiehas, and X.-Z. Zhou (2013), Plasmoid growth
1336 and expulsion revealed by two-point ARTEMIS observations, J. Geophys. Res. Space
1337 Physics, 118, 2133–2144, doi:10.1002/jgra.50105.

1338

1339 Liu, C., X. Feng, J. Guo, and Y. Ye (2013), Study of small-scale plasmoid structures in the
1340 magnetotail using Cluster observations and Hall MHD simulations, *J. Geophys. Res. Space*
1341 *Physics*, *118*, doi:10.1002/jgra.50248.

1342

1343 Lundquist, S. (1950), Magnetohydrostatic field, Ark. Fys., 2, 361.

1344

1345 McAndrews, H.J. M.F. Thomsen, C.S. Arridge, C.M. Jackman, R.J. Wilson, M.G.
1346 Henderson, R.L. Tokar, K.K. Khurana, E.C. Sittler, A.J. Coates, M.K. Dougherty (2009),
1347 Plasma in Saturn's nightside magnetosphere and the implications for global circulation,
1348 *Planet. Space Sci*, 57, 14-15, 1714-1722, doi:10.1016/j.pss.2009.03.003.

1349

1350

1351 Masters, A., M. F. Thomsen, S. V. Badman, C. S. Arridge, D. T. Young, A. J. Coates, and M.
1352 K. Dougherty (2011), Supercorotating return flow from reconnection in Saturn's magnetotail,
1353 *Geophys. Res. Lett.*, 38, L03103, doi:10.1029/2010GL046149.

1354

1355

1356 Mitchell, D. G., et al. (2005), Energetic ion acceleration in Saturn's magnetotail: Substorms
1357 at Saturn?, *Geophys. Res. Lett.*, 32, L20S01, doi:10.1029/2005GL022647.

1358

1359 Moldwin, M. and Hughes, W. (1992), On the Formation and Evolution of Plasmoids: A
1360 Survey of ISEE 3 Geotail Data, *J. Geophys. Res.*, 97, 19259–19282, doi:10.1029/92JA01598.
1361
1362
1363 Moldwin, M.B., Phillips, J.L., Gosling, J.T., Scime, E.E., McComas, D.J., Barne, S.J.,
1364 Balogh, A., Forsyth, R.J., (1995), Ulysses observations of a noncoronal mass ejection flux
1365 rope: evidence of interplanetary magnetic reconnection, *J. Geophys. Res.*, 100 (19), 903–910.
1366
1367
1368 Paschmann, G., and P. Daly (Eds.), (1998), Analysis methods for multi-spacecraft data, ISSI
1369 Science Report, SR-001.
1370
1371 Pontius, D., and T. W. Hill (2009), Inertial corotation lag and mass loading in Saturn's
1372 magnetosphere, *Geophys. Res. Lett.*, 36, L23103, doi:10.1029/2009GL041030.
1373
1374 Provan, G., D. J. Andrews, C. S. Arridge, A. J. Coates, S. W. H. Cowley, G. Cox, M. K.
1375 Dougherty, and C. M. Jackman (2012), Dual periodicities in planetary-period magnetic field
1376 oscillations in Saturn's tail, *J. Geophys. Res.*, 117, A01209, doi:10.1029/2011JA017104.
1377
1378 Richardson, I.G., S.W.H. Cowley, E.W. Hones, Jr., S.J. Bame, (1987), Plasmoid-associated
1379 energetic ion bursts in the deep geomagnetic tail: Properties of plasmoids and the post-
1380 plasmoid plasma sheet, *J. Geophys. Res.*, 92, 9997.
1381
1382 Runov, A.; Sergeev, V. A.; Nakamura, R.; Baumjohann, W.; Apatenkov, S.; Asano, Y.;
1383 Takada, T.; Volwerk, M.; Vörös, Z.; Zhang, T. L.; Sauvaud, J.-A.; Rème, H.; Balogh, A.,
1384 (2006), Local structure of the magnetotail current sheet: 2001 Cluster observations, *Ann.*
1385 *Geophys.*, 24, 1, 2006, 247-262.
1386
1387 Russell C.T. and R.C. Elphic, (1979), Observations of magnetic flux ropes in the Venus
1388 ionosphere, *Nature*, 279, 616.
1389

Russell, C. T. (1990), Magnetic flux ropes in the ionosphere of Venus, in Physics of Magnetic Flux Ropes, Geophys. Monogr. Ser., vol. 58, edited by C. T. Russell, E. R. Priest, and L. C. Lee, p. 413 – 213, AGU, Washington, D. C.

Russell C.T., C.M. Jackman, H.Y. Wei, C. Bertucci, M.K. Dougherty (2008), Titan's influence on Saturnian substorm occurrence, *Geophys. Res. Lett*., 35, L12105, doi:10.1029/2008GL034080.

Schindler, K. (1974), A theory of the substorm mechanism, *J. Geophys. Res.*, 79, 2803.

Sergis, N., C. S. Arridge, S. M. Krimigis, D. G. Mitchell, A. M. Rymer, D. C. Hamilton, N. Krupp, M. K. Dougherty, and A. J. Coates (2011), Dynamics and seasonal variations in Saturn□s magnetospheric plasma sheet, as measured by Cassini, *J. Geophys. Res.*, 116, A04203, doi:10.1029/2010JA016180.

Sibeck, D. G., G. L. Siscoe, J. A. Slavin, E. J. Smith, S. J. Bame, and F. L. Scarf, (1984), Magnetotail flux ropes, *Geophys. Res. Lett.*, 11, 1090.

Slavin, J., E. Smith, B. Tsurutani, D. Sibeck, H. Singer, D. Baker, J. Gosling, E. Hones, and F. Scarf (1984), Substorm-associated traveling compression regions in the distant tail: ISEE-3 geotail observations, *Geophys. Res. Lett.*, 11, 657–660, doi:10.1029/GL011i007p00657.

Slavin, J. A., E. J. Smith, D. G. Sibeck, D. N. Baker, R. D. Zwickl, and S.-I. Akasofu (1985), An ISEE 3 study of average and substorm conditions in the distant magnetotail, J. Geophys. Res., 90, 10,875–10,895.

Slavin, J. A., D. N. Baker, J. D. Craven, R. C. Elphic, D. H. Fairfield, L. A. Frank,A. B. Galvin, W. J. Hughes, R. H. Manka, D. G. Mitchell, I. G. Richardson, T. R. Sanderson, D. J. Sibeck, H. J. Singer, E. J. Smith, and R. D. Zwickl (1989), CDAW-8 observations of plasmoid signatures in the geomagnetic tail: An assessment, *J. Geophys. Res.,* 94, 15,153.

Slavin, J.A., M.F. Smith, E. L. Mazur, D. N. Baker, E. W. Hones, Jr., T. Iyemori, and E. W. Greenstadt, (1993), ISEE 3 Observations of Travelling Compression Regions in the Earth's Magnetotail, *J. Geophys. Res.*, 98, A9, 15425-15,446.

Slavin, J.A., C.J. Owen, M.M. Kuznetsova, M. Hesse, (1995), ISEE 3 observations of plasmoids with flux rope magnetic topologies, *Geophys. Res. Lett.*, 22, 15, 2061-2064.

Slavin, J. A., et al.,(2002), Simultaneous observations of earthward flow bursts and plasmoid ejection during magnetospheric substorms, *J. Geophys. Res.,* 107(A7), doi:10.1029/2000JA003501.

Slavin, J. A., R. P. Lepping, J. Gjerloev, D. H. Fairfield, M. Hesse, C. J. Owen, M. B. Moldwin, T. Nagai, A. Ieda, and T. Mukai, (2003a), Geotail observations of magnetic flux ropes in the plasma sheet, *J. Geophys. Res.*, 108(A1), 1015, doi:10.1029/2002JA009557.

Slavin, J. A., et al. (2003b), Cluster four spacecraft measurements of small traveling compression regions in the near‐tail, *Geophys. Res. Lett.*, 30, 2208, doi:10.1029/2003GL018438.

Slavin, J. A., Transkanen, E. I., Hesse, M., Owen, C. J., Dunlop, M. W., Imber, S., Lucek, E. A., Balogh, A., and Glassmier, K.-H. (2005), Cluster observations of traveling compression regions in the near-tail, *J. Geophys. Res.*, 110, A06207, doi:10.1029/2004JA010878.

Sonnerup, B.U.O ., Cahill Jr.,L.J.,(1967), Magnetopause structure and attitude from Explorer 12 observations, *J.Geophys.Res.*, 72,171–183.

1451 Szego, K., Z. Nemeth, G. Erdos, L. Foldy, Z. Bebesi, M. Thomsen, and D. Delapp (2012),
1452 Location of the magnetodisk in the nightside outer magnetosphere of Saturn near equinox
1453 based on ion densities, J. Geophys. Res., 177, A09225, doi:10.1029/2012JA017817

1454

1455 Thomsen, M.F., R.J. Wilson, R.L. Tokar, D.B. Reisenfeld, C.M. Jackman (2014),
1456 Cassini/CAPS Observations of Duskside Tail Dynamics at Saturn, 118, 5767-5781, doi:
1457 10.1002/jgra.50552..

1458

1459 Thomsen, M.F., C.M. Jackman, R.L. Tokar, R.J. Wilson, Plasma Flows in Saturn's Nightside
1460 Magnetosphere, J. Geophys. Res, submitted, 2014.

1461

1462 Vasyliunas, V. M. (1983), Plasma distribution and flow, in Physics of the Jovian
1463 Magnetosphere, edited by A. J. Dessler, pp. 395–453, Cambridge Univ. Press, New York,
1464 doi:10.1017/CBO9780511564574.013.

1465

1466 Vogt, M. F., M. G. Kivelson, K. K. Khurana, S. P. Joy, and R. J. Walker (2010),
1467 Reconnection and flows in the Jovian magnetotail as inferred from magnetometer
1468 observations, *J. Geophys. Res.*, 115, A06219, doi:10.1029/2009JA015098.

1469

1470 Vogt, M.F., C.M. Jackman, J.A. Slavin, E.J. Bunce, S.W.H. Cowley, M.G. Kivelson, K.K.
1471 Khurana (2014), Structure and Statistical Properties of Plasmoids in Jupiter's Magnetotail, J.
1472 Geophys. Res., 119*,* 821–843*, doi:10.1002/2013JA*019393

1473

1474 Volwerk, M., N. André, C.S. Arridge, C.M. Jackman, X. Jia, S.E. Milan, A. Radioti, M.F.
1475 Vogt, A.P. Walsh, R. Nakamura, A. Masters, and C. Forsyth (2013), Comparative
1476 magnetotail flapping: an overview of selected events at Earth, Jupiter and Saturn, *Ann.*
1477 *Geophys.*, 31, 817-833, doi:10.5194/angeo-31-817-2013.

1478

1479 Woch, J., N. Krupp, and A. Lagg (2002), Particle bursts in the Jovian magnetosphere:
1480 Evidence for a near-Jupiter neutral line, *Geophys. Res. Lett.*, 29(7), 1138,
1481 doi:10.1029/2001GL014080.

Zhang, H., et al. (2010), Evidence that crater flux transfer events are initial stages of typical flux transfer events, J. Geophys. Res., 115, A08229, doi:10.1029/2009JA015013.

Zhang, H., M. G. Kivelson, V. Angelopoulos, K. K. Khurana, Z. Y. Pu, R. J. Walker, R. L. McPherron, T.-S. Hsu,Q. G. Zong, and T. Phan (2012), Generation and properties of in vivo flux transfer events, J. Geophys. Res., 117, A05224, doi:10.1029/2011JA017166.

Zieger, B., K. C. Hansen, T. I. Gombosi, and D. L. De Zeeuw (2010), Periodic plasma escape from the mass-loaded Kronian magnetosphere, *J. Geophys. Res.*, 115, A08208, doi:10.1029/2009JA014951.

Zong, Q.-G., et al. (2004), Cluster observations of earthward flowing plasmoid in the tail, *Geophys. Res. Lett.*, 31, L18803, doi:10.1029/2004GL020692.

Tables:

Type	DOY	Time (Hr: Min:Sec)	Start Time (Hr Min sec)	End time (Hr min sec)	Range (R_S)	LT (Hr: Min)	Duration (mins)	ΔB_0 (nT)	B_0 change	Classification	Plasmaflow velocities
PLASMOID	32	12 58 00	12 47 00	13 11 00	65.99	4:26	24.00	2.13	south-north	isolated	V (W+) ~20 270 km/s
TCR	36	04 32 00	04 17 00	04 38 00	68.17	4:46	21.00	0.52	south-north	pair	
PLASMOID	36	05 41 00	05 34 00	06 02 00	68.17	4:46	28.00	0.63	south-north	pair	
PLASMOID	37	23 10 30	23 02 30	23 20 30	68.08	4:56	18.00	0.87	south-north	isolated	CAPS data
PLASMOID	60	07 33 00	07 30 20	07 36 00	32.33	2:17	5.67	2.16	south-north	multiple	V(W+) ~ 1 km/s
PLASMOID	60	08 27 00	08 25 30	08 28 00	32.50	2:17	2.00	0.94	south-north	multiple	
TCR	60	08 58 00	08 53 00	09 03 00	32.61	2:18	10.00	0.49	south-north	multiple	
TCR	60	09 34 00	09 33 00	09 36 00	32.71	2:18	3.00	0.12	south-north	multiple	
TCR	62	15 26 00	15 19 00	15 30 00	40.93	2:55	11	0.31	south-north	pair	
TCR	62	16 33 00	16 29 00	16 38 00	41.07	2:56	9.00	0.22	south-north	pair	
PLASMOID	63	22 07 00	22 06 00	22 09 00	44.10	3:10	3.00	1.70	south-north	pair	V (W+) ~20 km/s
PLASMOID	63	22 59 30	22 56 00	23 02 00	44.17	3:11	6	3.51	south-north	pair	V (W+) ~58 km/s V (H+) ~62 km/s
PLASMOID	64	08 50 00	08 48 00	08 54 00	44.9	3:15	6.00	0.90	south-north	multiple	V (W+) ~22

					8						km/s
PLASMOID	64	09 30 45	09 29 00	09 32 20	45.03	3:15	3.33	1.01	south-north	multiple	V (W+) ~29 km/s
PLASMOID	64	10 49 00	10 46 10	10 52 10	45.13	3:16	6.00	1.15	south-north	multiple	V (W+) ~22 km/s
PLASMOID	64	19 56 30	19 49 00	20 04 00	45.78	3:20	15.00	1.19	south-north	isolated	
PLASMOID	65	06 34 00	06 28 00	06 39 00	46.45	3:24	11.00	0.78	south-north	isolated	
PLASMOID	65	17 03 00	17 00 45	17 05 00	47.00	3:29	4.25	0.61	south-north	pair	
PLASMOID	65	17 24 00	17 22 00	17 27 15	47.02	3:29	5.25	1.31	south-north	pair	
PLASMOID	65	21 08 00	20 59 00	21 17 00	47.20	3:30	18.00	0.97	south-north	isolated	
TCR	66	06 23 00	06 17 00	06 30 00	47.6	3.36	13	0.6	south-north	pair	
TCR	66	08 42 00	08 40 00	08 51 00	47.7	3.36	11	0.7	south-north	pair	
TCR	83	18 34 30	18 18 30	18 46 00	34.03	0:33	27.50	2.22	south-north	isolated	
PLASMOID	84	02 31 30	02 30 30	02 32 30	35.8	0.7	2	1.9	south-north	isolated	Outward: V (W+) ~24 km/s
PLASMOID	85	00 16 00	00 09 00	00 20 00	40.22	0:58	11.00	1.85	south-north	isolated	
TCR	85	04 20 00	04 01 00	04 25 00	40.9	1.0	24	0.6	south-north	isolated	
TCR	124	08 33 00	08 32 00	08 42 00	38.40	0:43	10.00	0.62	south-north	isolated	
TCR	124	13 13 00	13 05 00	13 20 00	39.05	0:45	15.00	0.20	north-south	pair	
TCR	124	14 19 30	14 06 00	14 30 00	39.20	0:46	24.00	0.65	north-south	pair	
PLASMOID	131	13 55 00	13 40 30	14 16 30	48.28	2:01	36.00	1.35	south-north	isolated	
TCR	131	22 48 00	22 19 00	22 57 00	48.09	2:05	38	0.84	south-north	isolated	
TCR	169	00 34 00	00 32 00	00 39 00	62.32	1:34	7.00	1.47	south-north	isolated	V (H+) ~62 km/s
PLASMOID	193	07 28 30	07 27 00	07 43 00	48.42	23:52	16	2.1	south-north	isolated	V (W+) ~12 km/s V (H+) ~67 km/s
PLASMOID	195	01 48 00	01 42 00	02 05 00	47.61	0:09	23.00	2.22	south-north	Pair	
TCR	195	04 08 00	04 07 00	04 13 00	47.52	0:10	6.00	0.38	south-north	Pair	
TCR	195	12 44 00	12 38 00	12 53 00	47.16	0:13	15	0.69	south-north	isolated	
PLASMOID	195	23 38 30	23 31 00	23 45 00	46.5	0.3	14	1.6	south-north	isolated	
PLASMOID	196	08 56 00	08 54 00	09 01 00	46.05	0:22	7.00	1.15	south-north	Pair	V (W+) ~20 km/s
PLASMOID	196	10 22 00	10 15 00	10 24 00	45.96	0:23	9.00	1.40	south-north	Pair	V (W+) ~20 km/s
PLASMOID	196	18 28 00	18 24 00	18 30 00	45.41	0:26	6.00	1.25	south-north	isolated	V (W+) ~18 km/s
PLASMOID	197	07 09 00	07 05 00	07 12 00	44.41	0:32	7.00	1.60	south-north	Pair	
TCR	197	07 44 00	07 40 00	07 51 00	44.36	0:32	11.00	0.38	south-north	Pair	
PLASMOID	197	16 34 00	16 25 00	16 41 00	43.5	0.6	16	0.9	south-north	isolated	V (W+) ~17 km/s
PLASMOID	198	14 45 30	14 43 30	14 52 30	41.25	0:48	9.00	1.75	south-north	isolated	
PLASMOID	199	23 06 45	23 02 00	23 08 30	36.88	1:08	6.5	1.80	south-north	isolated	
PLASMOID	209	20 34 00	20 17 00	20 38 30	36.85	22:24	21.50	2.58	south-north	isolated	
PLASMOID	212	04 49 00	04 39 00	04 57 00	43.85	22:56	18.00	0.84	south-north	Pair	

PLASMOID	212	05 27 00	05 15 00	05 57 00	43.91	22:56	42.00	0.65	south-north	Pair	
PLASMOID	212	10 07 00	10 05 00	10 08 00	44.34	22:58	3.00	0.68	south-north	Pair	
PLASMOID	212	10 54 00	10 48 00	10 58 00	44.41	22:36	10.00	1.08	south-north	Pair	
PLASMOID	212	14 57 00	14 50 00	15 00 00	44.76	23:00	10.00	0.91	south-north	isolated	
PLASMOID	212	23 19 30	23 17 30	23 20 30	45.4	23.1	3	1.1	south-north	isolated	
PLASMOID	213	11 50 00	11 32 00	12 12 00	46.4	23.2	40	1.5	south-north	isolated	
PLASMOID	214	18 32 00	18 29 00	18 35 00	48	23.4	6	0.8	south-north	isolated	
PLASMOID	215	10 36 30	10 30 00	10 38 30	48.5	23.5	8.5	1.1	south-north	isolated	
PLASMOID	215	17 27 00	17 20 00	17 35 00	48.7	23:31	15.0	0.83	south-north	isolated	V(W+)~2 km/s
PLASMOID	216	16 47 30	16 45 00	16 51 15	49.00	23:41	6.25	3.39	south-north	Pair	V (W+) ~24 km/s
PLASMOID	216	17 51 00	17 47 30	17 55 30	49.01	23:50	8	0.82	south-north	Pair	
PLASMOID	217	17 42 00	17 28 20	17 59 00	48.85	23:13	21.67	0.65	south-north	isolated	V (W+) ~15 km/s V (H+) ~62 km/s
PLASMOID	218	15 27 00	14 47 00	16 05 00	48.31	23:59	78.00	0.92	south-north	isolated	
PLASMOID	219	11 20 00	10 45 00	12 20 00	47.48	00:07	95.00	1.03	south-north	isolated	
PLASMOID	223	14 40 00	14 26 00	15 07 00	37.99	00:56	41.00	1.21	south-north	isolated	V(W+)~2 km/s
PLASMOID	232	10 01 00	09 46 00	10 07 00	30.76	21:54	21.00	1.91	south-north	isolated	
PLASMOID	234	14 50 30	14 45 00	15 03 00	39.6	22.6	18	1.8	south-north	isolated	
PLASMOID	236	18 05 30	18 04 30	18 11 00	45	23	6.5	0.95	south-north	Pair	
PLASMOID	238	18 16 00	18 15 00	18 18 30	47.9	23.3	3.5	1.3	south-north	isolated	V (W+) ~14 km/s
PLASMOID	240	00 41 00	00 33 00	00 44 00	48.73	23:32	11.00	1.20	south-north	isolated	
PLASMOID	240	06 48 00	06 46 00	06 55 00	48.81	23:34	9.00	0.66	south-north	isolated	V(W+)~1 km/s V(H+)~44 km/s
PLASMOID	240	23 38 30	23 28 00	23 54 00	48.8	23.6	26	1.5	south-north	multiple	V (W+) ~24 km/s
PLASMOID	241	01 38 30	01 34 30	01 53 30	48.8	23.6	20	1.1	south-north	multiple	
PLASMOID	241	03 40 30	03 25 00	03 45 00	48.8	23.7	5	0.55	south-north	multiple	
PLASMOID	242	17 30 00	17 02 00	17 50 00	48.02	23:57	48.0	0.98	south-north	isolated	
PLASMOID	243	09 05 00	08 52 00	09 10 00	47.3	0.1	18	1.4	south-north	isolated	V (W+) ~3 km/s
PLASMOID	243	21 47 00	21 22 00	21 58 00	46.64	00:09	36.00	0.64	south-north	isolated	
PLASMOID	244	15 17 00	15 11 00	15 19 00	45.45	00:16	8.00	1.15	south-north	isolated	

PLASMOID	246	22 45 00	22 18 00	22 51 00	39.74	00:45	33.00	2.02	south-north	isolated	V(W+)~3 km/s
PLASMOID	248	17 50 00	17 45 00	18 00 00	32.8	1.3	15	1.6	south-north	Pair	V (W+) ~1 km/s
PLASMOID	248	18 30 00	18 29 00	18 31 00	32.8	1.3	2	1.4	south-north	Pair	V (W+) ~3 km/s
PLASMOID	249	12 04 00	12 02 30	12 04 30	29.14	01:34	2.00	2.00	south-north	Pair	V(W+)~2 km/s
PLASMOID	249	15 34 00	15 32 15	15 36 45	28.35	1:38	4.50	4.42	south-north	isolated	V (W+) ~4 km/s
PLASMOID	250	00 32 30	00 11 30	00 33 45	26.22	01:49	22.25	2.25	south-north	isolated	
PLASMOID	258	10 05 00	09 20 00	10 10 00	35.4	23.9	50	2.2	south-north	isolated	V (W+) ~4 km/s
PLASMOID	258	21 00 00	20 20 00	21 20 00	36.2	0	60	2.1	south-north	isolated	
PLASMOID	261	04 01 00	03 58 30	04 05 45	37.52	00:31	7.25	1.66	south-north	isolated	V(W+) >6 km/s
PLASMOID	262	08 45 00	08 30 30	08 49 00	36.54	00:47	18.50	1.10	south-north	isolated	V(W+)~2 km/s
PLASMOID	264	02 08 30	02 00 30	02 09 30	32.99	01:12	9.00	1.59	south-north	isolated	

Table 1: Timings and properties of plasmoids and TCRs observed during 2006. Flow speeds are estimated from the energy of the peak counts and thus they represent upper limits.

Figures:

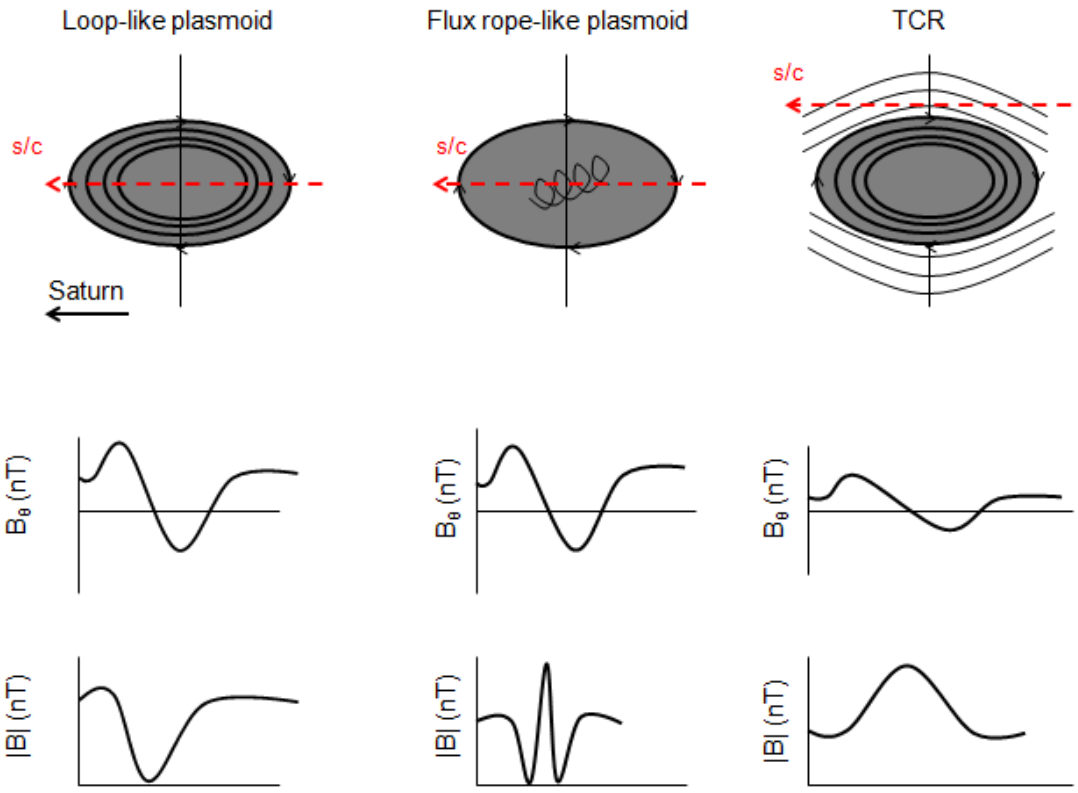

1505

1506 Figure 1: Schematic sketch of spacecraft trajectory through a) tailward-moving loop-like
1507 plasmoid, b) tailward-moving flux rope-like plasmoid, c) tailward-moving TCR (adapted
1508 from Zong et al., 2004].

1509

1510

1511

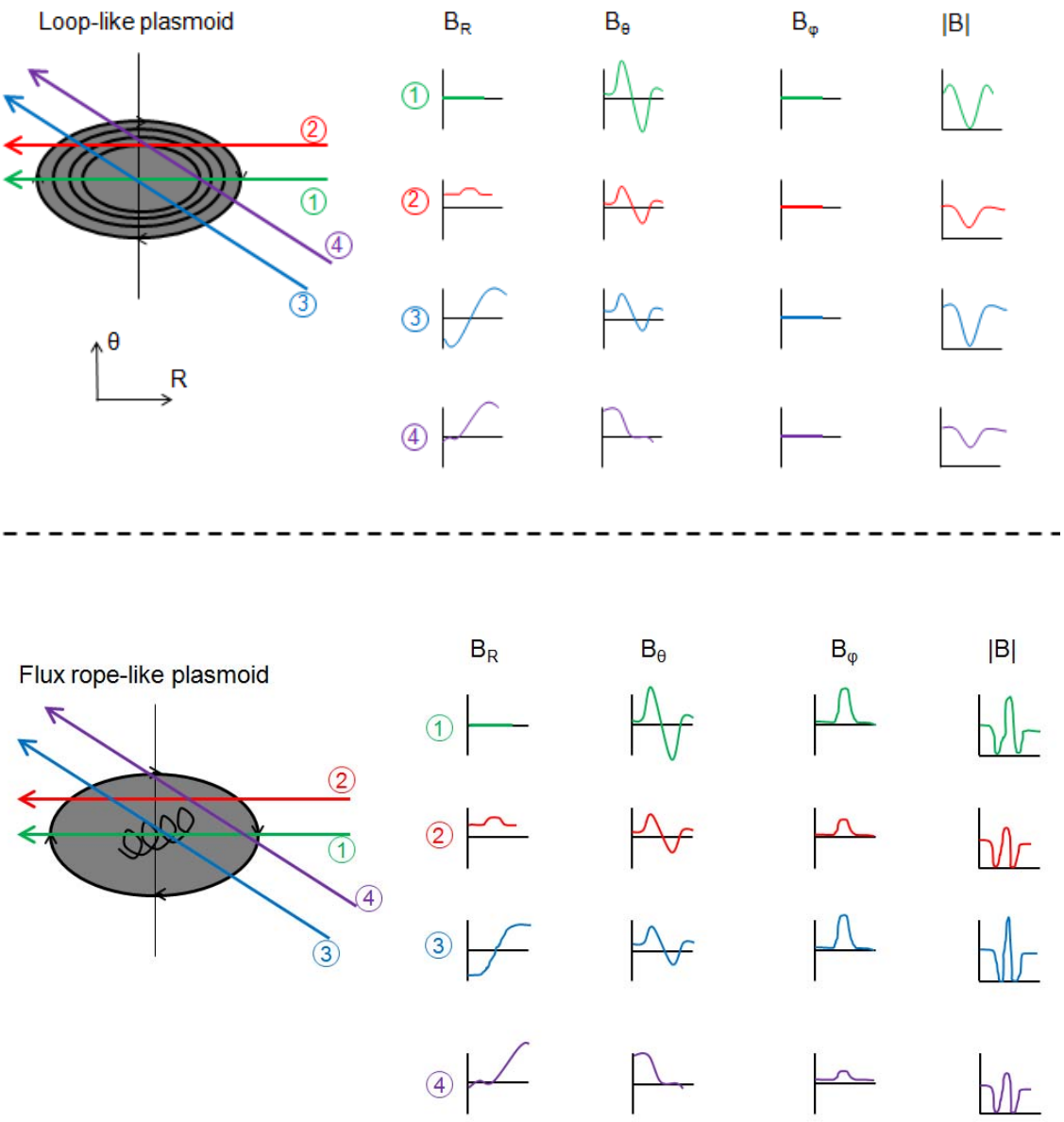

Figure 2: Schematic of various possible spacecraft trajectories through model tailward-moving loop-like and flux rope-like plasmoids and the field signatures (in KRTP co-ordinates) that would result. B_R is positive above the current sheet, B_θ is positive southward, and B_φ is positive in the corotation direction. The various straight line trajectories assume that the encounters occur in a time scale short compared with the times for dynamical changes of the local magnetosphere. [After Borg et al., 2012].

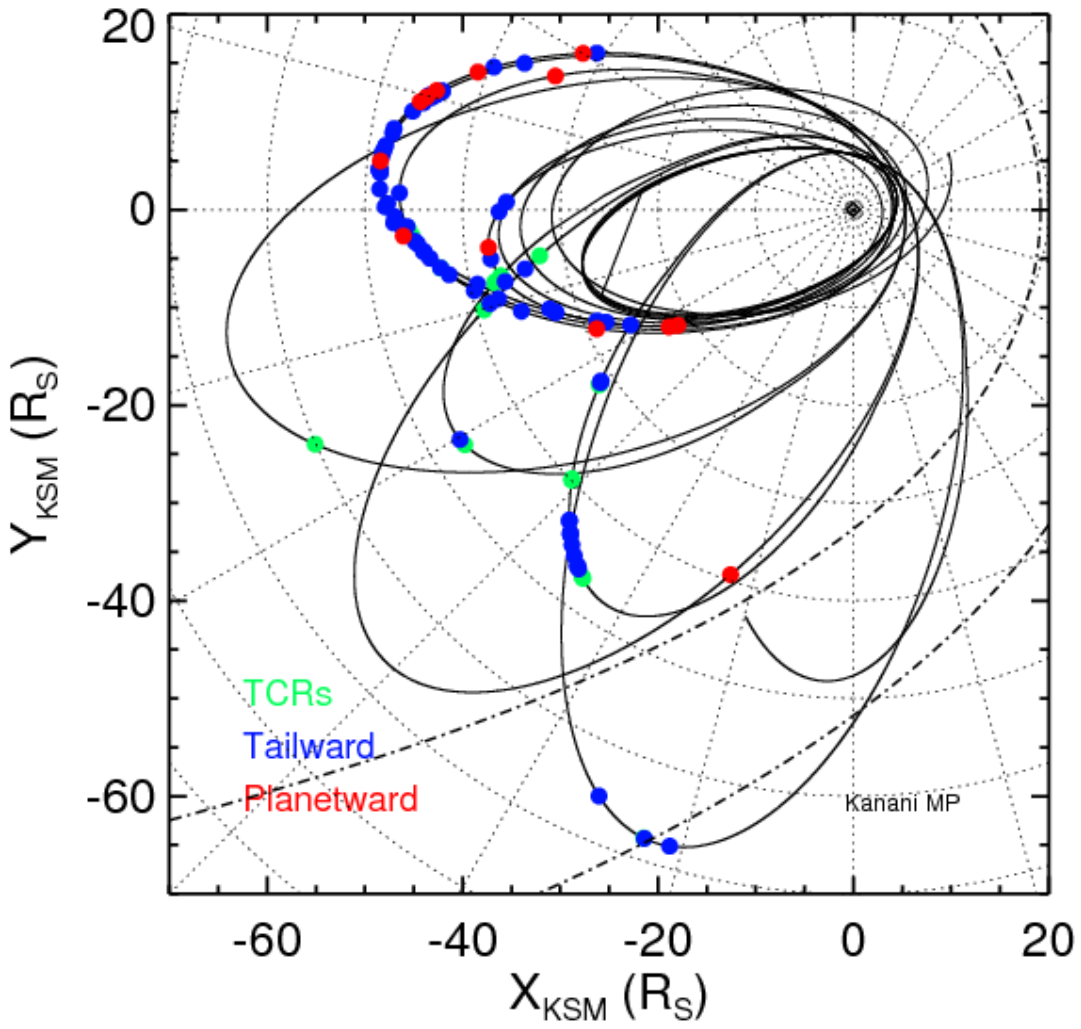

1520

1521 Figure 3: Cassini trajectory for 2006 day 18-291 in the Kronocentric Solar Magnetospheric
1522 (KSM) co-ordinate system. KSM is the kronian analogue of GSM where the X axis coincides
1523 with the direction to the Sun, the XZ plane contains the planetary dipole axis, and the Y
1524 component is azimuthal, positive toward dusk. Blue, red and green dots show the location of
1525 tailward and planetward-moving structures, and TCRs respectively. a)X-Y KSM view. The
1526 Kanani et al. [2010] model magnetopause is overplotted for solar wind dynamic pressures of
1527 0.1 and 0.01 nPa.

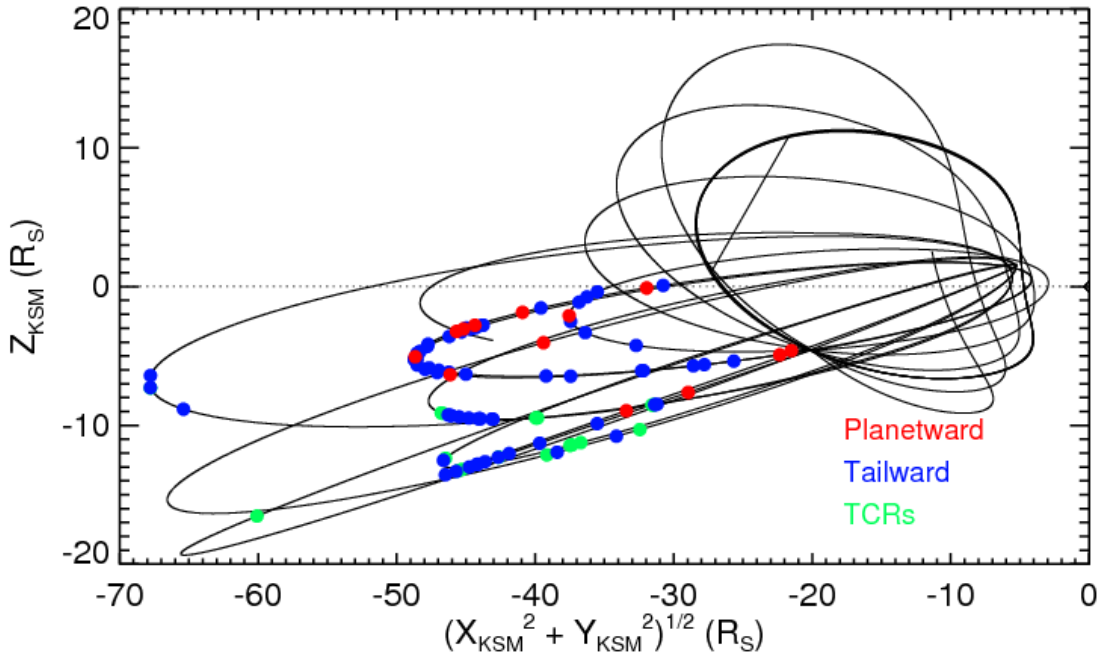

b) ρ-Z KSM view.

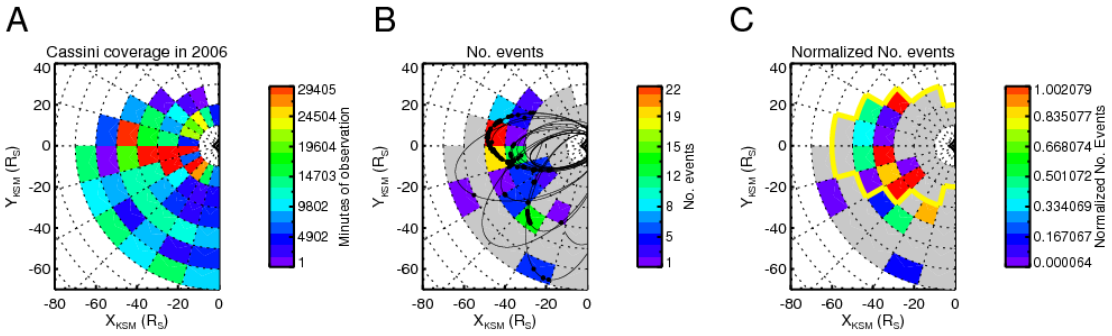

Figure 4: Colour-coded plots of Saturn's nightside showing the properties of particular radial distance and local time sectors. All plots are equatorial plane views with the Sun to the right. In all panels, white represents bins with no spacecraft coverage, and grey represents bins with trajectory coverage but no reconnection events. A) Plot showing the number of minutes the Cassini spacecraft spent on the nightside during 2006, in bins of 10 R_S in radial distance by 1 hour in local time. B) Plot showing the number of reconnection events seen in each sector by Cassini. The spacecraft trajectory during 2006 is overlaid, as are black points to illustrate the precise locations of tailward-moving plasmoids, TCRs and planetward-moving events. C) Plot showing the number of reconnection events normalized to observation time. Thick yellow lines surround bins symmetric either side of midnight where there was spacecraft coverage.

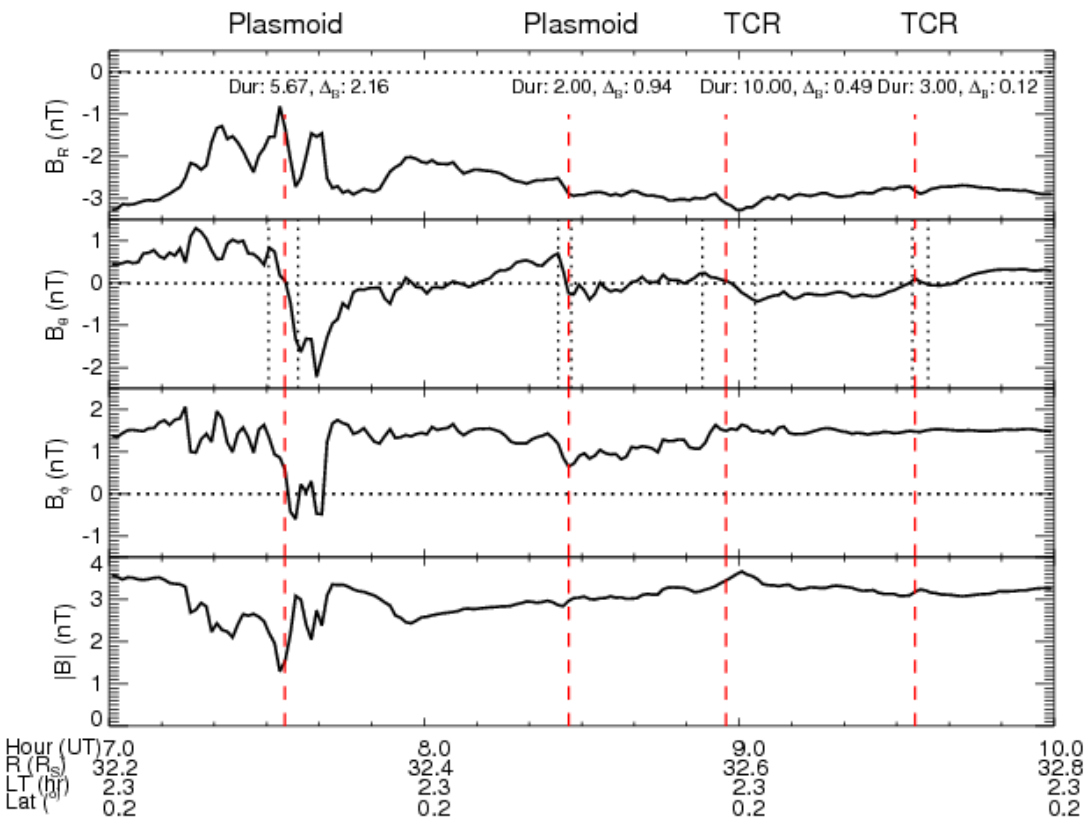

1543

1544 Figure 5: a) Cassini magnetic field data in KRTP co-ordinates for 2006 day 60 07:00-10:00. The
1545 positions of two plasmoids and two TCRs are marked with vertical lines, and the amplitude and
1546 duration in minutes of the signatures are listed in the top panel.

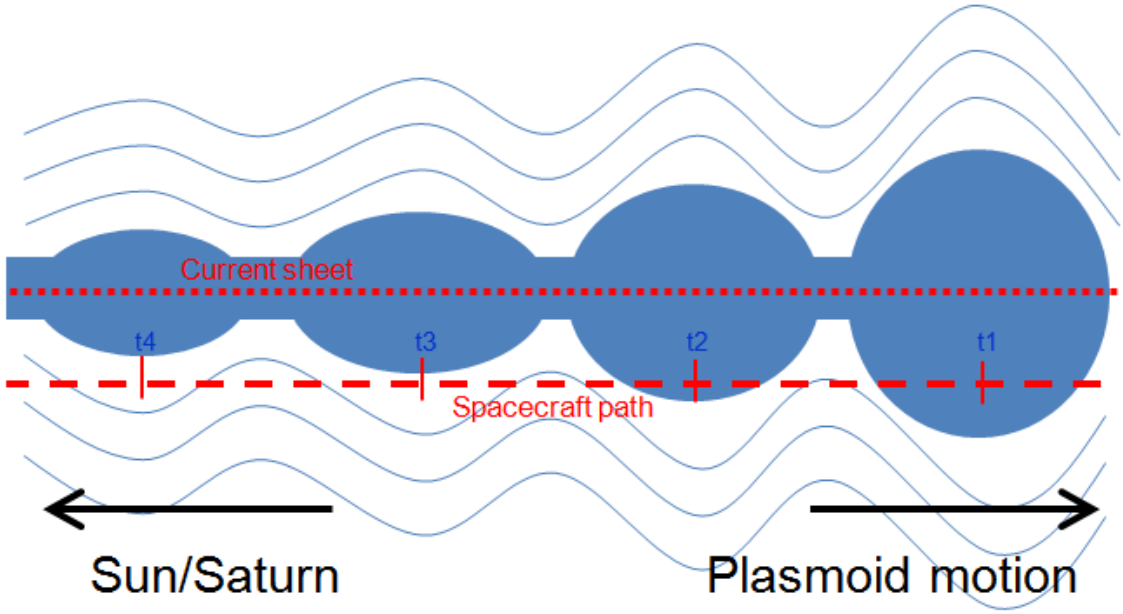

1547

1548 b) Schematic of expected geometry of the magnetotail during the passage of the plasmoids and TCRs

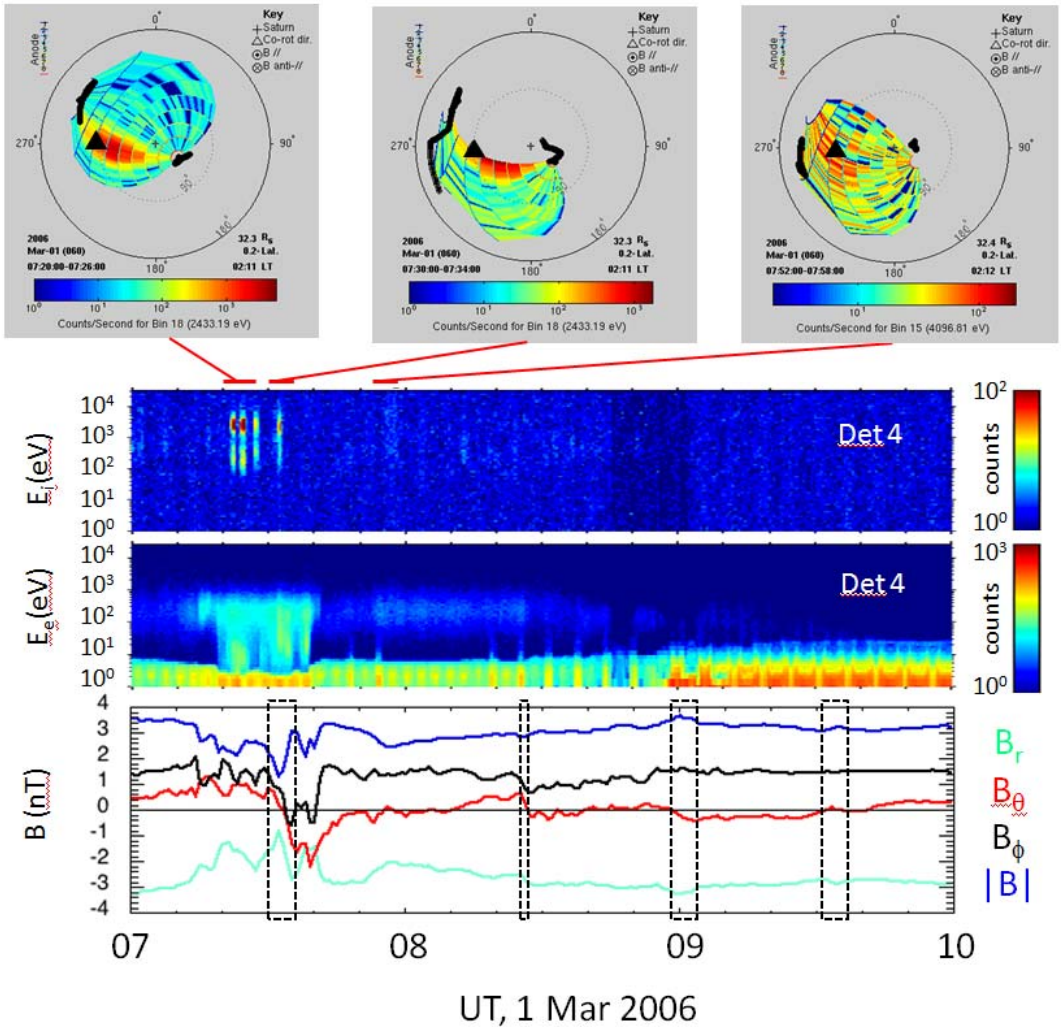

c) Plasma and magnetic field observations for two plasmoids and two TCRs identified on 1 Mar 2006. The bottom panel reproduces the magnetic field measurements in Figure 6a, while the two panels above show the color-coded count rate in the CAPS Ion Mass Spectrometer (above) and Electron Spectrometer (below) as a function of energy and time through the event. The black dashed boxes surround the intervals defined as the "duration" of the events from Figure 6a. The top row of panels shows all-sky images of the ion distribution at 2.4 keV (first two) and 4.1 keV (third). In this format, the look direction toward Saturn is in the center. The radial distance from the center is proportional to the polar angle of the viewing direction relative to Saturn's direction. Thus, the entire outer circle corresponds to the anti-Saturnward look direction, and the dashed circle halfway to the outer boundary indicates look directions that are 90° away from Saturn's direction. The azimuth in the plots (indicated by the angle markings around the circumference of the outer circle, given in degrees) corresponds to the azimuth of the look direction relative to a meridian containing the direction to Saturn and Saturn's spin (and magnetic dipole) axis, measured about the axis pointing toward Saturn. Thus, the corotation look direction (indicated by the filled triangle) lies at a polar angle of 90° and an azimuthal angle of 270°. Particles coming from the

direction of Saturn are seen at look directions interior to the dashed 90° circle, and particles flowing toward Saturn are seen at look directions exterior to that circle.

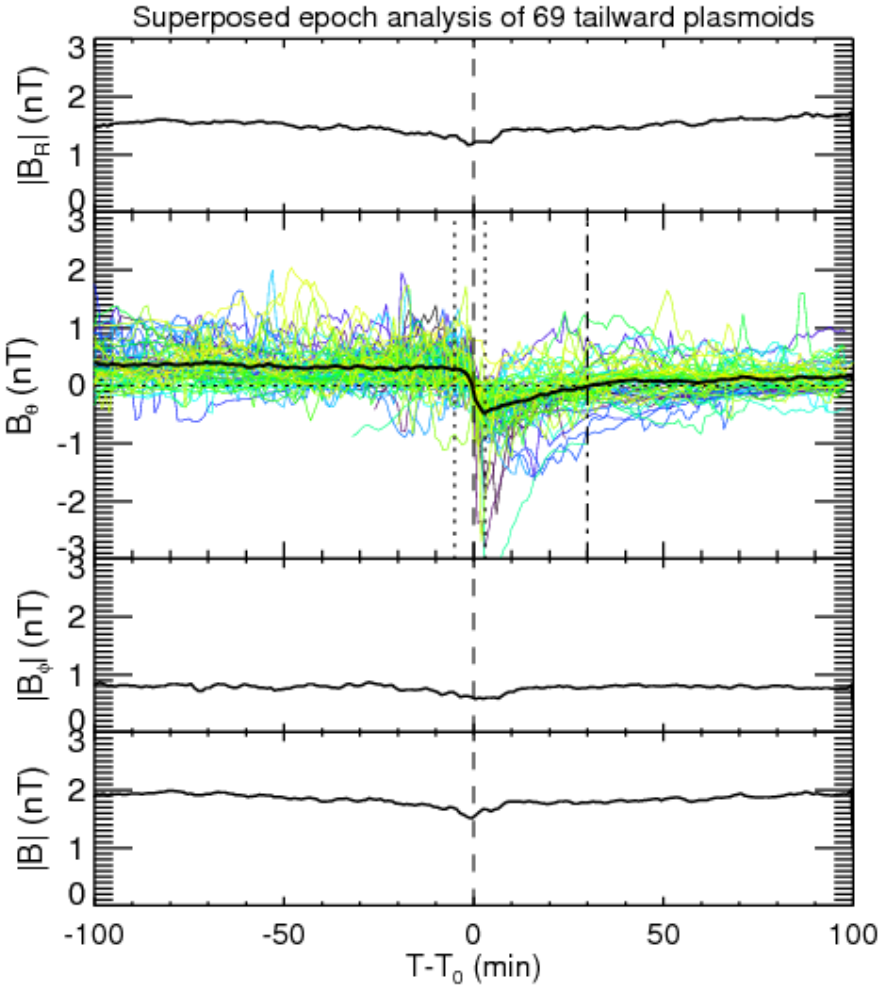

Figure 6: Superposed epoch analyses of (a) plasmoids. The second panel is twice the size and range of the other panels, and the coloured lines in the second panel show the individual traces for 69 events to illustrate the spread. The thick black line shows the average trace from the superposed epoch analysis. The vertical dotted lines at T=-5 min and T=+3 min bracket the central plasmoid passage time as determined from the superposed epoch analysis. The vertical dot-dashed line marks the end of the PPPS (27 minutes long).

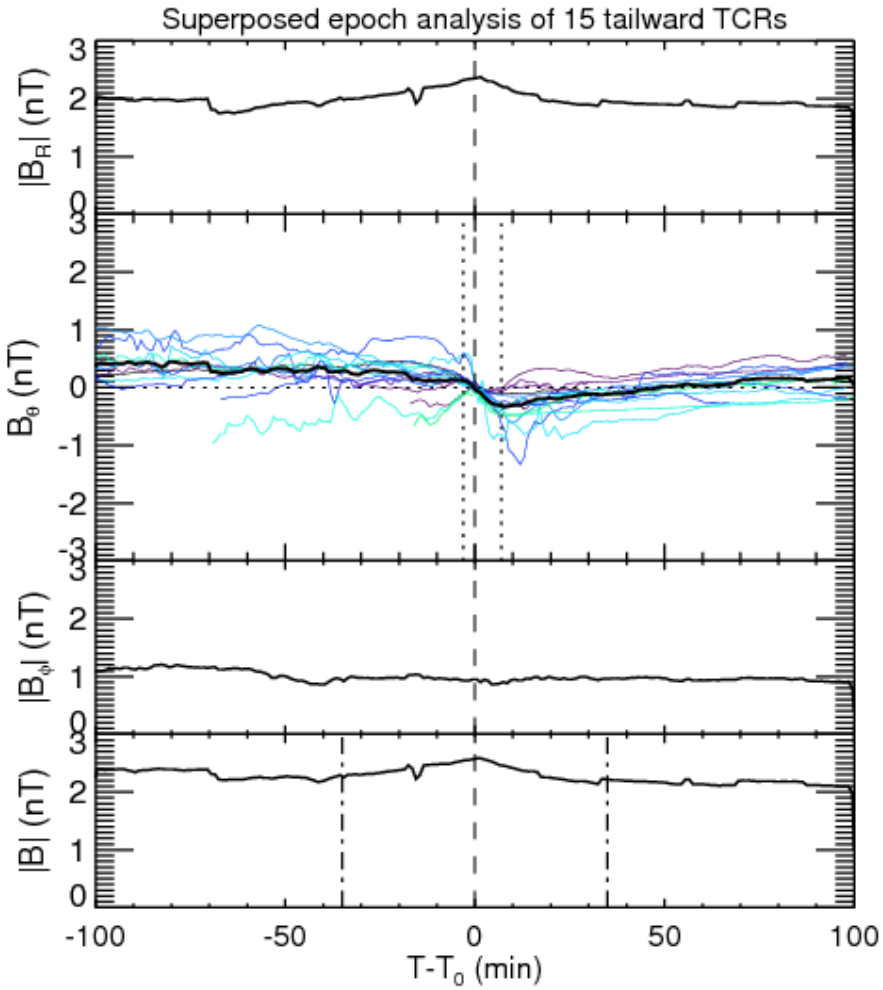

1577

1578 (b) TCRs in the same format as Figure 6a.

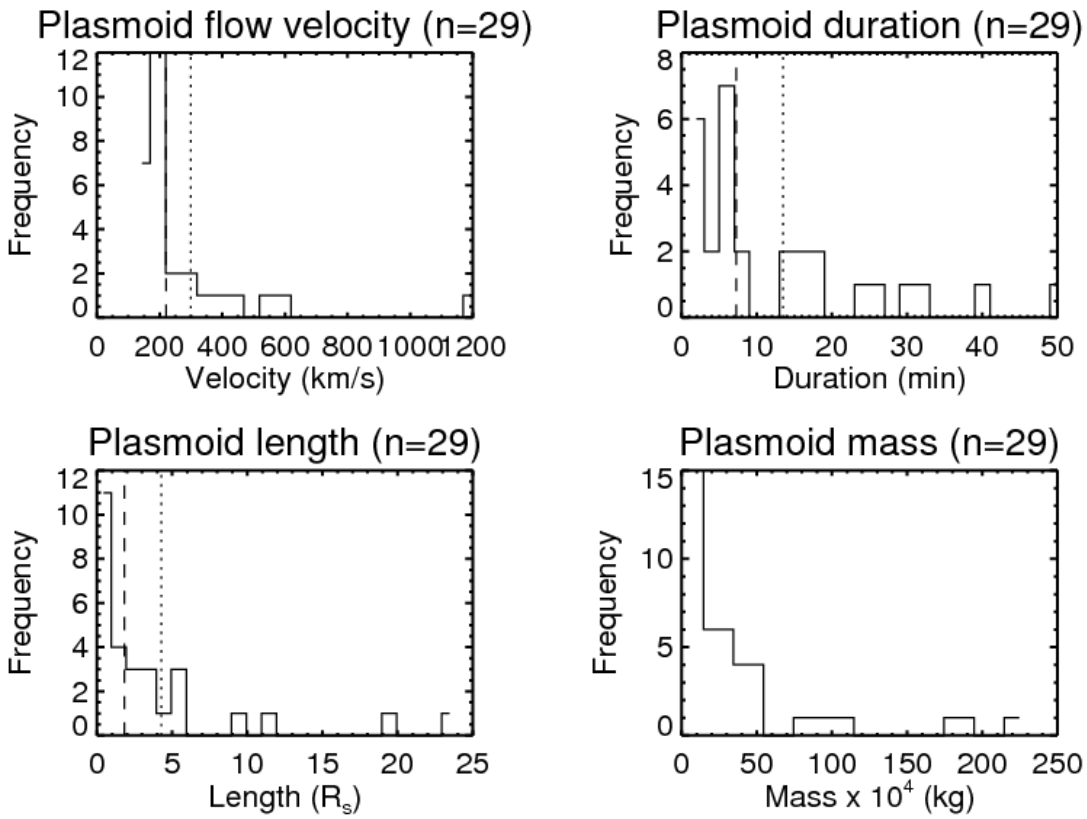

Figure 7: Histograms of plasmoid (a) flow velocity, (b) duration, (c) length, and (d) mass for the 29 plasmoid for which magnetometer and plasma data were available. These represent a subset of the total of 69 plasmoids listed in Table 1. The vertical dotted lines are the mean values and the vertical dashed lines are the medians.

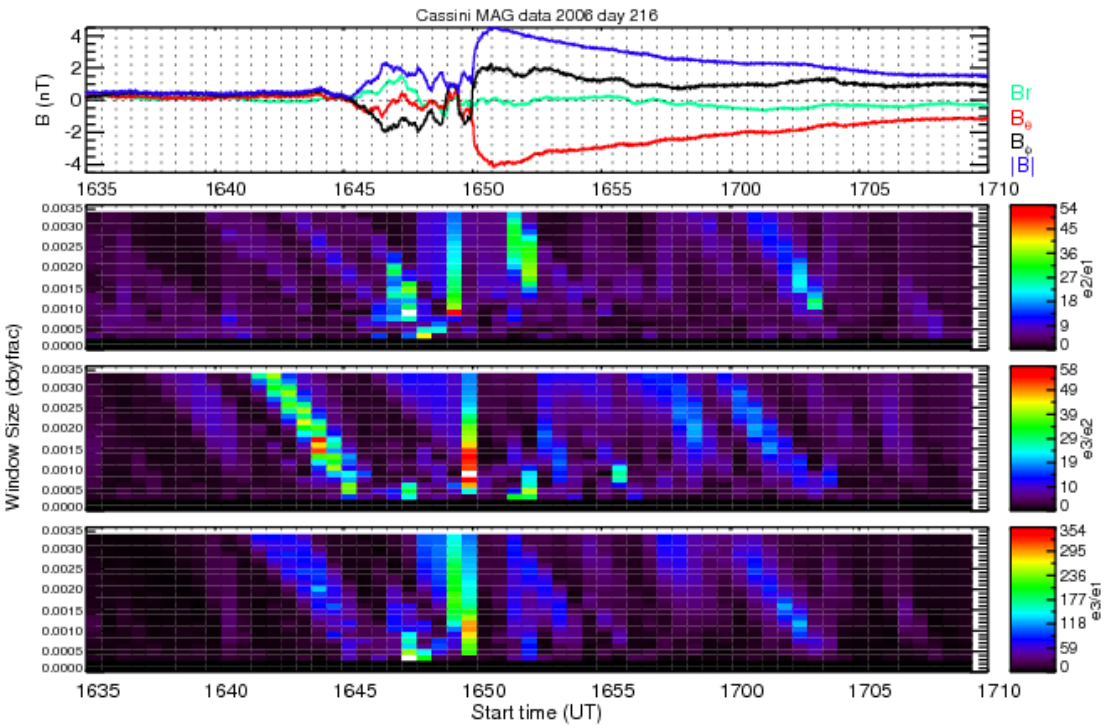

Figure 8: Example of MVA optimization technique applied to magnetometer data from 2006 day 216 16:35-17:10. The top panel shows the magnetic field data in KRTP co-ordinates, colour-coded according to the legend on the top right. The next three panels show the results of the application of a sliding window for MVA. On the x-axis are the various start times of the MVA windows (also denoted by the vertical dashed lines in the top panel). The y-axis shows the window sizes, applied from each start point. Thus the plots are comprised of a selection of boxes which represent various start times and window lengths over which MVA was applied. The colours (coded as per the colour bars on the right-hand side of the plots), show the eigenvalue ratios, for e2/e1, e3/e2, e3/e1 respectively. B1 is the direction of minimum variance, and B2 and B3 refer to the intermediate and maximum variance directions.

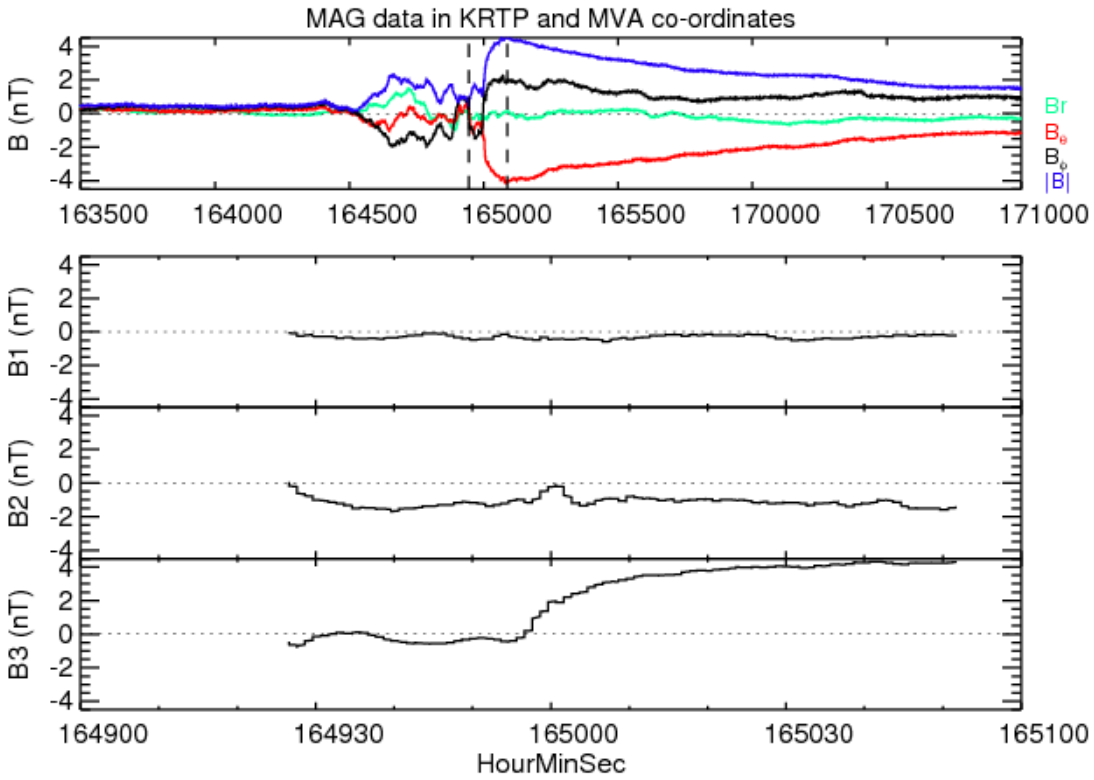

Figure 9a: Results of minimum variance analysis on an interval of magnetic field data from 2006 day 216. The top panel shows the magnetic field in KRTP co-ordinates. The vertical dashed lines denote the interval over which MVA was applied. The selection of this interval was guided by the optimisation technique outlined in Figure 8. The lower three panels show the field minimum, intermediate and maximum variance directions

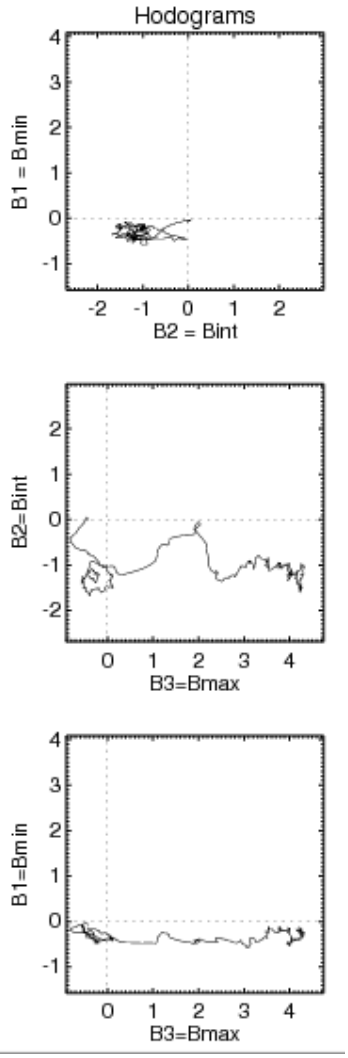

Figure 9b: Field hodograms for the interval selected in Figure 9a.

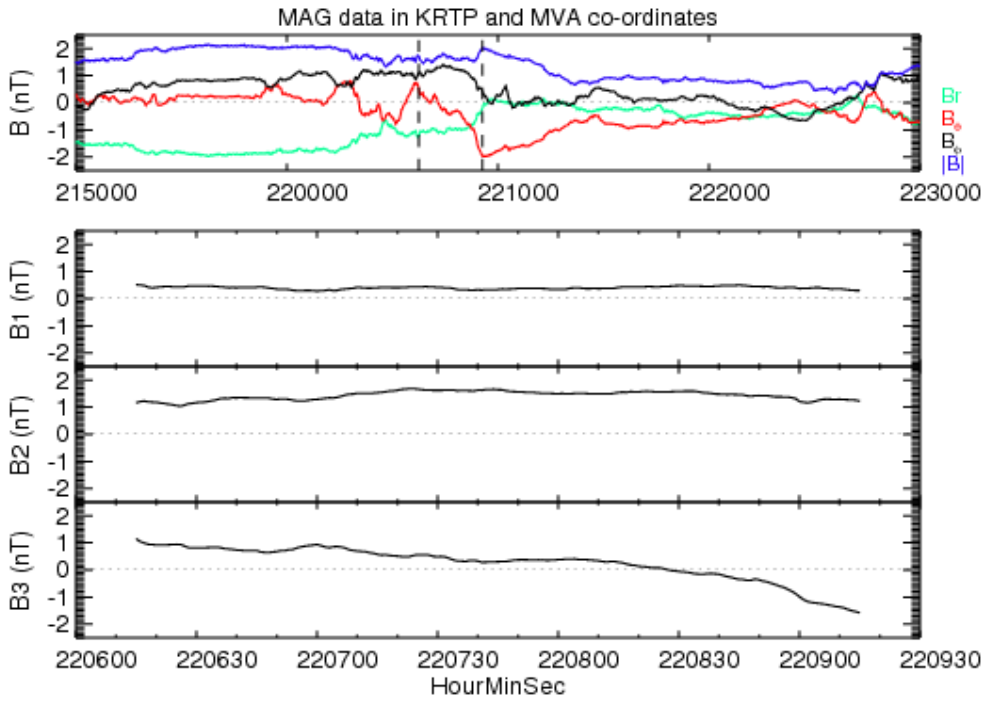

Figure 10a: Magnetic field in KRTP and MVA co-ordinates surrounding a plasmoid observation on 2006 day 63 at 22:07. The figure is in the same format as Figure 9a.

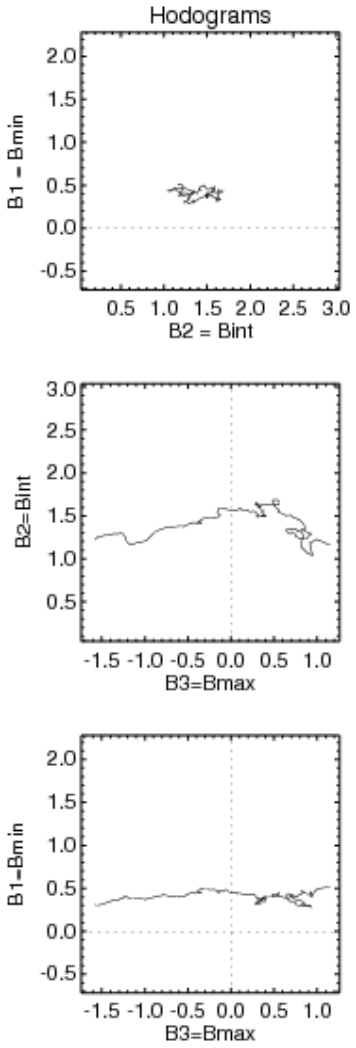

Figure 10b: Field hodograms corresponding to the interval depicted in Figure 10a.

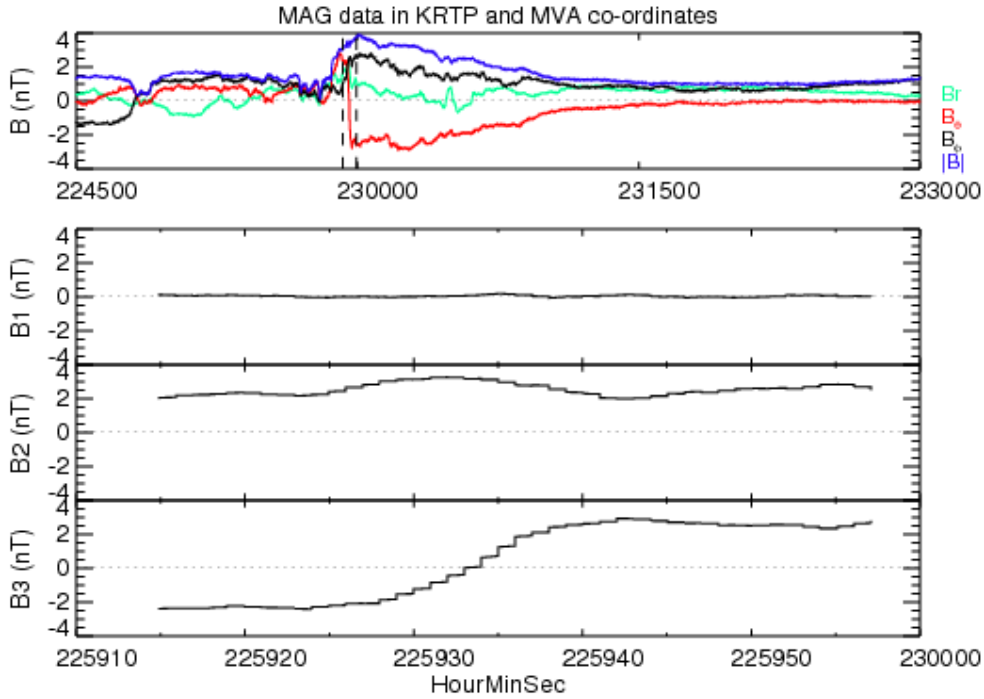

Figure 11a: Magnetic field in KRTP and MVA co-ordinates surrounding a plasmoid observation on 2006 day 63 22:59. The figure is in the same format as Figure 9a.

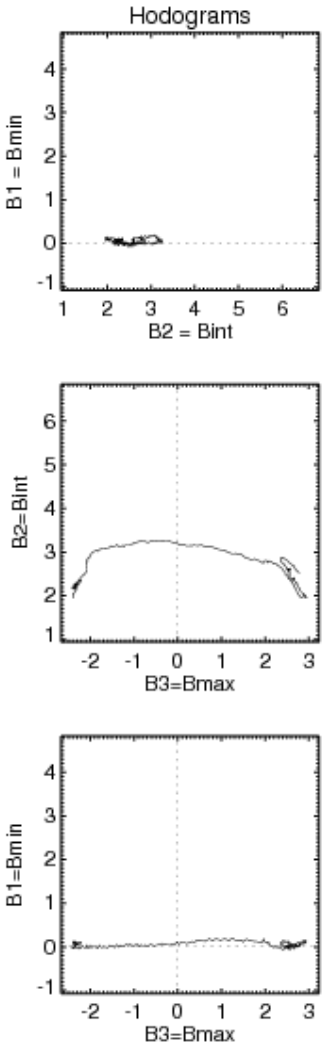

b) Field hodograms corresponding to the interval depicted in Figure 11a.

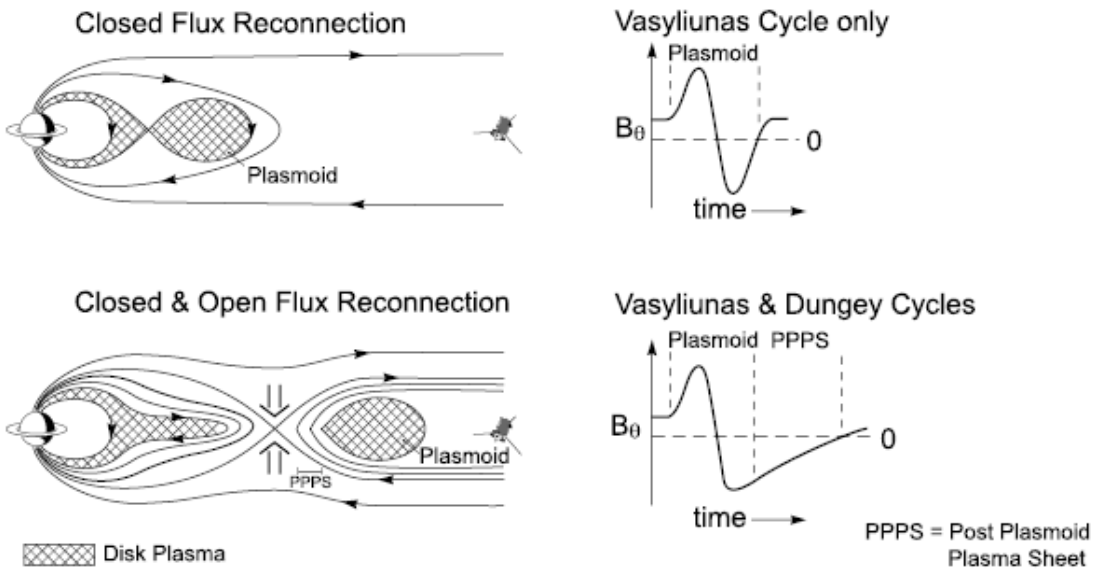

Figure 12: a) Schematic of the expected field signatures for reconnection on closed and open field lines

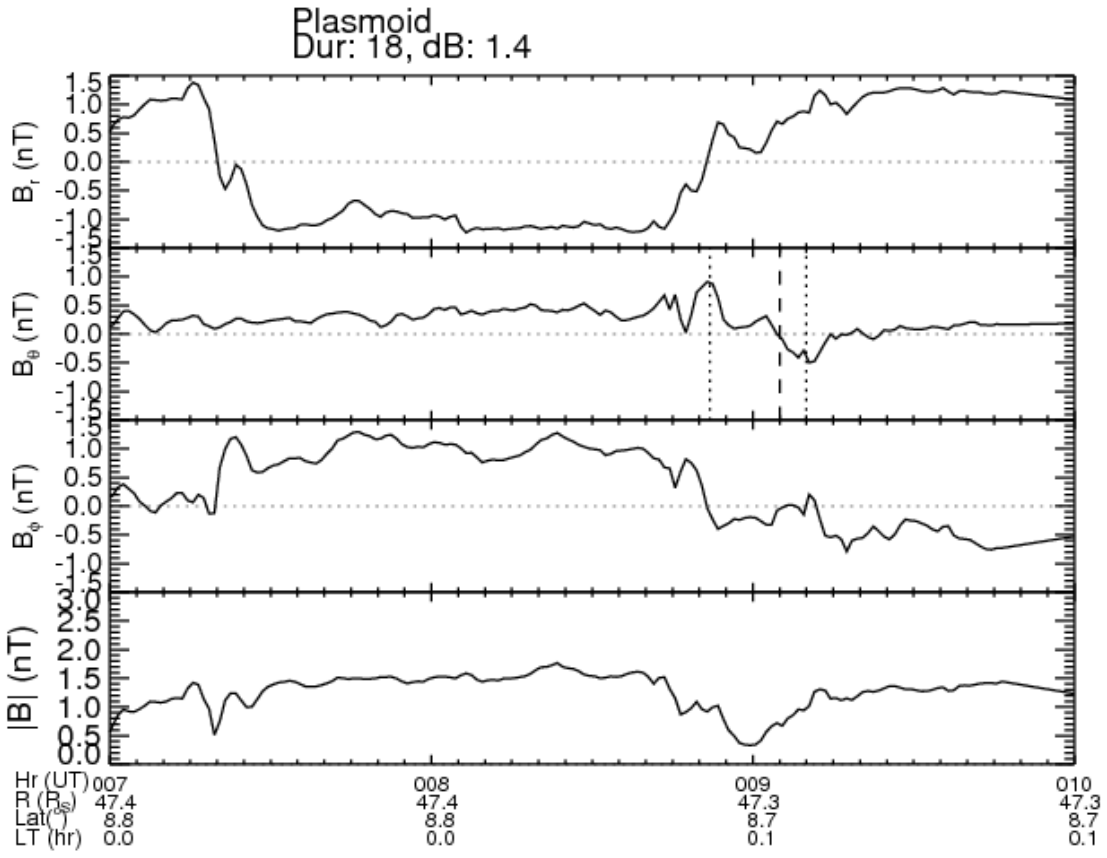

1625 b) Cassini magnetometer data from 2006 day 243 07:00-10:00. A plasmoid was observed at
1626 09:05. The central event time (where B_θ) goes through zero, is marked by the vertical dashed
1627 line, while vertical dotted lines either side of this mark the start and end points of the event.

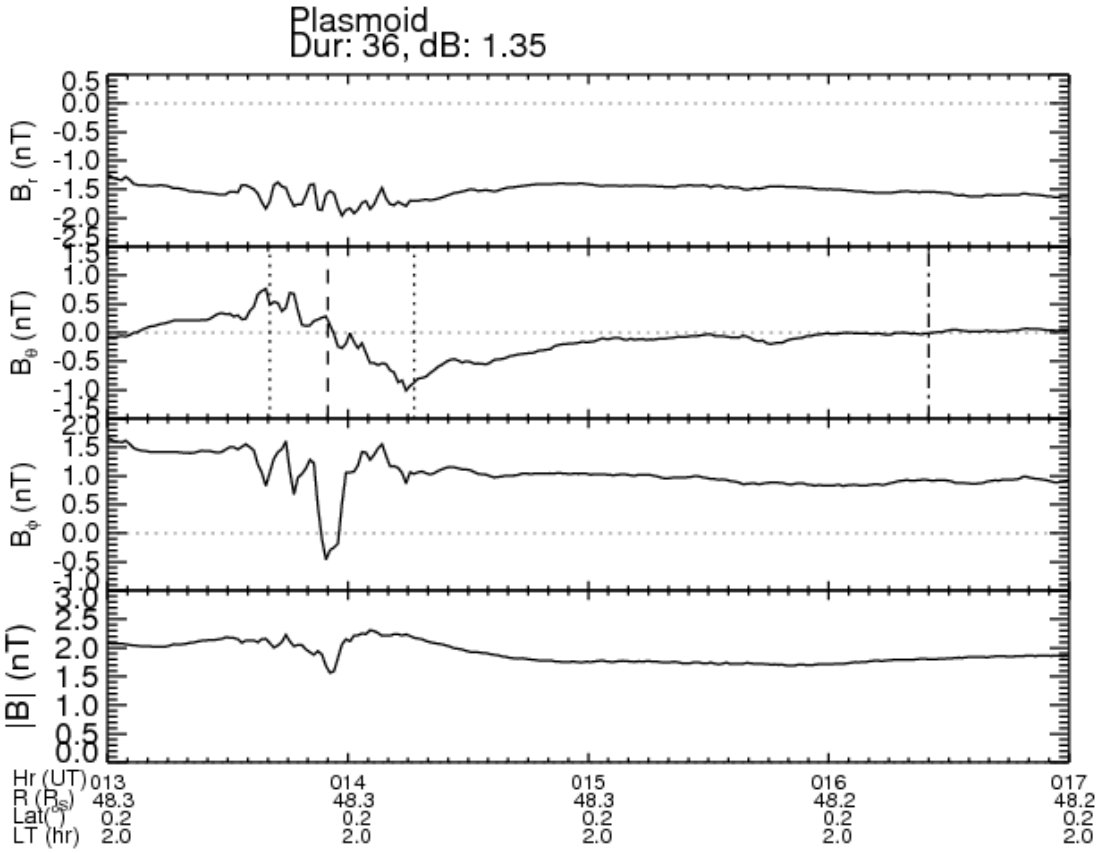

1628

1629 c) Cassini magnetometer data from 2006 day 131 13:00-17:00 in the same format as Figure
1630 12b. The vertical dot-dashed line marks the end of the PPPS.

1631

1632

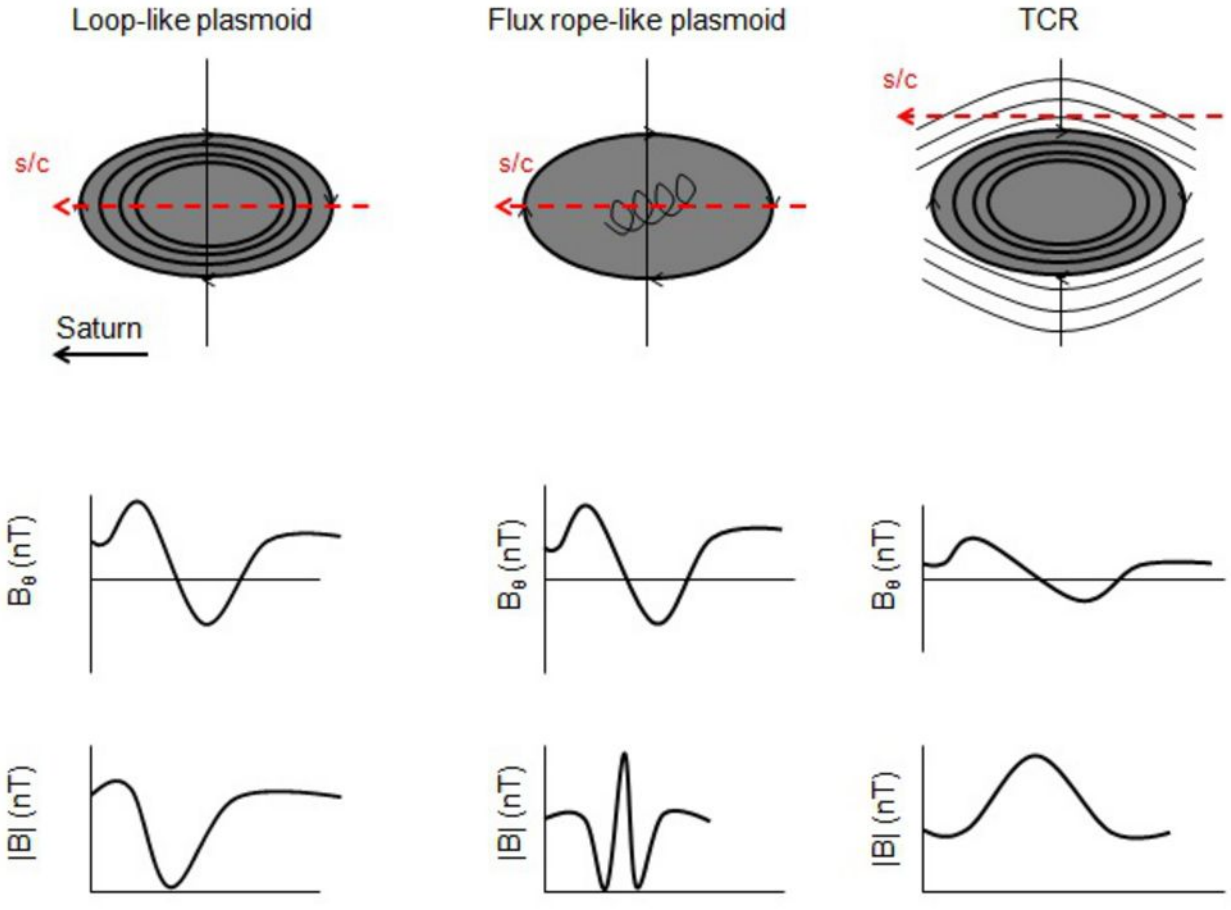
Loop-like plasmoid
Flux rope-like plasmoid
TCR
s/c
s/c
s/c
Saturn
B_θ (nT)
B_θ (nT)
B_θ (nT)
|B| (nT)
|B| (nT)
|B| (nT)

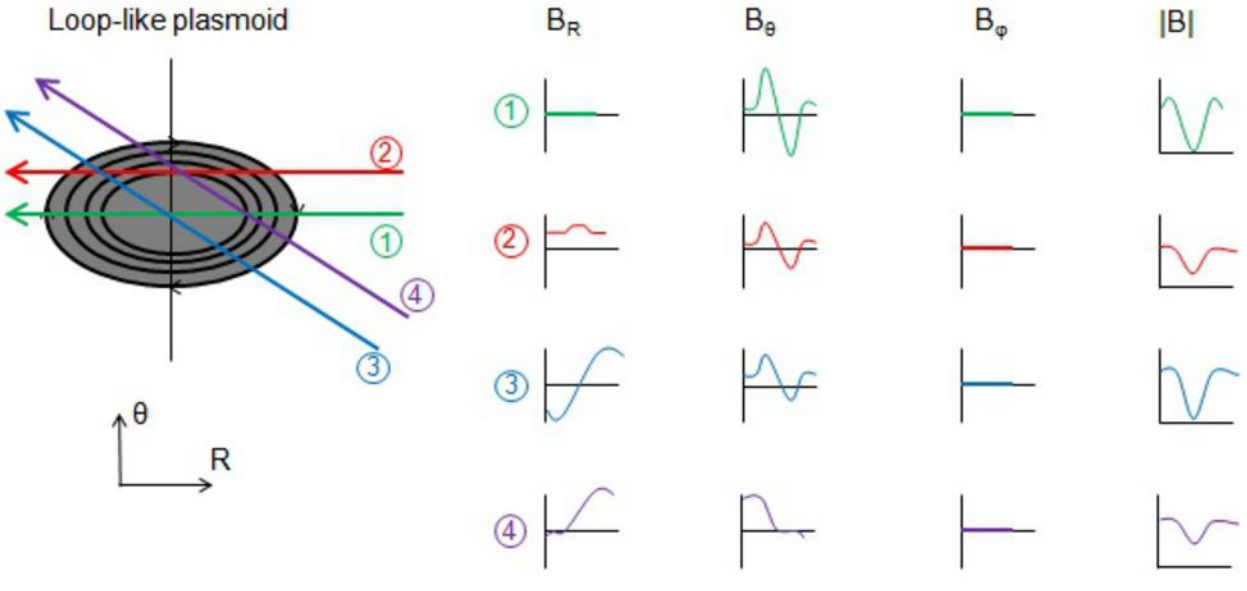
Loop-like plasmoid
B_R
B_θ
B_φ
|B|
①
②
③
④
θ
R

Flux rope-like plasmoid

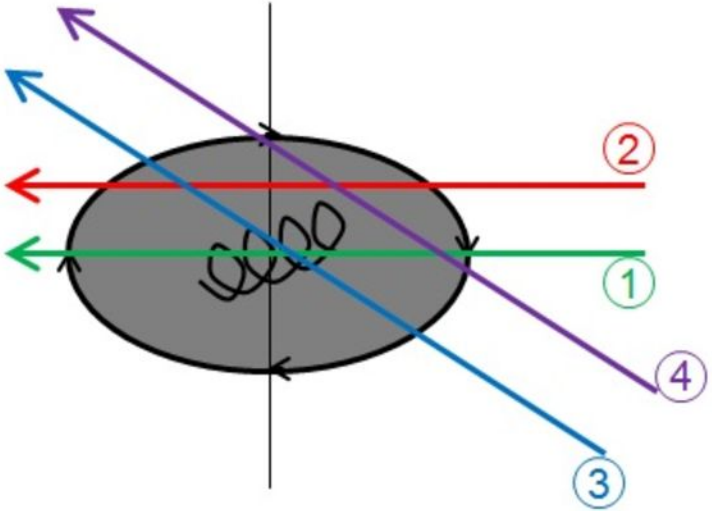

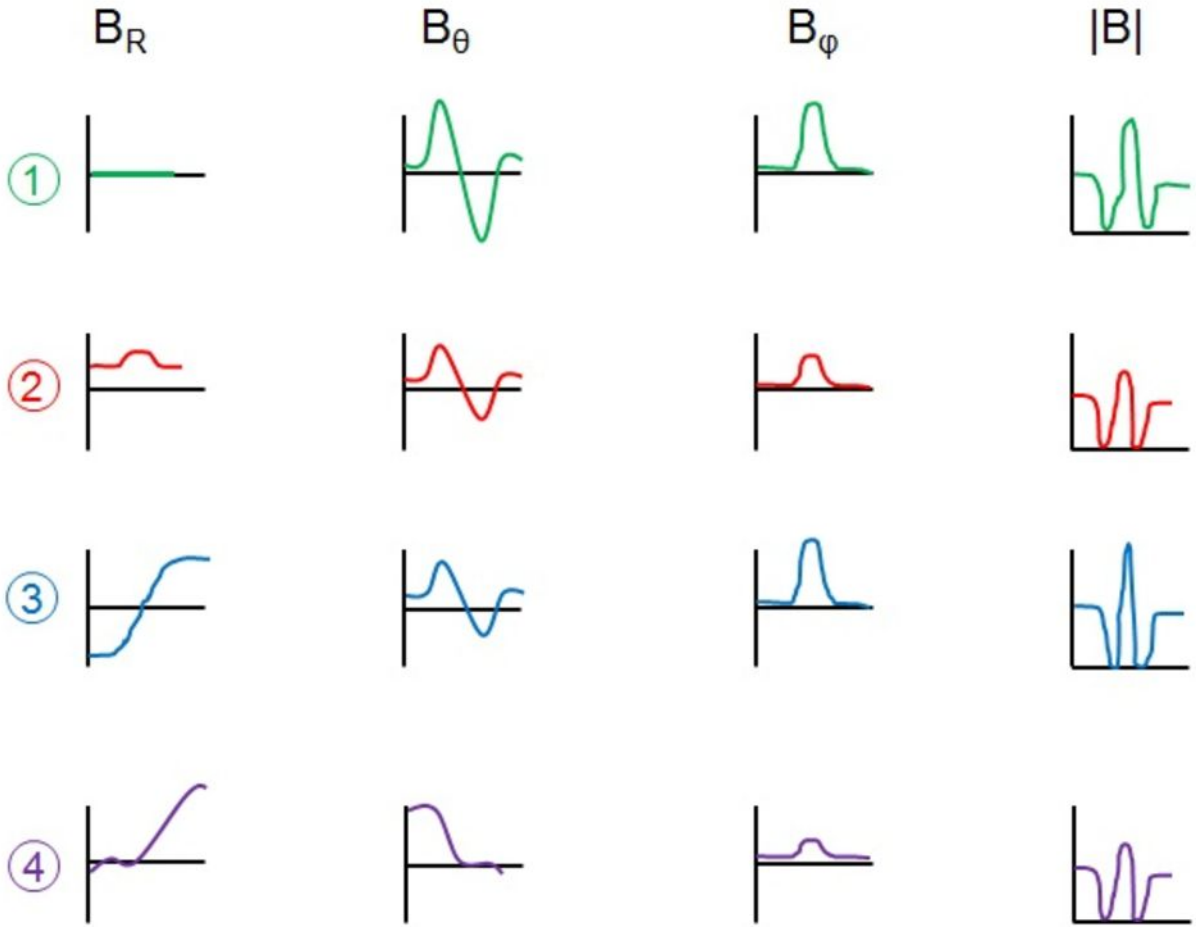

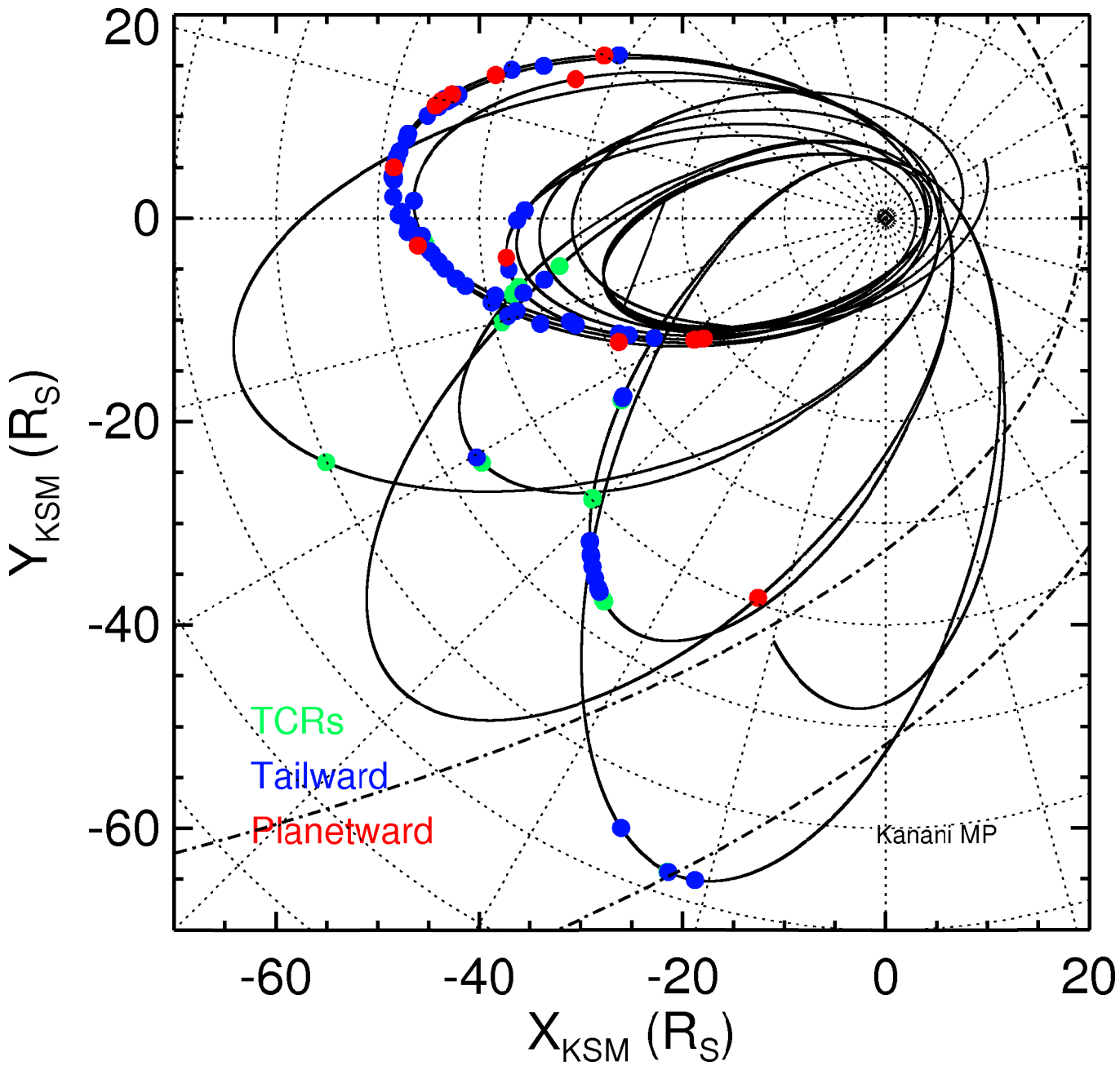
20
0
-20
-40
-60
Y_{KSM} (R_S)
-60
-40
-20
0
20
X_{KSM} (R_S)
TCRs
Tailward
Planetward
Kanani MP

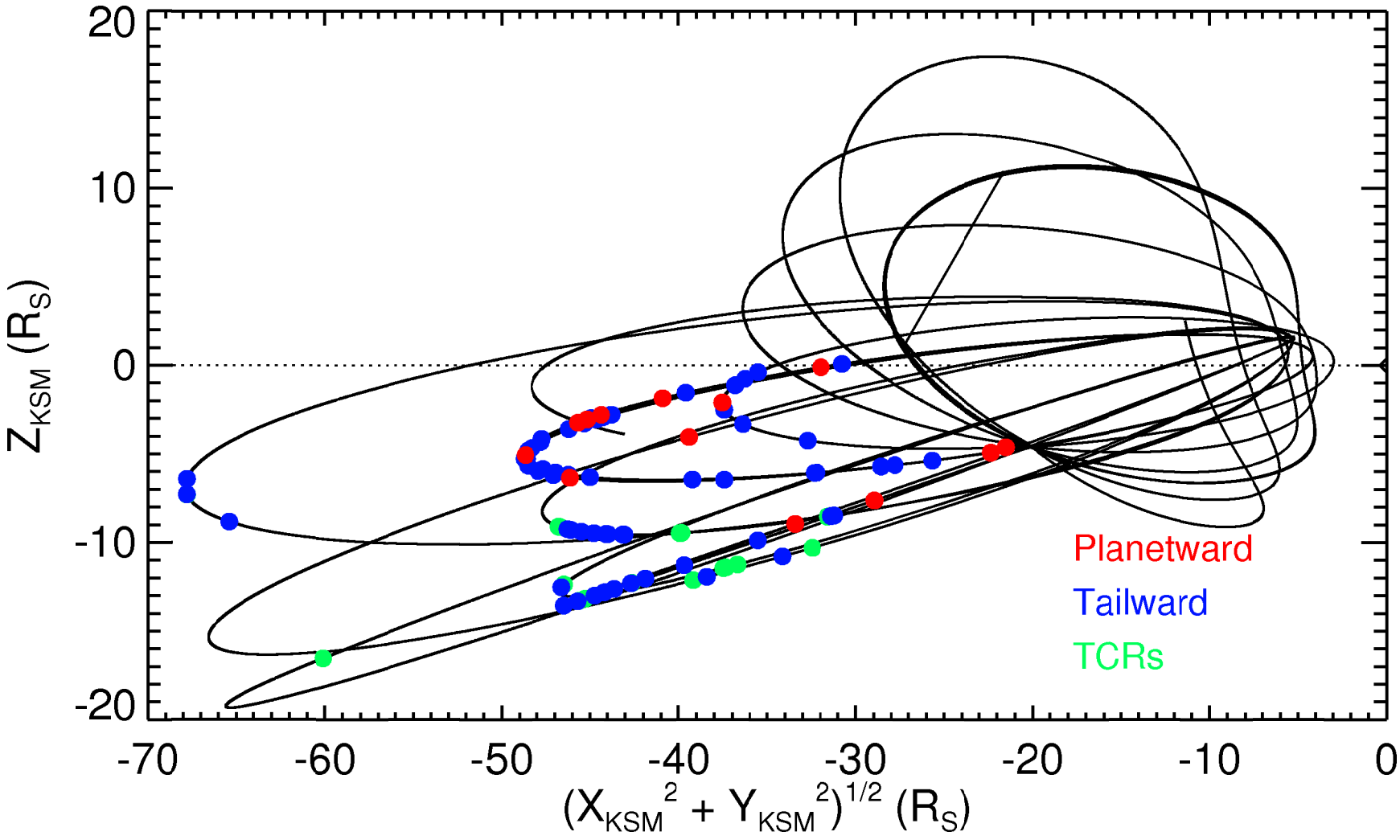
20
10
0
-10
-20
-70
-60
-50
-40
-30
-20
-10
0
Z_{KSM} (R_S)
$(X_{KSM}^2 + Y_{KSM}^2)^{1/2}$ (R_S)
Planetward
Tailward
TCRs

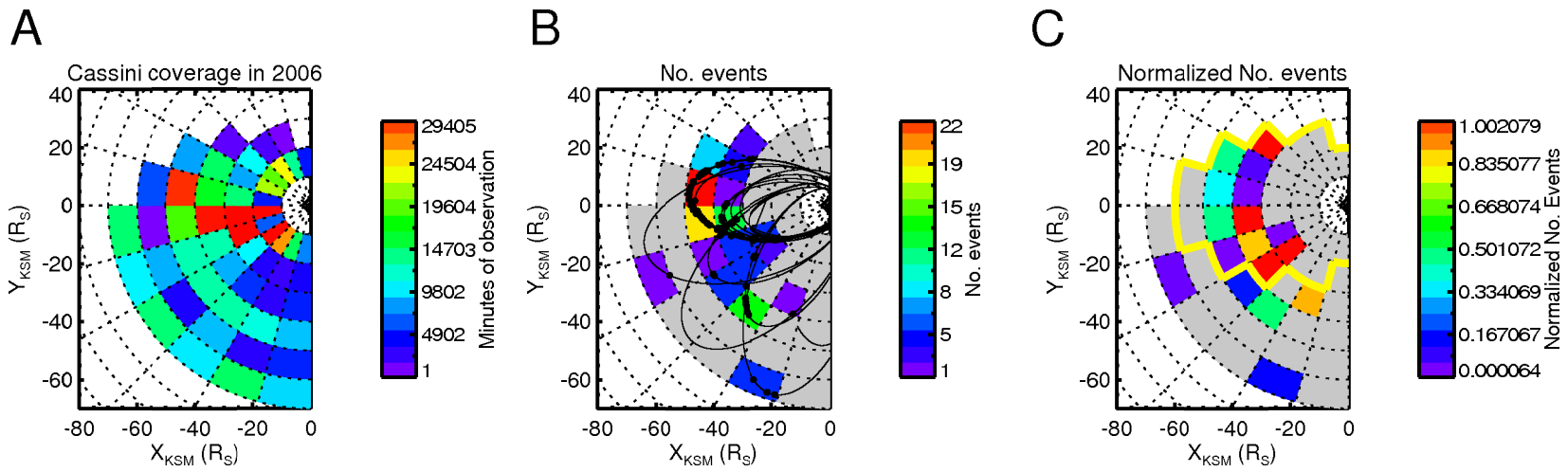
A
Cassini coverage in 2006
40
20
0
-20
-40
-60
-80 -60 -40 -20 0
Y_{KSM} (R_S)
X_{KSM} (R_S)
29405
24504
19604
14703
9802
4902
1
Minutes of observation
B
No. events
22
19
15
12
8
5
1
No. events
C
Normalized No. events
1.002079
0.835077
0.668074
0.501072
0.334069
0.167067
0.000064
Normalized No. Events

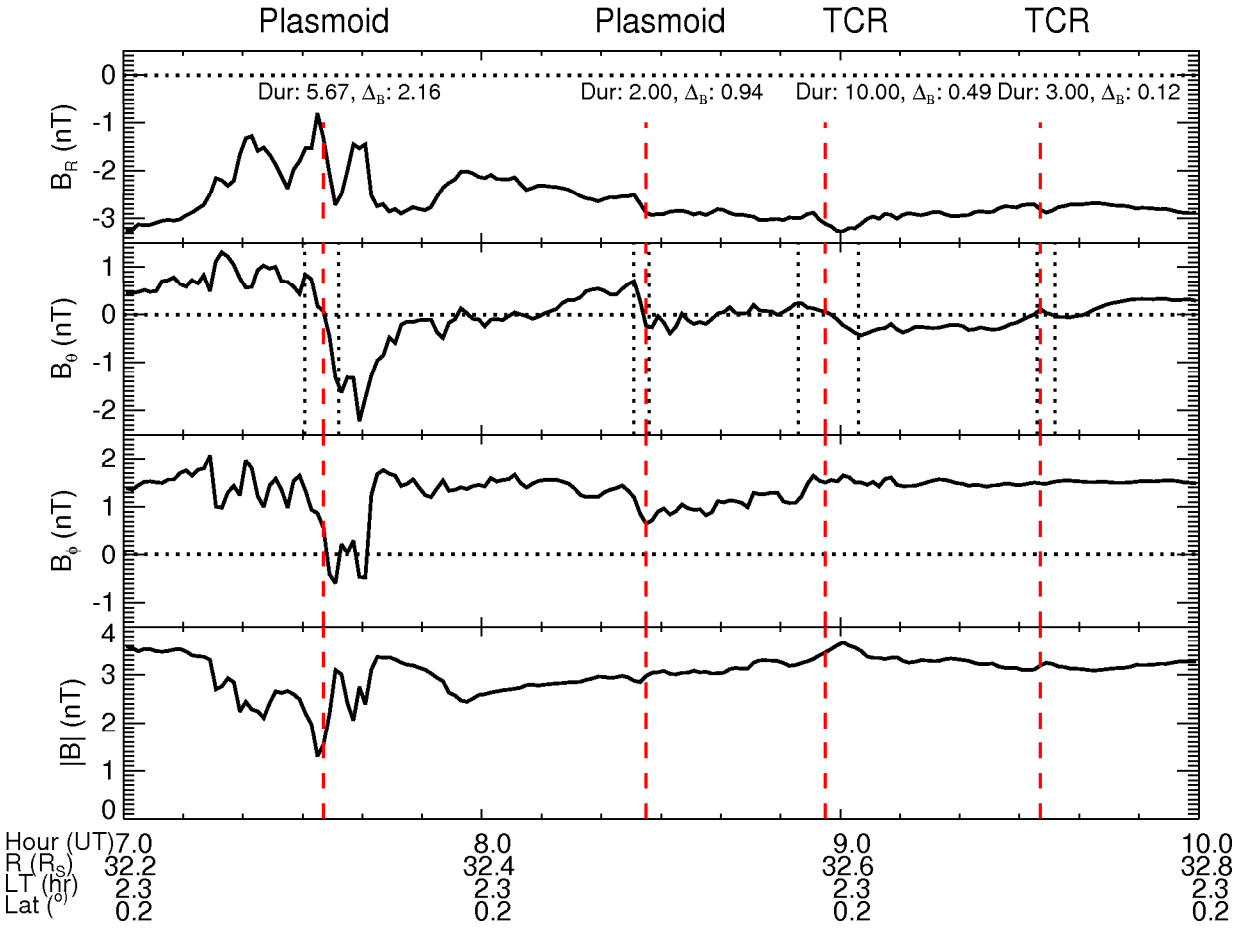
Plasmoid
Plasmoid
TCR
TCR
Dur: 5.67, Δ_B: 2.16
Dur: 2.00, Δ_B: 0.94
Dur: 10.00, Δ_B: 0.49
Dur: 3.00, Δ_B: 0.12
B_R (nT)
B_θ (nT)
B_ϕ (nT)
|B| (nT)
Hour (UT) 7.0 8.0 9.0 10.0
R (R_S) 32.2 32.4 32.6 32.8
LT (hr) 2.3 2.3 2.3 2.3
Lat (°) 0.2 0.2 0.2 0.2

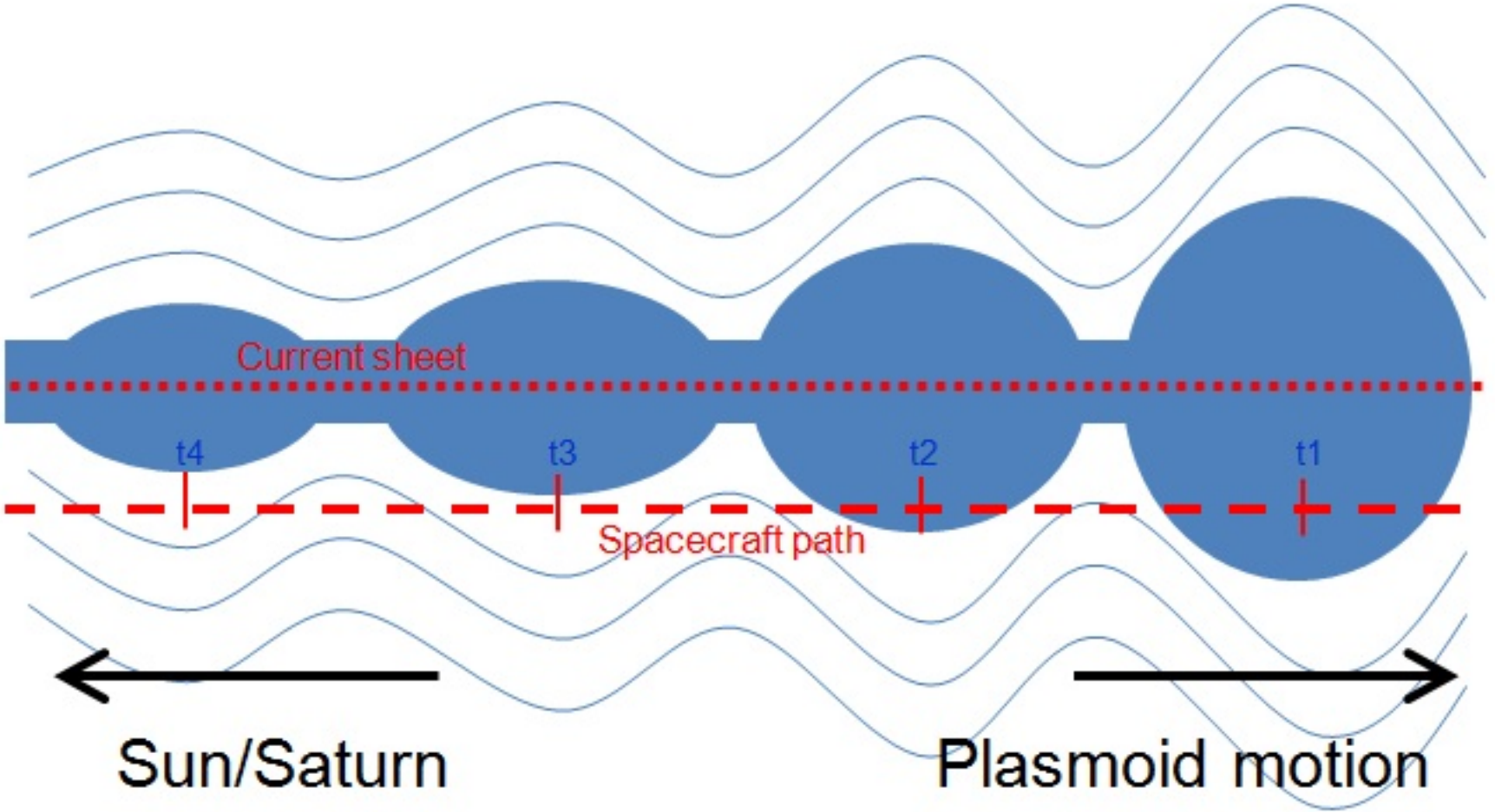
Current sheet
t4
t3
t2
t1
Spacecraft path
Sun/Saturn
Plasmoid motion

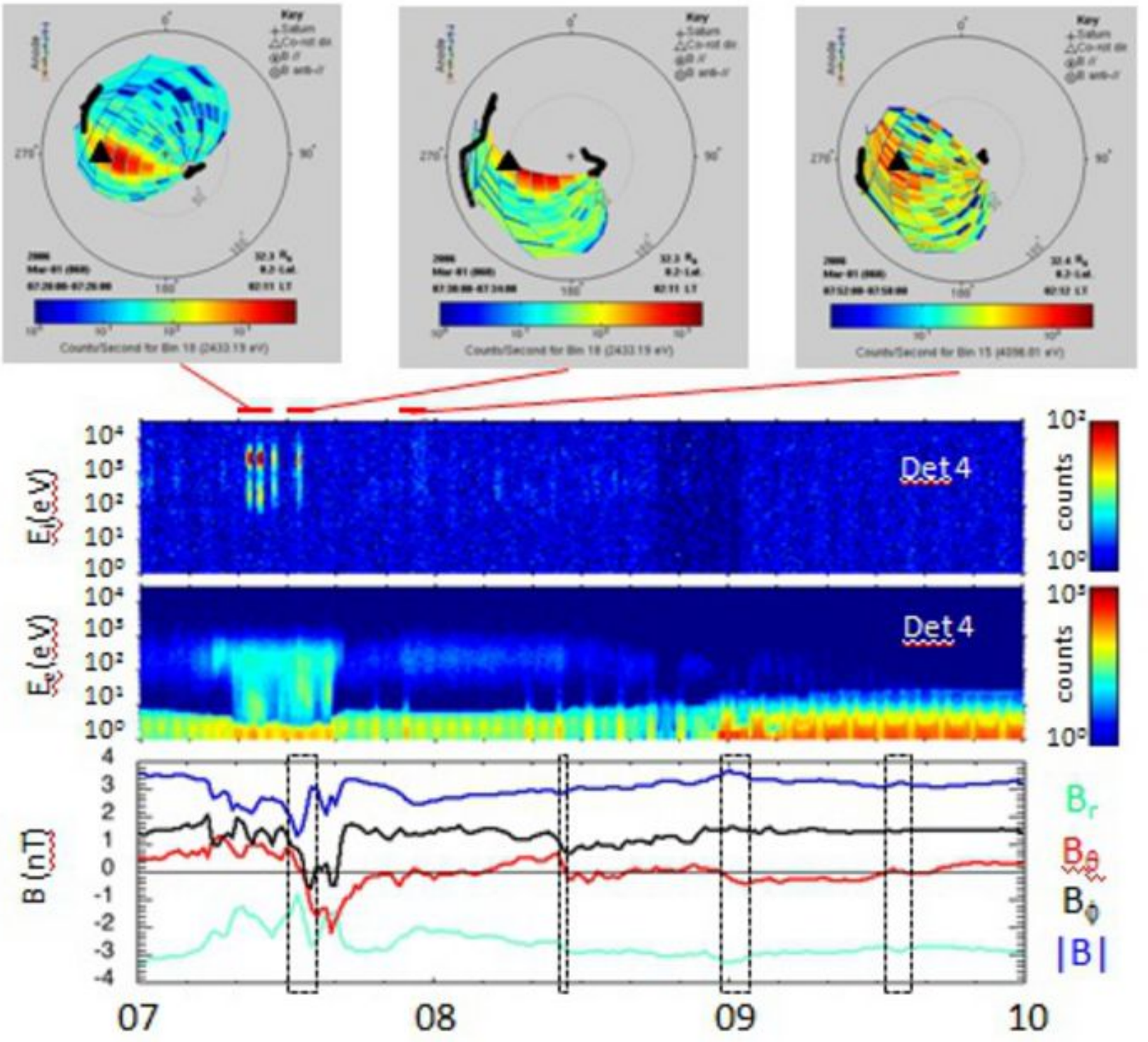
Det 4
Det 4
E_i(eV)
E_e(eV)
counts
counts
B (nT)
B_r
B_θ
B_ϕ
|B|
07
08
09
10
UT, 1 Mar 2006

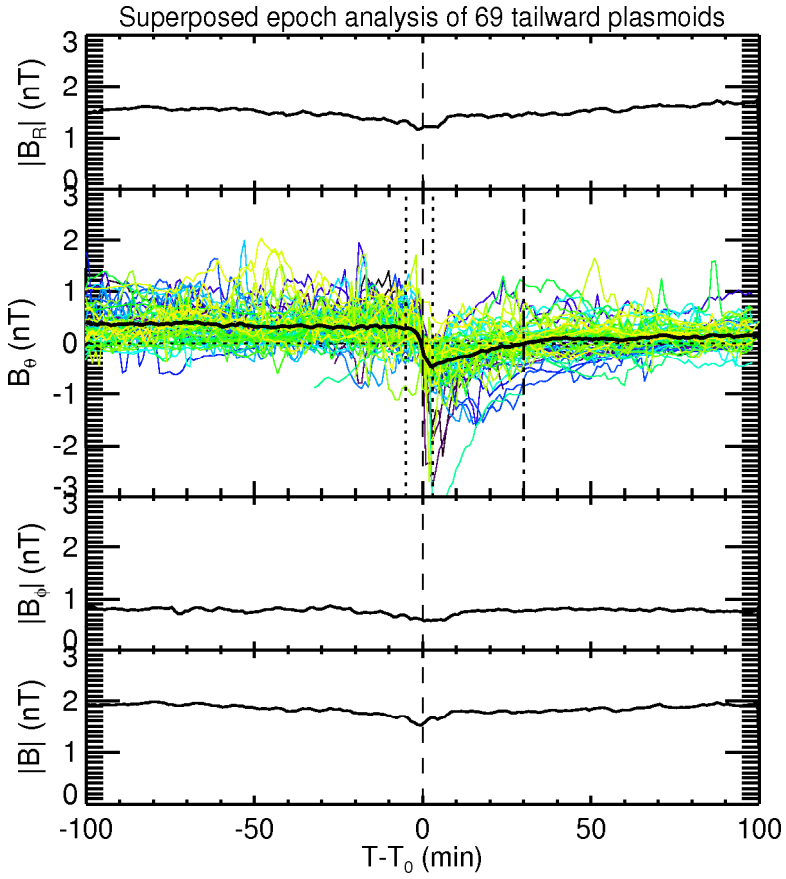
Superposed epoch analysis of 69 tailward plasmoids
|B_R| (nT)
B_θ (nT)
|B_φ| (nT)
|B| (nT)
T-T_0 (min)
-100
-50
0
50
100

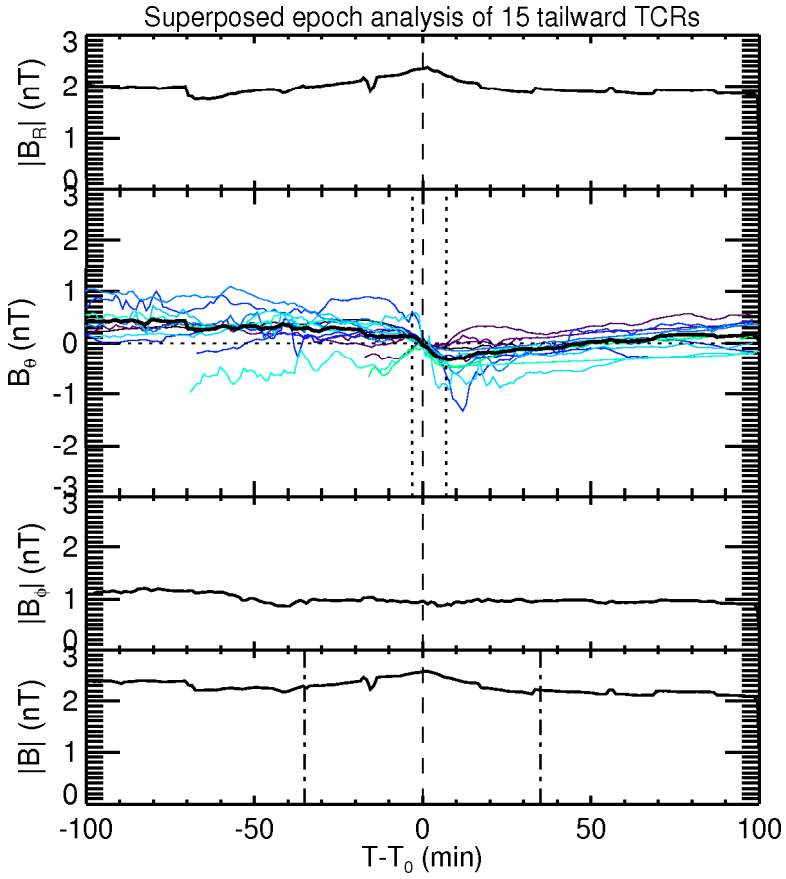
Superposed epoch analysis of 15 tailward TCRs
|B_R| (nT)
B_θ (nT)
|B_φ| (nT)
|B| (nT)
T-T_0 (min)

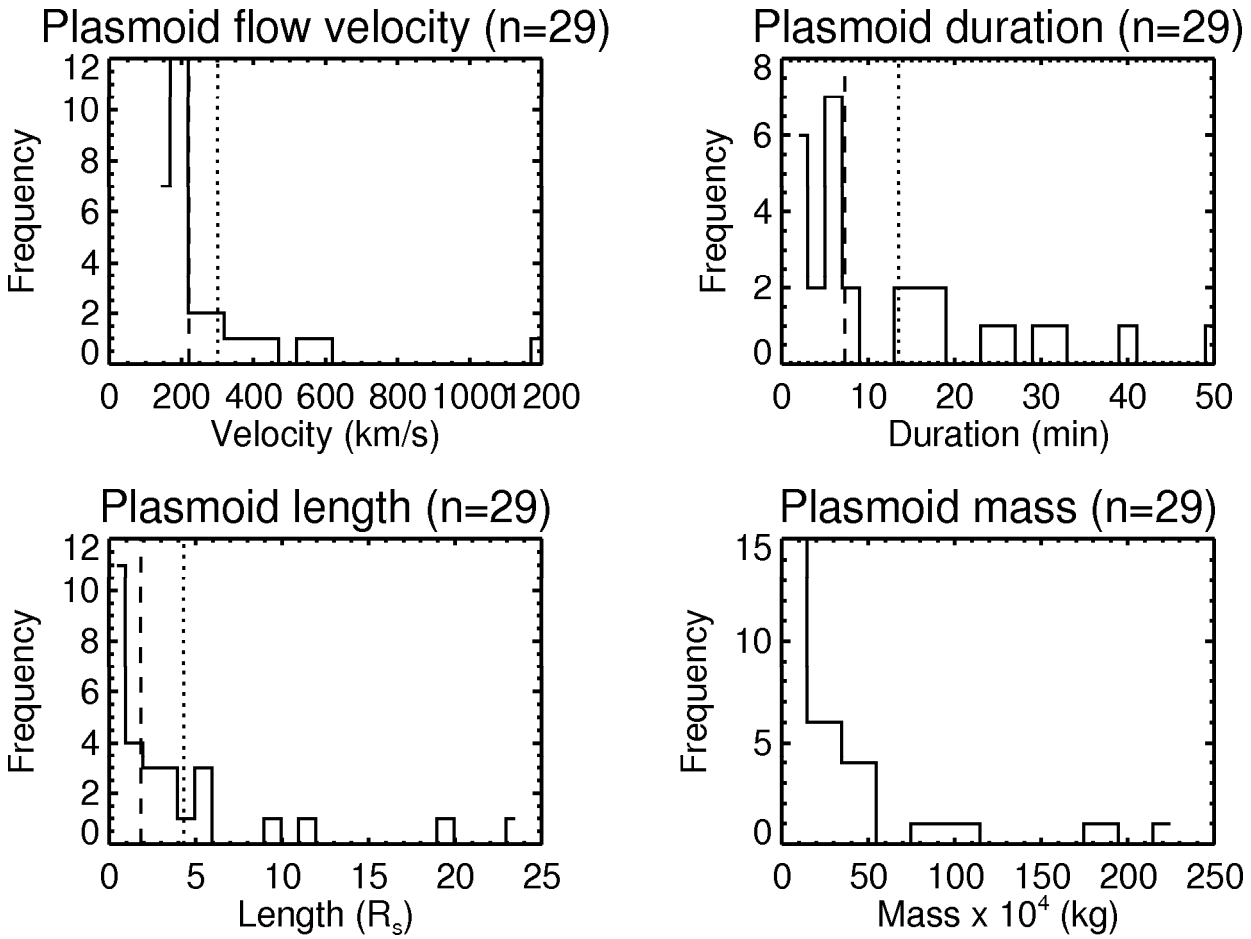
Plasmoid flow velocity (n=29)
Frequency
Velocity (km/s)
Plasmoid duration (n=29)
Frequency
Duration (min)
Plasmoid length (n=29)
Frequency
Length (R_s)
Plasmoid mass (n=29)
Frequency
Mass x 10^4 (kg)

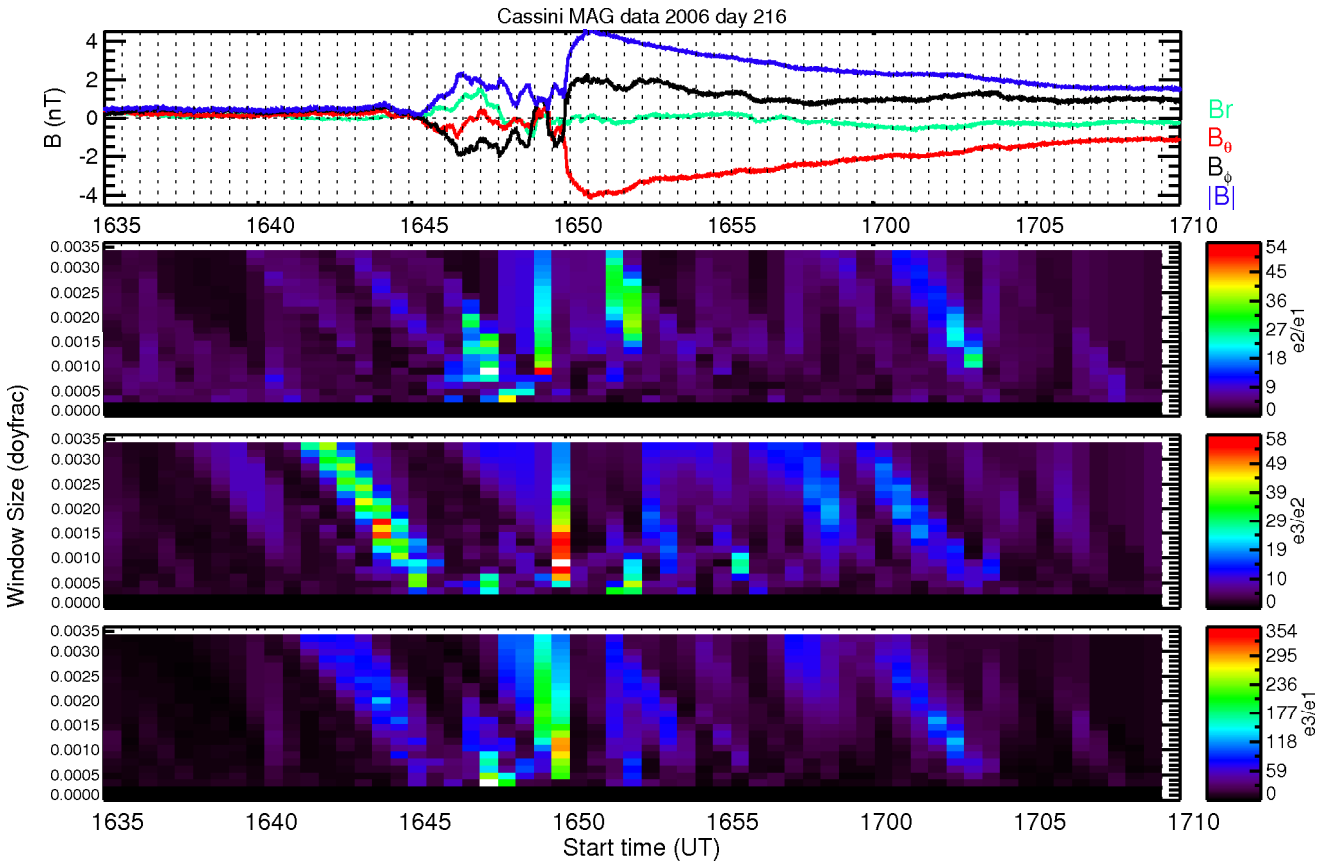
Cassini MAG data 2006 day 216
B (nT)
Br
Bθ
Bφ
|B|
Window Size (doyfrac)
e2/e1
e3/e2
e3/e1
Start time (UT)

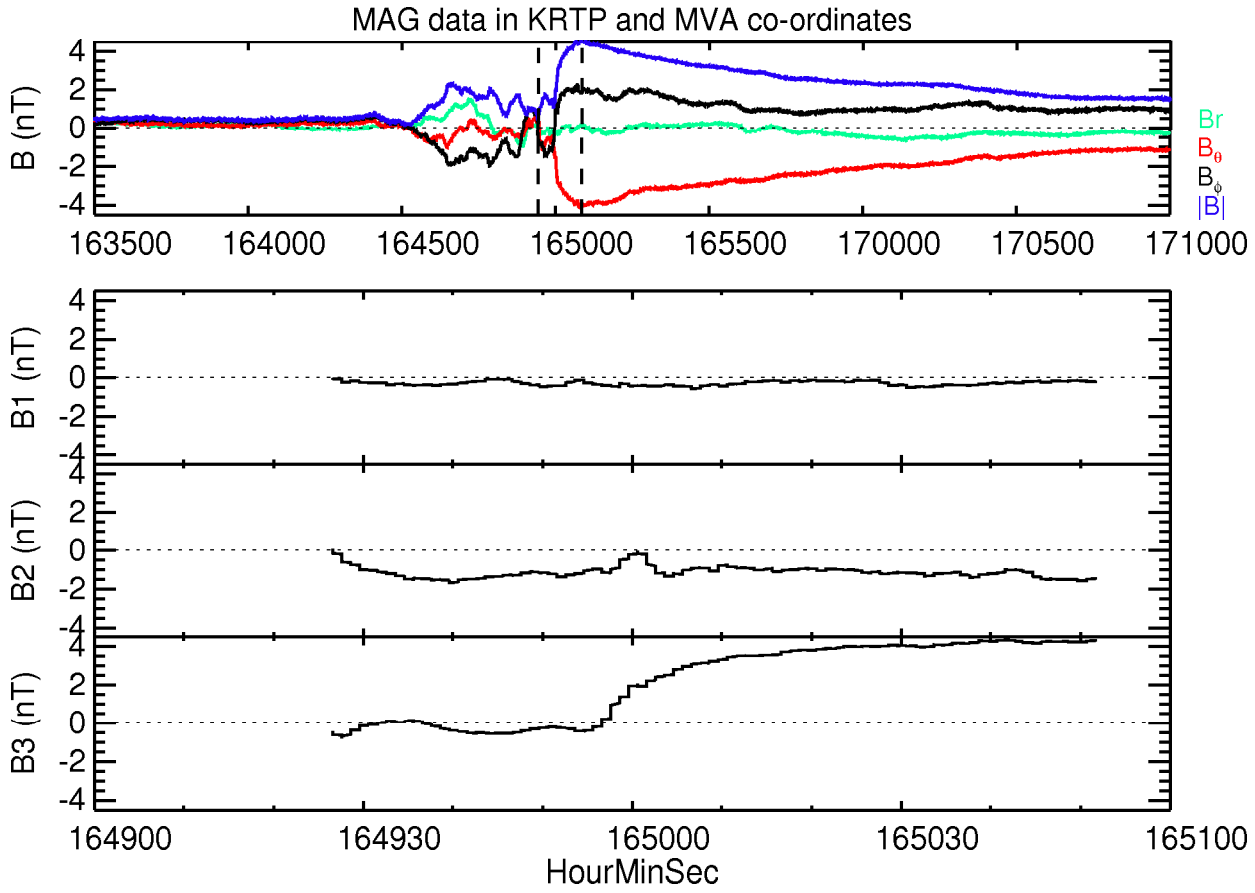
MAG data in KRTP and MVA co-ordinates
B (nT)
Br
B_θ
B_ϕ
|B|
B1 (nT)
B2 (nT)
B3 (nT)
163500
164000
164500
165000
165500
170000
170500
171000
164900
164930
165000
165030
165100
HourMinSec

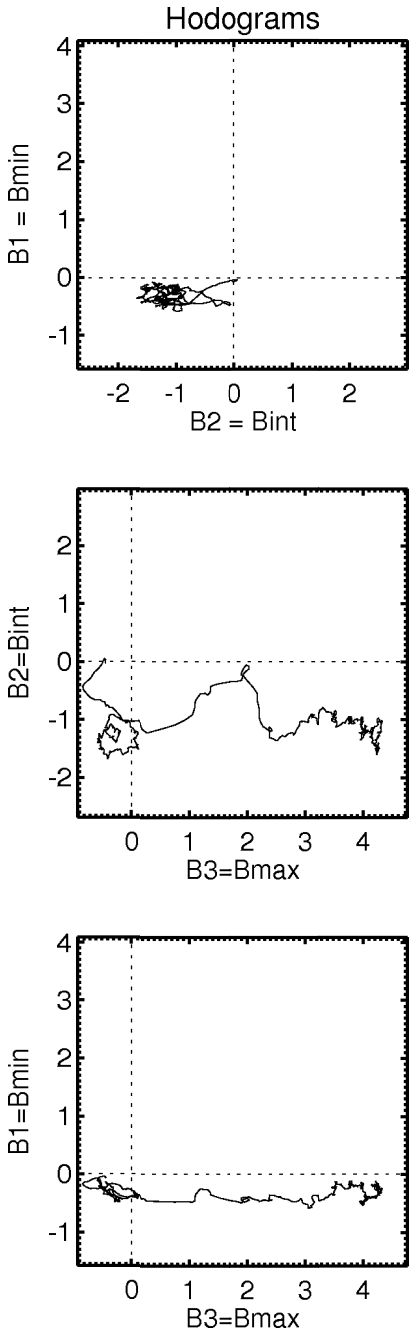
Hodograms
B1 = Bmin
B2 = Bint
B2=Bint
B3=Bmax
B1=Bmin
B3=Bmax

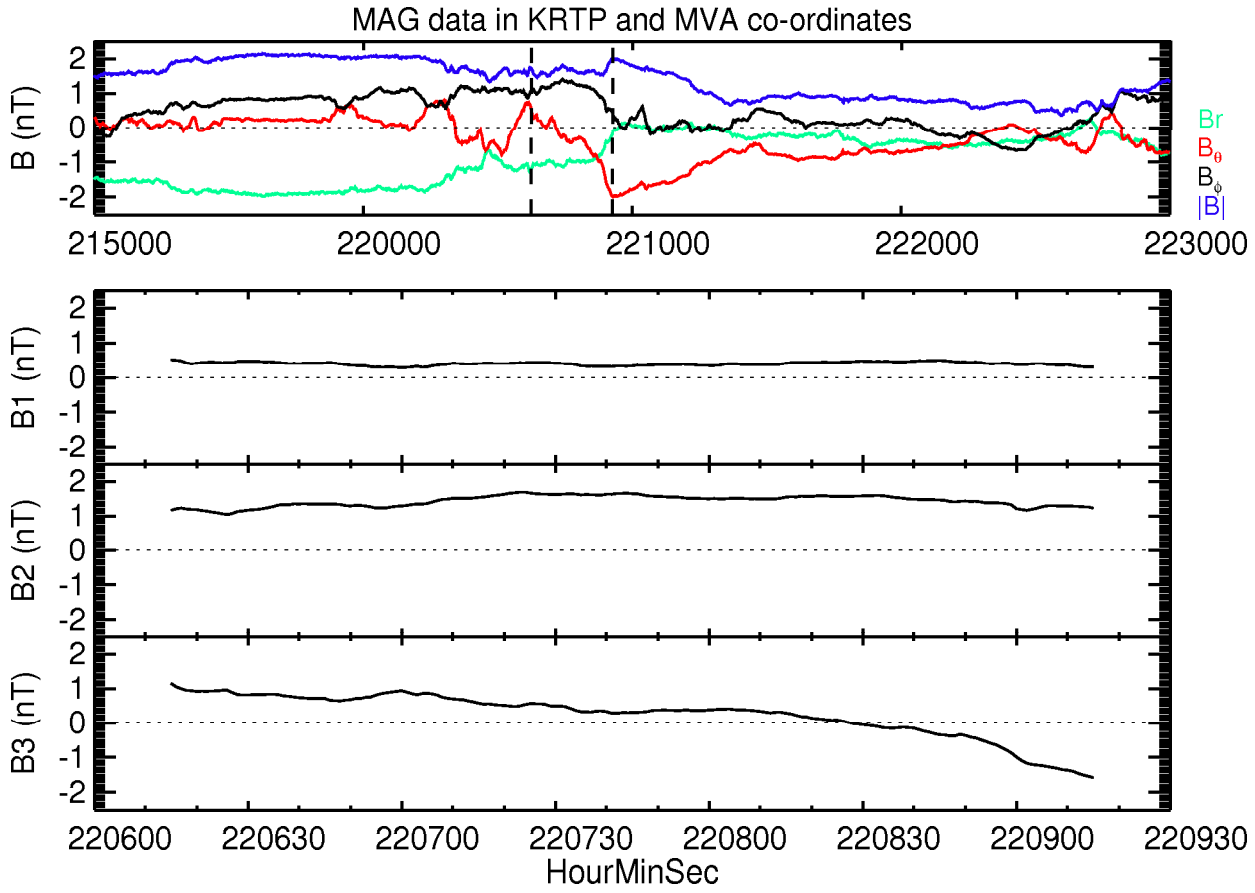
MAG data in KRTP and MVA co-ordinates
B (nT)
Br
B_θ
B_ϕ
|B|
B1 (nT)
B2 (nT)
B3 (nT)
215000
220000
221000
222000
223000
220600
220630
220700
220730
220800
220830
220900
220930
HourMinSec

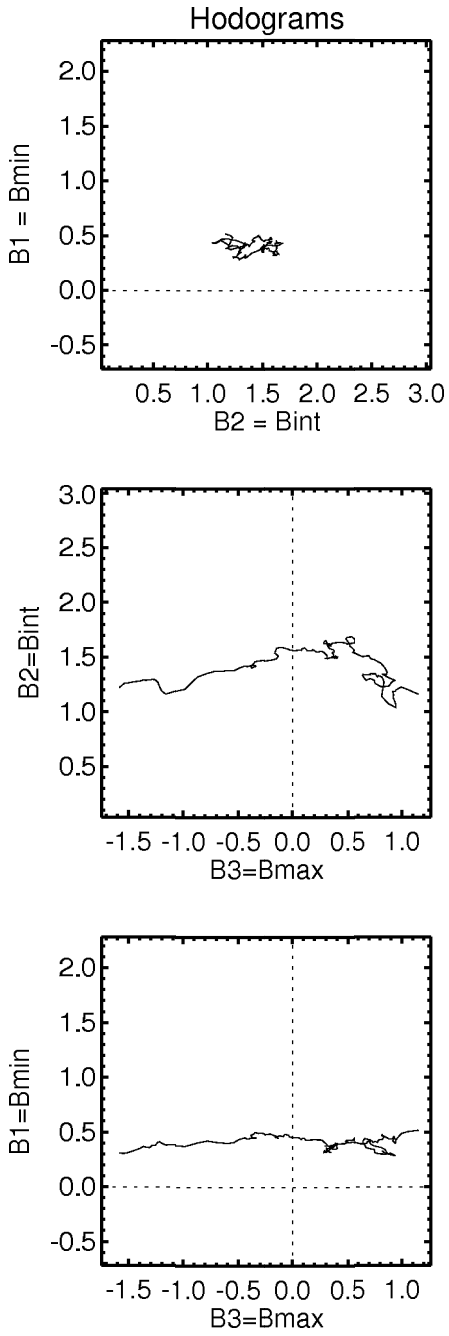
Hodograms
B1 = Bmin
B2 = Bint
B2=Bint
B3=Bmax
B1=Bmin
B3=Bmax

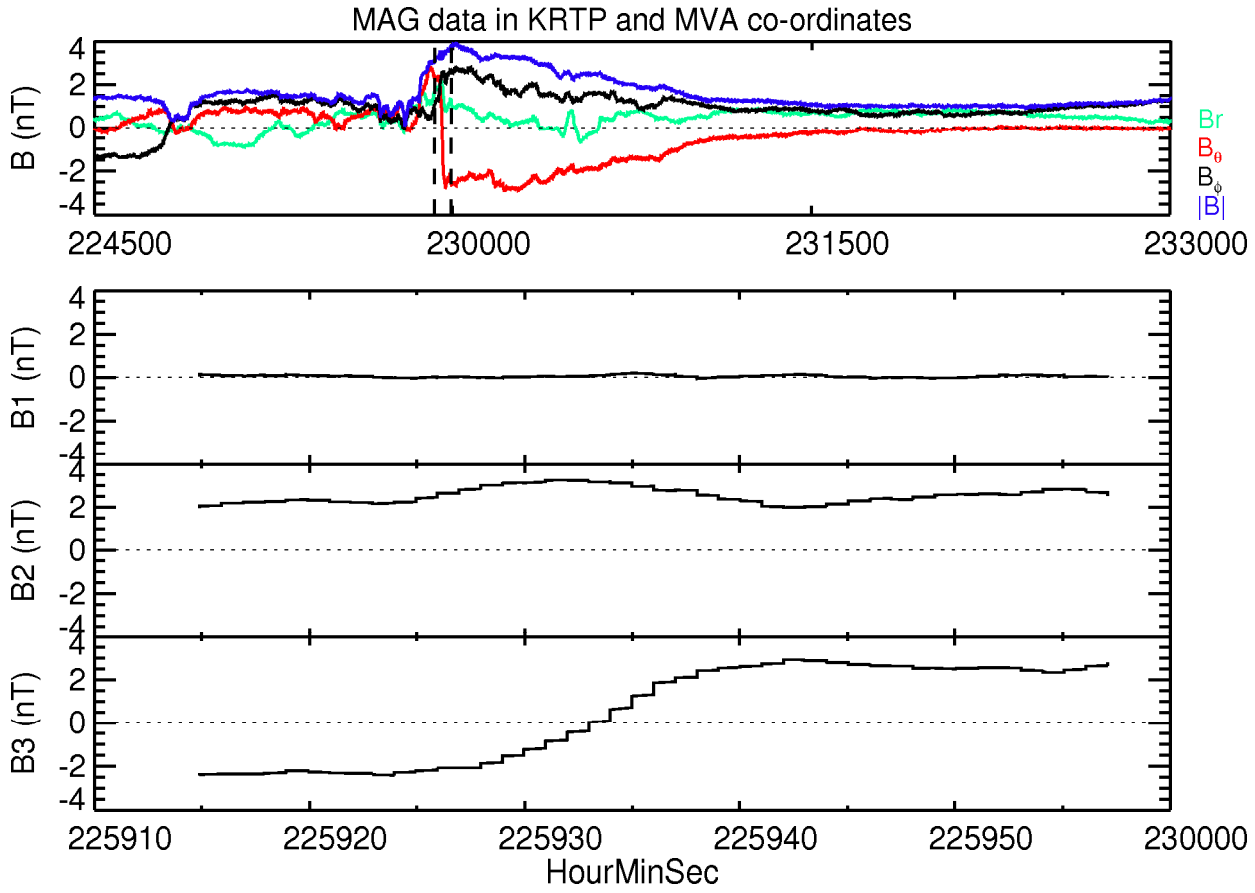
MAG data in KRTP and MVA co-ordinates
B (nT)
Br
Bθ
Bϕ
|B|
224500
230000
231500
233000
B1 (nT)
B2 (nT)
B3 (nT)
225910
225920
225930
225940
225950
230000
HourMinSec

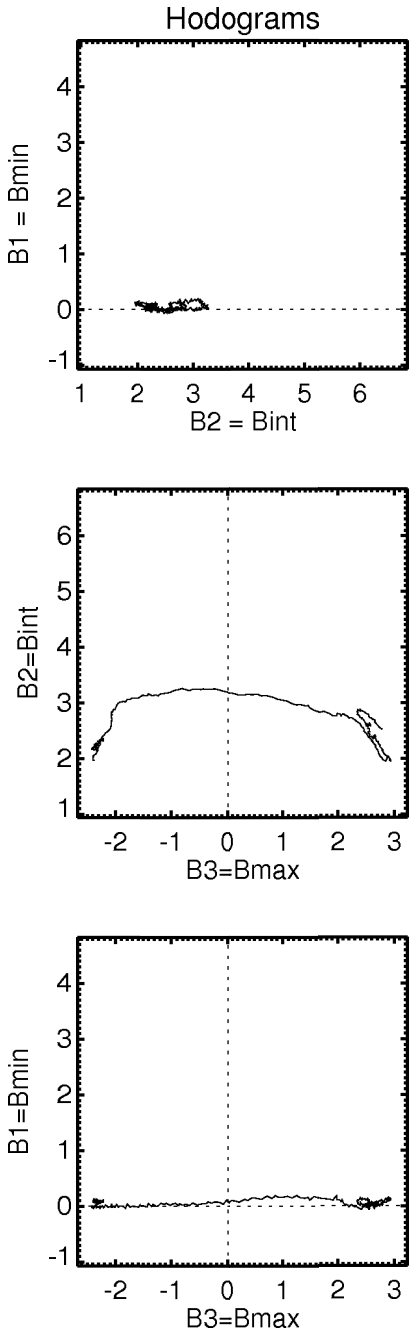
Hodograms
B1 = Bmin
B2 = Bint
B2=Bint
B3=Bmax
B1=Bmin
B3=Bmax

Closed Flux Reconnection

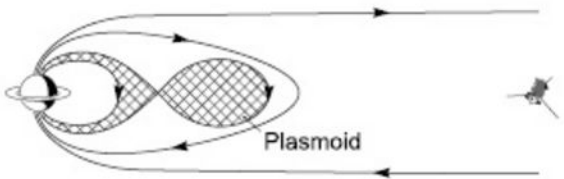

Vasyliunas Cycle only

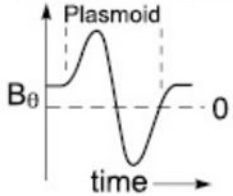

Closed & Open Flux Reconnection

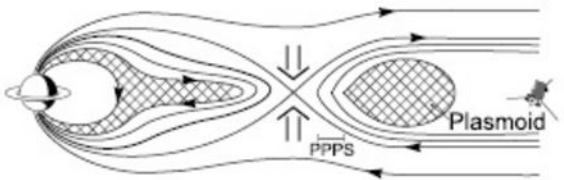

Disk Plasma

Vasyliunas & Dungey Cycles

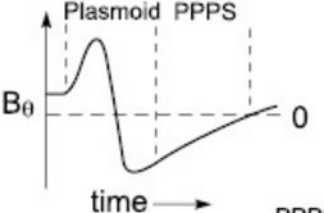

PPPS = Post Plasmoid Plasma Sheet

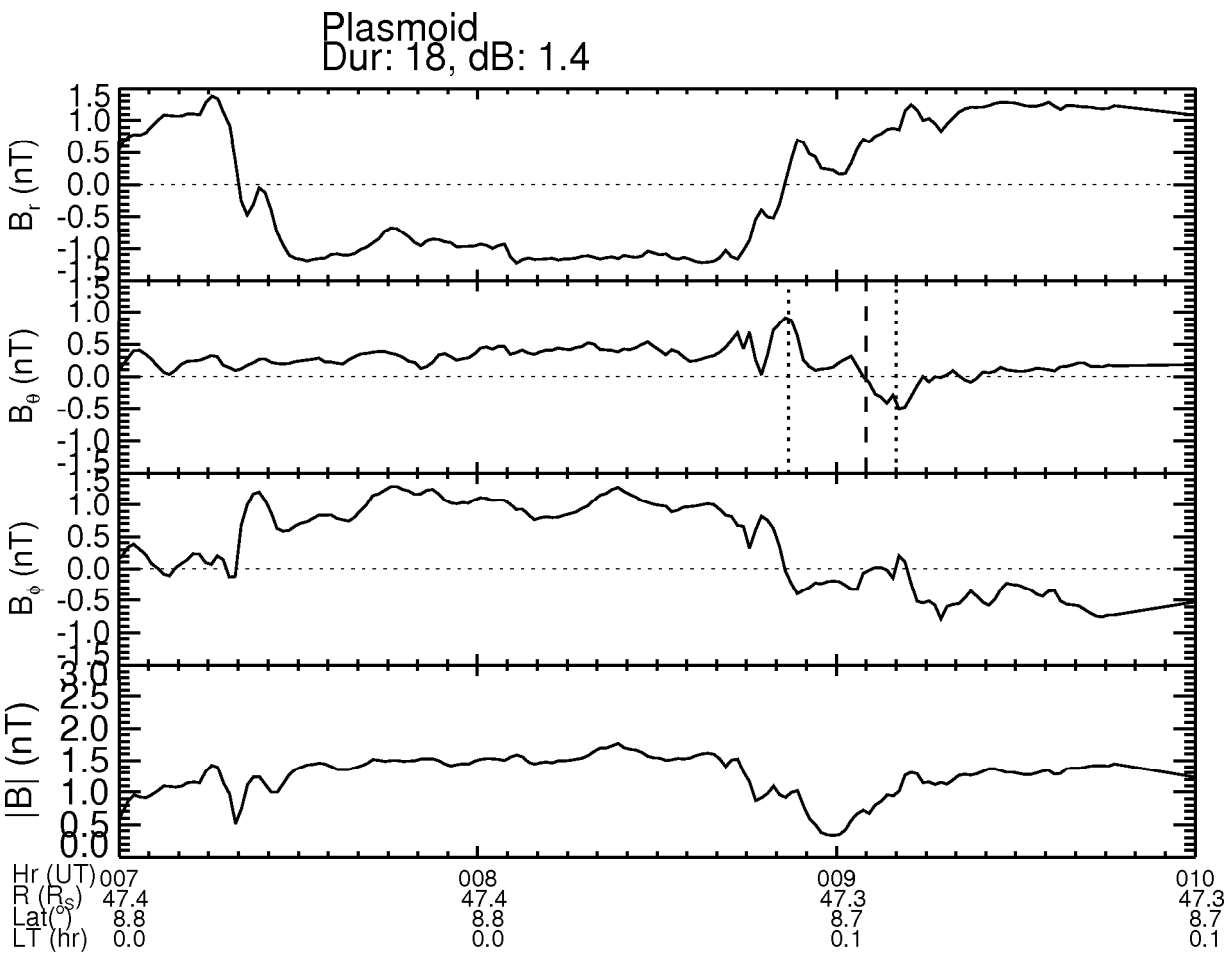
Plasmoid
Dur: 18, dB: 1.4
B_r (nT)
B_θ (nT)
B_φ (nT)
|B| (nT)
Hr (UT) 007 008 009 010
R (R_S) 47.4 47.4 47.3 47.3
Lat(°) 8.8 8.8 8.7 8.7
LT (hr) 0.0 0.0 0.1 0.1

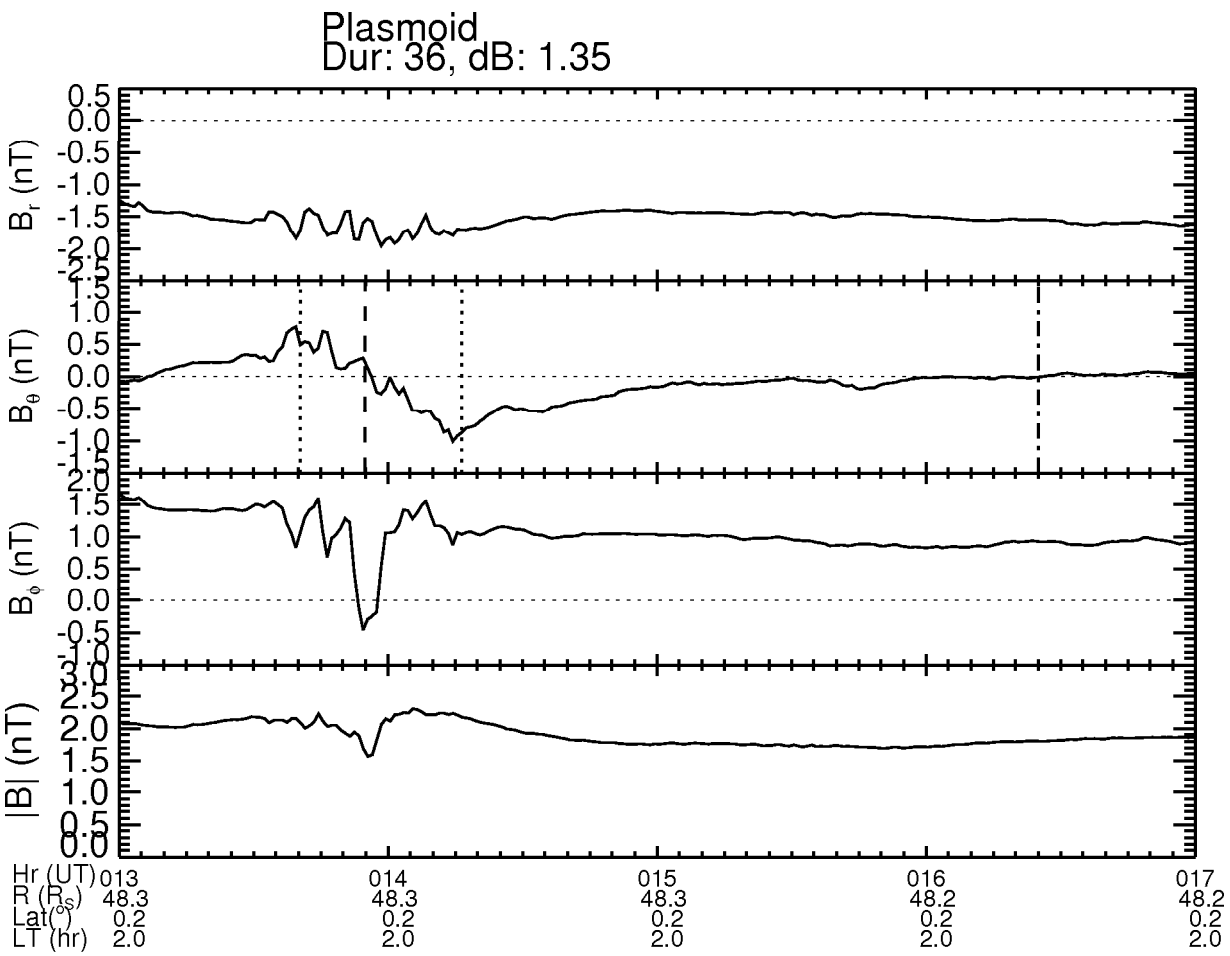
Plasmoid
Dur: 36, dB: 1.35
B_r (nT)
B_θ (nT)
B_φ (nT)
|B| (nT)
Hr (UT) 013 014 015 016 017
R (R_S) 48.3 48.3 48.3 48.2 48.2
Lat(°) 0.2 0.2 0.2 0.2 0.2
LT (hr) 2.0 2.0 2.0 2.0 2.0

Type	DOY	Time (Hr: Min:Sec)	Start Time (Hr Min sec)	End time (Hr min sec)	Range (R_S)	LT (Hr: Min)	Duration (mins)	ΔB_θ (nT)	B_θ change	Classification	Plasmaflow velocities	Ion flow direction
PLASMOID	32	12 58 00	12 47 00	13 11 00	65.99	4:26	24.00	2.13	south-north	isolated	V (W+) ~200-270 km/s	Strongly outward
TCR	36	04 32 00	04 17 00	04 38 00	68.17	4:46	21.00	0.52	south-north	pair		
PLASMOID	36	05 41 00	05 34 00	06 02 00	68.17	4:46	28.00	0.63	south-north	pair		
PLASMOID	37	23 10 30	23 02 30	23 20 30	68.08	4:56	18.00	0.87	south-north	isolated	CAPS data gap	CAPS data gap
PLASMOID	60	07 33 00	07 30 20	07 36 00	32.33	2:17	5.67	2.16	south-north	multiple	V(W+) ~ 170 km/s	Corotation and outward
PLASMOID	60	08 27 00	08 25 30	08 28 00	32.50	2:17	2.00	0.94	south-north	multiple		
TCR	60	08 58 00	08 53 00	09 03 00	32.61	2:18	10.00	0.49	south-north	multiple		
TCR	60	09 34 00	09 33 00	09 36 00	32.71	2:18	3.00	0.12	south-north	multiple		
TCR	62	15 26 00	15 19 00	15 30 00	40.93	2:55	11	0.31	south-north	pair		
TCR	62	16 33 00	16 29 00	16 38 00	41.07	2:56	9.00	0.22	south-north	pair		
PLASMOID	63	22 07 00	22 06 00	22 09 00	44.10	3:10	3.00	1.70	south-north	pair	V (W+) ~200 km/s	Halfway between corotation and outward
PLASMOID	63	22 59 30	22 56 00	23 02 00	44.17	3:11	6	3.51	south-north	pair	V (W+) ~580 km/s V (H+) ~620 km/s	Outward, from above, and slightly westward
PLASMOID	64	08 50 00	08 48 00	08 54 00	44.98	3:15	6.00	0.90	south-north	multiple	V (W+) ~220 km/s	Outward
PLASMOID	64	09 30 45	09 29 00	09 32 20	45.03	3:15	3.33	1.01	south-north	multiple	V (W+) ~290 km/s	Strongly outward
PLASMOID	64	10 49 00	10 46 10	10 52 10	45.13	3:16	6.00	1.15	south-north	multiple	V (W+) ~220 km/s	Strongly outward
PLASMOID	64	19 56 30	19 49 00	20 04 00	45.78	3:20	15.00	1.19	south-north	isolated		
PLASMOID	65	06 34 00	06 28 00	06 39 00	46.45	3:24	11.00	0.78	south-north	isolated		
PLASMOID	65	17 03 00	17 00 45	17 05 00	47.00	3:29	4.25	0.61	south-north	pair		
PLASMOID	65	17 24 00	17 22 00	17 27 15	47.02	3:29	5.25	1.31	south-north	pair		
PLASMOID	65	21 08 00	20 59 00	21 17 00	47.2	3:30	18.00	0.97	south-north	isolated		

					0							
TCR	66	06 23 00	06 17 00	06 30 00	47.6	3.36	13	0.6	south-north	pair		
TCR	66	08 42 00	08 40 00	08 51 00	47.7	3.36	11	0.7	south-north	pair		
TCR	83	18 34 30	18 18 30	18 46 00	34.03	0:33	27.50	2.22	south-north	isolated		
PLASMOID	84	02 31 30	02 30 30	02 32 30	35.8	0.7	2	1.9	south-north	isolated	Outward: V (W+) ~245 km/s	Outward
PLASMOID	85	00 16 00	00 09 00	00 20 00	40.22	0:58	11.00	1.85	south-north	isolated		Outward
TCR	85	04 20 00	04 01 00	04 25 00	40.9	1.0	24	0.6	south-north	isolated		
TCR	124	08 33 00	08 32 00	08 42 00	38.40	0:43	10.00	0.62	south-north	isolated		
TCR	124	13 13 00	13 05 00	13 20 00	39.05	0:45	15.00	0.20	north-south	pair		
TCR	124	14 19 30	14 06 00	14 30 00	39.20	0:46	24.00	0.65	north-south	pair		
PLASMOID	131	13 55 00	13 40 30	14 16 30	48.28	2:01	36.00	1.35	south-north	isolated		Progression from eastward to radial outward to westward flow
TCR	131	22 48 00	22 19 00	22 57 00	48.09	2:05	38	0.84	south-north	isolated		
TCR	169	00 34 00	00 32 00	00 39 00	62.32	1:34	7.00	1.47	south-north	isolated	V (H+) ~620 km/s	Outward
PLASMOID	193	07 28 30	07 27 00	07 43 00	48.42	23:52	16	2.1	south-north	isolated	V (W+) ~1240 km/s V (H+) ~679 km/s	Strongly outward and slightly westward (field-aligned)
PLASMOID	195	01 48 00	01 42 00	02 05 00	47.61	0:09	23.00	2.22	south-north	Pair		
TCR	195	04 08 00	04 07 00	04 13 00	47.52	0:10	6.00	0.38	south-north	Pair		
TCR	195	12 44 00	12 38 00	12 53 00	47.16	0:13	15	0.69	south-north	isolated		
PLASMOID	195	23 38 30	23 31 00	23 45 00	46.5	0.3	14	1.6	south-north	isolated		
PLASMOID	196	08 56 00	08 54 00	09 01 00	46.05	0:22	7.00	1.15	south-north	Pair	V (W+) ~202 km/s	Strongly outward
PLASMOID	196	10 22 00	10 15 00	10 24 00	45.96	0:23	9.00	1.40	south-north	Pair	V (W+) ~202 km/s	Outward
PLASMOID	196	18 28 00	18 24 00	18 30 00	45.41	0:26	6.00	1.25	south-north	isolated	V (W+) ~186 km/s	Outward
PLASMOID	197	07 09 00	07 05 00	07 12 00	44.41	0:32	7.00	1.60	south-north	Pair		Slightly outward

TCR	197	07 44 00	07 40 00	07 51 00	44.36	0:32	11.00	0.38	south-north	Pair		
PLASMOID	197	16 34 00	16 25 00	16 41 00	43.5	0.6	16	0.9	south-north	isolated	V (W+) ~170 km/s	Outward
PLASMOID	198	14 45 30	14 43 30	14 52 30	41.25	0:48	9.00	1.75	south-north	isolated		
PLASMOID	199	23 06 45	23 02 00	23 08 30	36.88	1:08	6.5	1.80	south-north	isolated		
PLASMOID	209	20 34 00	20 17 00	20 38 30	36.85	22:24	21.50	2.58	south-north	isolated		
PLASMOID	212	04 49 00	04 39 00	04 57 00	43.85	22:56	18.00	0.84	south-north	Pair		
PLASMOID	212	05 27 00	05 15 00	05 57 00	43.91	22:56	42.00	0.65	south-north	Pair		
PLASMOID	212	10 07 00	10 05 00	10 08 00	44.34	22:58	3.00	0.68	south-north	Pair		Corotation
PLASMOID	212	10 54 00	10 48 00	10 58 00	44.41	22:36	10.00	1.08	south-north	Pair		Corotation
PLASMOID	212	14 57 00	14 50 00	15 00 00	44.76	23:00	10.00	0.91	south-north	isolated		Uncertain direction. Spacecraft rolling but CAPS not looking in corotation direction
PLASMOID	212	23 19 30	23 17 30	23 20 30	45.4	23.1	3	1.1	south-north	isolated		
PLASMOID	213	11 50 00	11 32 00	12 12 00	46.4	23.2	40	1.5	south-north	isolated		
PLASMOID	214	18 32 00	18 29 00	18 35 00	48	23.4	6	0.8	south-north	isolated		
PLASMOID	215	10 36 30	10 30 00	10 38 30	48.5	23.5	8.5	1.1	south-north	isolated		
PLASMOID	215	17 27 00	17 20 00	17 35 00	48.7	23:31	15.0	0.83	south-north	isolated	V(W+)~220 km/s	Outward
PLASMOID	216	16 47 30	16 45 00	16 51 15	49.00	23:41	6.25	3.39	south-north	Pair	V (W+) ~242 km/s	Strongly outward
PLASMOID	216	17 51 00	17 47 30	17 55 30	49.01	23:50	8	0.82	south-north	Pair		
PLASMOID	217	17 42 00	17 28 20	17 59 00	48.85	23:13	21.67	0.65	south-north	isolated	V (W+) ~155 km/s V (H+) ~620 km/s	Corotation or very slightly outward
PLASMOID	218	15 27 00	14 47 00	16 05 00	48.31	23:59	78.00	0.92	south-north	isolated		
PLASMOID	219	11 20 00	10 45 00	12 20 00	47.48	00:07	95.00	1.03	south-north	isolated		
PLASMOID	223	14 40 00	14 26 00	15 07 00	37.9	00:56	41.00	1.21	south-north	isolated	V(W+)~240	Very weak

					9						km/s	ions, apparently outward
PLASMOID	232	10 01 00	09 46 00	10 07 00	30.76	21:54	21.00	1.91	south-north	isolated		Very weak ions, uncertain flow direction
PLASMOID	234	14 50 30	14 45 00	15 03 00	39.6	22.6	18	1.8	south-north	isolated		No discernible ion flow
PLASMOID	236	18 05 30	18 04 30	18 11 00	45	23	6.5	0.95	south-north	Pair		
PLASMOID	238	18 16 00	18 15 00	18 18 30	47.9	23.3	3.5	1.3	south-north	isolated	V (W+) ~144 km/s	Outward
PLASMOID	240	00 41 00	00 33 00	00 44 00	48.73	23:32	11.00	1.20	south-north	isolated		
PLASMOID	240	06 48 00	06 46 00	06 55 00	48.81	23:34	9.00	0.66	south-north	isolated	V(W+)~190 km/s V(H+)~440 km/s	Initially, flow outward and from above; subsequently, largely corotating
PLASMOID	240	23 38 30	23 28 00	23 54 00	48.8	23.6	26	1.5	south-north	multiple	V (W+) ~242 km/s	Outward
PLASMOID	241	01 38 30	01 34 30	01 53 30	48.8	23.6	20	1.1	south-north	multiple		
PLASMOID	241	03 40 30	03 25 00	03 45 00	48.8	23.7	5	0.55	south-north	multiple		
PLASMOID	242	17 30 00	17 02 00	17 50 00	48.02	23:57	48.0	0.98	south-north	isolated		
PLASMOID	243	09 05 00	08 52 00	09 10 00	47.3	0.1	18	1.4	south-north	isolated	V (W+) ~314 km/s	Uncertain flow direction (probably corotational)
PLASMOID	243	21 47 00	21 22 00	21 58 00	46.64	00:09	36.00	0.64	south-north	isolated		
PLASMOID	244	15 17 00	15 11 00	15 19 00	45.45	00:16	8.00	1.15	south-north	isolated		Outward flowing H+ precedes event, which coincides with departure from electron plasma sheet
PLASMOID	246	22 45 00	22 18 00	22 51 00	39.74	00:45	33.00	2.02	south-north	isolated	V(W+)~350 km/s	Viewing away from corotation, but clearly outward
PLASMOID	248	17 50 00	17 45 00	18 00 00	32.8	1.3	15	1.6	south-north	Pair	V (W+) ~170	Probably

											km/s	outward
PLASMOID	248	18 30 00	18 29 00	18 31 00	32.8	1.3	2	1.4	south-north	Pair	V (W+) ~340 km/s	Outward
PLASMOID	249	12 04 00	12 02 30	12 04 30	29.14	01:34	2.00	2.00	south-north	Pair	V(W+)~220 km/s	Slightly outward on both sides of event
PLASMOID	249	15 34 00	15 32 15	15 36 45	28.35	1:38	4.50	4.42	south-north	isolated	V (W+) ~407 km/s	Outward
PLASMOID	250	00 32 30	00 11 30	00 33 45	26.22	01:49	22.25	2.25	south-north	isolated		Uncertain flow direction (not actuating)
PLASMOID	258	10 05 00	09 20 00	10 10 00	35.4	23.9	50	2.2	south-north	isolated	V (W+) ~480 km/s	Flow from above (inward/outward uncertain)
PLASMOID	258	21 00 00	20 20 00	21 20 00	36.2	0	60	2.1	south-north	isolated		
PLASMOID	261	04 01 00	03 58 30	04 05 45	37.52	00:31	7.25	1.66	south-north	isolated	V(W+) >600 km/s	Inward?
PLASMOID	262	08 45 00	08 30 30	08 49 00	36.54	00:47	18.50	1.10	south-north	isolated	V(W+)~220 km/s	Corotation
PLASMOID	264	02 08 30	02 00 30	02 09 30	32.99	01:12	9.00	1.59	south-north	isolated		

Table 1: Timings and properties of plasmoids and TCRs observed during 2006. Flow speeds are estimated from the energy of the peak counts and thus they represent upper limits.